

STEADY CAPILLARY-GRAVITY  
WAVES ON DEEP WATER

Thesis by  
Benito Miguel Chen Charpentier

In Partial Fulfillment of the Requirements  
for the Degree of  
Doctor of Philosophy

California Institute of Technology  
Pasadena, California

1979  
(Submitted April 16, 1979)

## ACKNOWLEDGEMENTS

I like to thank my adviser, Professor Philip G. Saffman, for suggesting the topic of this thesis and for his invaluable help and patience during its development. I would also like to express my gratitude to the faculty, fellow students and staff of the Applied Mathematics department for many useful suggestions and for these interesting years.

My stay at Caltech was possible thanks to support by the Consejo Nacional de Ciencia y Tecnología, México, and to a Graduate Research Assistantship. I am indebted to Control Data Corporation for providing me with time on their STAR 100 computer, without which the calculations would not have been possible.

I wish to thank my family for believing in me, and last but not most, to Esther, to whom I dedicate this thesis, for everything.

ABSTRACT

The properties of capillary-gravity waves of permanent form on deep water are studied. Two different formulations to the problem are given. The theory of simple bifurcation is reviewed. For small amplitude waves a formal perturbation series is used. The Wilton ripple phenomenon is re-examined and shown to be associated with a bifurcation in which a wave of permanent form can double its period. It is shown further that Wilton's ripples are a special case of a more general phenomenon in which bifurcation into subharmonics and factorial higher harmonics can occur. Numerical procedures for the calculation of waves of finite amplitude are developed. Bifurcation and limit lines are calculated. Pure and combination waves are continued to maximum amplitude. It is found that the height is limited in all cases by the surface enclosing one or more bubbles. Results for the shape of gravity waves are obtained by solving an integro-differential equation. It is found that the family of solutions giving the waveheight or equivalent parameter has bifurcation points. Two bifurcation points and the branches emanating from them are found specifically, corresponding to a doubling and tripling of the wavelength. Solutions on the new branches are calculated.

TABLE OF CONTENTS

CHAPTER		PAGE
	Acknowledgements	ii
	Abstract	iii
	Table of Contents	iv
	INTRODUCTION	1
1.	FORMULATION OF THE PROBLEM	8
	1.1 The Fourier Series Expansion	8
	1.2 The Vortex Sheet Formulation	14
	1.3 Some Integral Properties	18
	1.4 Simple Bifurcation	22
2.	WEAKLY NON-LINEAR WAVES	27
	2.1 Pure and Combination Waves	27
	2.2 Wilton Ripples	33
	2.3 Wilton Ripples as a $2 \rightarrow 1$ Bifurcation	39
	2.4 Combination (N,M) Waves	42
	2.5 The $M \rightarrow N$ and $N \rightarrow M$ Bifurcations, $N > \frac{1}{2}M$	46
	2.6 The Case $1 < N < \frac{1}{2}M$	48
	2.7 The Case $N=1, M \geq 4$	49
	2.8 Bifurcation of (1,3) Combination Waves	52
3.	NUMERICAL PROCEDURES	56
	3.1 The Fourier Series Method	56
	3.2 The Vortex Sheet Method	60

CHAPTER	PAGE
3.3 Arclength Continuation	66
4. FINITE AMPLITUDE CAPILLARY-GRAVITY WAVES	72
4.1 Introduction	72
4.2 The Finite Amplitude $2 \rightarrow 1$ and $2 \rightarrow 3$ Bifurcations	74
4.3 The Finite Amplitude $M \leftrightarrow N$ Bifurcation with $N > \frac{1}{2}$	79
4.4 The $1 \rightarrow M$ Limit Line	81
4.5 Waves of Maximum Height on Deep Water	83
5. FINITE AMPLITUDE GRAVITY WAVES	89
5.1 Introduction	89
5.2 Numerical Results for Regular Waves of Class 1	95
5.3 Bifurcation of Regular Class 2 Waves: a New Type of Symmetrical Solution	98
5.4 Bifurcation of Regular Class 3 Waves	102
5.5 Discussion	106
APPENDIX A	108
APPENDIX B	110
FIGURES	112
TABLES	139
REFERENCES	142

## INTRODUCTION

Since the last century, there has been an undecaying interest in the study of periodic, irrotational, permanent surface waves on a deep heavy inviscid fluid. Most of the work done considers gravity as the only restoring force. In his now classic paper of 1847, Stokes (27) proposed the existence of a solution for the non-linear problem as a perturbation series in the amplitude. He calculated the first three terms of the series and found that the speed of propagation  $c$  depends on the amplitude. When he revised this paper in 1880 (28), he found it simpler to reformulate the problem using the complex potential as the independent variable. He also added an appendix proving that if the surface has a cusp, the internal angle is  $120^\circ$ . Since, as the amplitude grows, the crests become steeper and the troughs shallower, he speculated that the highest wave would have a  $120^\circ$  corner and a wide shallow trough. Michell (17) and Yamada (32) incorporated this singular behavior into the approximate calculation of waves of maximum height, and found that  $h/\lambda \approx 0.1412$ , where  $h$  is the vertical distance between crest and trough, and  $\lambda$  is the wavelength. Schwartz (23), using Padé approximants to sum a Stokes type expansion to high order, calculated numerical

solutions for waves of any height up to almost the maximum. His surface profiles tend to those of Michell and Yamada, as the waveheight increases. Longuet-Higgins (13), using the same method as Schwartz, found that the wavespeed and the energy are not monotonic functions of the waveheight, and established some integral and differential properties of gravity waves. Longuet-Higgins and Fox (15) constructed asymptotic expansions close to the  $120^\circ$ -cusped wave of greatest height and showed that both the wavespeed and the energy oscillate infinitely often as the limiting wave is approached, and moreover, the maximum slope is greater than  $30^\circ$ . The stability of finite amplitude, steady gravity waves to infinitesimal sinusoidal disturbances has also been investigated by Longuet-Higgins (14). He determined that for a superharmonic perturbation (the wavelength of the perturbation is less than that of the unperturbed steady wave) there is an instability at  $h/\lambda = 0.139$ , which is also the value for which the wavespeed has a maximum. When the perturbations are subharmonic, he found that for small amplitudes all modes are neutrally stable; become unstable when the waveheight reaches a certain value corresponding to the Benjamin & Feir (1) instability; and, as the amplitude continues to increase, become stable and then unstable again at about  $h/\lambda = 0.129$ .

If we include the effects of surface tension, the results are fewer. However, if surface tension is the only

force, Crapper (4) solved the problem analytically. He found that the wavespeed decreases monotonically with the waveheight, and that the highest wave encloses a bubble. For higher amplitudes the surface crosses itself making the solution unphysical.

Harrison (6) approximated the solution to the problem with both surface tension and gravity by a Fourier series using Stokes' hypothesis that the  $n$ th Fourier coefficient is  $n$ th order in the amplitude. He calculated three terms and found that the approximation broke down when the wavelength was such that the wavespeed was the same as the speed of waves with a half or a third of the wavelength. He showed that the profiles for waves of very short and very long wavelength are essentially different. Wilton (31) extended the expansion to fifth order and showed how to correct the inconsistency at the critical wavelengths  $\lambda_N = 2\pi(N\tau/\rho g)^{1/2}$ , where  $N$  is an integer greater than 1,  $\tau$  the surface tension,  $\rho$  the density of the fluid and  $g$  the acceleration due to gravity. He proposed that at the critical wavelengths, the first and  $N$ th harmonics are of the same order and all the others of smaller order. He found further that two different solutions exist at  $\lambda_2 = 2\pi(2\tau/\rho g)^{1/2}$ , the so-called Wilton ripples.

Pierson and Fife (21) using the method of strained coordinates extended Wilton's solutions to wavelengths near  $\lambda_2$  ( $\lambda_2 = 2.44$  cm in water). Nayfeh (19) obtained a

second order expansion valid near  $\lambda_3$  ( $\lambda_3 = 2.99$  cm in water) using the technique of multiple scales and found three different profiles.

Schooley (22) observed experimentally in wind generated waves profiles close to those predicted by Wilton near  $\lambda = 2.44$  cm. However, McGoldrick (16) using a wavemaker could not produce a uniform profile for  $\lambda = 2.44$  cm. The physical existence of capillary-gravity waves near the critical wavelengths is still an open question.

Results about the mathematical existence and uniqueness are few and most are limited to small amplitude. For gravity waves ( $\mathcal{T} = 0$ ), Nekrasov (20) formulated the problem, for symmetric waves about verticals through the crest and trough, as a non-linear integral equation. He proposed a series solution and proved the convergence for sufficiently small amplitude, but did not give the radius of convergence. Levi-Civita (12) used a similar series to prove the existence of water waves for sufficiently small amplitude. His proof yields solutions that are symmetric with respect to crest and trough, but, contrary to popular belief, he did not prove that all gravity waves must be symmetric. More recently, Krasovskii (9) gave an existence proof valid for waves of finite amplitude with slopes measured from the horizontal less than  $30^\circ$ . Keady and Norbury (7) reformulated the problem using the inverse of the speed at the crest as the expansion parameter and proved convergence of the

series for all crest speeds down to but not including zero. The highest wave with an stagnation point at the crest is the only wave not included in the proof, which allows even for the existence of waves with slopes greater than  $30^\circ$ . Garabedian (5) using variational methods gave another existence proof and, under the assumption that there is only one crest and trough per period, proved that the waves are symmetric about the crest and trough. A corollary of his proof is the uniqueness of symmetric waves with the same crests and troughs. He could not prove symmetry for waves whose crests or troughs have unequal heights. Toland (30) proved the existence of the highest wave having a stagnation point at the crest, and showed that the crest has to be either a  $120^\circ$  cusp or the limit point of a sequence of steep ripples.

For capillary-gravity waves, Sekerzh-Zen'kovich (24) gave the outline of an existence proof. Zeidler (33) did a comprehensive study of existence and uniqueness proofs, together with the functional analysis methods used. One of the most important results is his constructive proof of existence and uniqueness for capillary-gravity waves of sufficiently small amplitude for all wavelengths, except the critical ones found by Wilton. He supposed symmetry of the waves.

The existence, uniqueness and symmetry of capillary-gravity waves is still not completely solved. They exist

for sufficiently small amplitude and it is likely that they cease to exist when the amplitude reaches some finite critical value. Gravity waves do not appear to exist when  $h/\lambda > 0.142$ . Also, capillary waves cease to exist for  $h/\lambda > 0.730$ . The limiting wave touches itself and encloses a bubble but the shape is otherwise smooth. The results of Wilton (31), Pierson and Fife (21) and Nayfeh (19) show that capillary-gravity waves are not unique, even for wavelengths not equal to the critical ones. It is not obvious that permanent nonsymmetrical capillary-gravity waves of sufficiently large amplitude do not exist. Wilton ripples are not symmetric with respect to all their crests or troughs.

Our main objective is to investigate the properties of capillary-gravity waves, analytically for small amplitude and numerically for amplitudes up to the maximum. We will study the bifurcation of waves into subharmonics and fractional higher harmonics, and show that finite amplitude capillary-gravity waves are not unique. We will also give evidence of nonuniqueness for gravity waves. We will restrict ourselves mainly to symmetrical waves about a crest or a trough. But for gravity waves we will explore the possibility of nonsymmetrical solutions. The mathematical existence and stability of the solutions are beyond the scope of this work.

In chapter 1, the physical problem is established and the mathematical equations derived. Some integral and differential properties of water waves are formulated. A review of simple bifurcation and arclength continuation is given.

In chapter 2, we consider the form of weakly non-linear waves of permanent shape on deep water under the effects of both surface tension and gravity. A formal perturbation series is used to find uniformly valid solutions and to establish the bifurcation of waves. Wilton ripples are a special case of this phenomenon.

Chapter 3 is the development of the numerical procedures used to solve the problem for finite amplitude.

Chapter 4 contains the numerical results for finite amplitude capillary-gravity waves.

Chapter 5 is the numerical study of high amplitude gravity waves and their subharmonic bifurcation.

CHAPTER 1

FORMULATION OF THE PROBLEM

1.1 The Fourier series expansion.

We consider periodic, steady or permanent, one-dimensional, inviscid, irrotational, progressive water waves of finite amplitude on deep water otherwise at rest, under the influence of both gravity and surface tension. The density of the upper fluid, usually air, is neglected.

We take rectangular coordinate axes  $Ox'y'$ , with  $Ox'$  horizontal and  $Oy'$  vertically upwards in a frame of reference moving with the wave. Let  $z=x+iy$  denote the complex physical coordinate. We study the wave in a window of horizontal extent  $L$ , where  $L$  is an integral multiple of the wavelength  $\lambda$ , that is defined as the shortest period of the wave. Let  $c$  be the wave speed and  $h$  the height, defined as the vertical distance between the top of the highest crest and the bottom of the lowest trough. Denote the components of the velocity vector in the direction  $Ox'$  and  $Oy'$  by  $u$  and  $v$ , respectively, the pressure by  $p$  and the acceleration of gravity (positive downwards) by  $g$ . The

density  $\rho$  of the fluid will be taken equal to 1 with no loss of generality.

Since in this frame of reference the motion is steady, the equations of motion for an inviscid, incompressible and one-dimensional fluid are

$$\frac{\partial u}{\partial x} + \frac{\partial v}{\partial y} = 0 \quad (1.1.1)$$

$$u \frac{\partial u}{\partial x} + v \frac{\partial u}{\partial y} = - \frac{\partial p}{\partial x} \quad (1.1.2)$$

$$u \frac{\partial v}{\partial x} + v \frac{\partial v}{\partial y} = -g - \frac{\partial p}{\partial y} . \quad (1.1.3)$$

Further, since the motion is irrotational,

$$\frac{\partial v}{\partial x} - \frac{\partial u}{\partial y} = 0 \quad (1.1.4)$$

and there exists a complex potential  $w = \phi + i\psi$  such that

$$u - iv = \frac{dw}{dz} . \quad (1.1.5)$$

For incompressible fluids, we have Bernoulli's integral

$$\frac{1}{2}(u^2 + v^2) + gy + p = A \quad (1.1.6)$$

where  $A$  is a constant.

Next consider the boundary conditions. Let  $F(x,y)=0$  describe the surface, then the condition that there is no transfer of matter across the surface gives the first boundary condition

$$u \frac{\partial F}{\partial x} + v \frac{\partial F}{\partial y} = 0 . \quad (1.1.7)$$

That is, the velocity at the surface is tangential to the surface. Since the surface is not known a priori, we need an additional condition. This is the dynamic condition

$$p = -\frac{T}{R}, \quad (1.1.8)$$

where  $T$  is the surface tension and  $R$  the radius of curvature of the interface taken positive when the surface is concave upwards.

Since the surface is a streamline, say  $\psi=0$ , it is more convenient to work with  $z$  as a function of the complex potential. The fluid occupies the region  $\psi \leq 0$ . See figure 1. The equation of continuity (1.1.1) and the irrotationality of the fluid (1.1.4) give

$$\nabla^2 z \equiv \frac{\partial^2 z}{\partial \phi^2} + \frac{\partial^2 z}{\partial \psi^2} = 0 \quad (1.1.9)$$

on  $\psi \leq 0$ . The boundary conditions imply that

$$q^2 + 2gY - \frac{2T}{R} = c^2(1-b) \quad (1.1.10)$$

on  $\psi=0$ . In (1.1.10)  $q = |dz/dw|^{-1}$  evaluated on the surface,  $Y$  is the height of the free surface above some origin. Bernoulli's constant is written as  $c^2(1-b)$ , where  $c$  is the wavespeed. The magnitude of the wave determines the parameter  $b$ , but its precise specification depends upon the choice of origin for  $Y$ . For instance, if  $Y$  is measured from the mean water level, then the argument in Lamb (10, section 250) is easily extended to include surface tension

to show that  $b=0$ . (See appendix A). However, we find it convenient in our discussion to measure  $\Upsilon$ , and the horizontal coordinate, from a crest or a trough (i.e. a local maximum or minimum of  $\Upsilon$ ) where  $w$  is also supposed to vanish. In this case

$$b = 1 - \frac{u_0^2}{c^2} + \frac{2T}{R_0 c^2}, \quad (1.1.11)$$

where suffix  $_0$  refers to the origin and  $u_0$  is the speed at the crest or trough.

We are going to use two completely different methods to find solutions to the problem. The first one consists in expressing  $z$  in terms of the complex potential  $w$  by a Stokes type expansion. The second is to consider the surface as a vortex sheet and obtain an integro-differential equation for the problem. This method will be developed in section 1.2.

Returning to the first method, let

$$z = \frac{w}{c} + i \frac{L}{2\pi} \sum_1^{\infty} \frac{C_n}{n} \exp(-2\pi n i w / cL) + i \frac{L C_0}{2\pi} \quad (1.1.12)$$

which satisfies Laplace's equation (1.1.9). Since  $z(0)=0$ , we have that  $C_0$  is given in terms of all the other  $C_n$ 's. The unknowns are the complex constants  $C_n$ , the wavespeed and the parameter  $b$ . They are determined by Bernoulli's equation (1.1.10) and by the amplitude of the wave.

Equation (1.1.12) evaluated at  $\Psi = 0$  gives parametric equations for  $X$  and  $Y$  as functions of the velocity

potential  $\phi$ . Evaluation of  $q$  and  $R$  and substitution into (1.1.10), which must be satisfied for  $0 \leq \phi \leq cL$ , together with a specification of the amplitude, provides the necessary equations for the unknowns.

We now assume further that the waves are symmetrical about the origin; that is, we suppose that a crest or a trough exists about which the wave is symmetrical and choose it as the origin. It was proved by Levi-Civita (12) and others that permanent symmetric gravity waves exist. Zeidler (33) proved the same for capillary-gravity waves. To our knowledge, it has not been proved that all waves must be symmetric. However, this is a matter for further study and we shall restrict attention to symmetrical waves. Then it can be supposed that the constants  $C_n = A_n + iB_n$ , say, are real (i.e.  $B_n = 0$ ) and the parametric equation of the interface is

$$X = \frac{L\xi}{2\pi} + \frac{L}{2\pi} \sum_1^{\infty} \frac{A_n}{n} \sin n\xi \quad (1.1.13)$$

$$Y = \frac{L}{2\pi} \sum \frac{A_n}{n} (\cos n\xi - 1), \quad (1.1.14)$$

where

$$\xi = 2\pi \phi / cL, \quad (1.1.15)$$

and the origin is taken at  $\xi = 0$ . Since  $q/c = (X'^2 + Y'^2)^{-1/2}$  and  $R^{-1} = (X'Y'' - X''Y') / (X'^2 + Y'^2)^{3/2}$ , where  $' = d/d\xi$ , equation (1.1.10) gives

$$\begin{aligned}
 & gL \sum_1^{\infty} \frac{A_n}{n} (\cos n\xi - 1) - \pi c^2(1-b) + \pi c^2 \left[ \left( 1 + \sum_1^{\infty} A_n \cos n\xi \right)^2 + \left( \sum_1^{\infty} A_n \sin n\xi \right)^2 \right]^{-1} \\
 & + \frac{4\pi^2 T}{L} \left\{ \left( \sum_1^{\infty} A_n \sin n\xi \right) \left( \sum_1^{\infty} n A_n \sin n\xi \right) + \left( 1 + \sum_1^{\infty} A_n \cos n\xi \right) \left( \sum_1^{\infty} n A_n \cos n\xi \right) \right\} \\
 & \times \left\{ \left( 1 + \sum_1^{\infty} A_n \cos n\xi \right)^2 + \left( \sum_1^{\infty} A_n \sin n\xi \right)^2 \right\}^{-3/2} = 0. \tag{1.1.16}
 \end{aligned}$$

Because of the assumed symmetry,  $\xi = \pi$  is also a crest or trough and it is sufficient to satisfy (1.1.16) for  $0 \leq \xi \leq \pi$ . This equation was given by Wilton (31), with a slightly different notation.

The unknowns in (1.1.16) are the  $A_n$ ,  $n = 1, 2, \dots$ , the wave speed  $c$ , and the parameter  $b$ . The period  $L$  is supposed known. Therefore a further condition is necessary to specify the solution. This is usually taken to be the wave-height  $h$ , say, i.e. vertical distance between crest and trough, or perhaps the energy of the wave measured relative to a fixed frame, or the leading coefficient  $A_1$ . We found from experience that none of these parameters were universally useful for describing the bifurcation phenomenon to be described in this work, and in fact we have been unable to construct a parameter which characterized the magnitude of the wave for all the phenomena in a satisfactory way. For the computations we used the following method of characterizing the wave magnitude in terms of an amplitude parameter  $\epsilon$ . The sequence  $\lambda_1, \lambda_2, \lambda_3, \dots$  is chosen so that

$\sum_1^{\infty} |\lambda_n| = 1$ . Then we take

$$\sum_1^{\infty} \lambda_n A_n = \varepsilon \quad (1.1.17)$$

Different classes of waves correspond to various choices of the sequence  $\lambda_n$ . The parameter  $\varepsilon$  may be positive or negative. This approach is not particularly elegant and lacks a clear physical interpretation, but it is the most convenient one we have found so far. The basic difficulty is the lack of a parameter which is a monotonic function of a physically significant wave magnitude. An alternative approach is to specify  $b$  as the amplitude parameter.

Our task will be to study the solutions of (1.1.16).

## 1.2 The vortex sheet formulation.

There are several alternative schemes which reduce the calculation of the wave profile to the solution of non-linear integro-differential equations. See, for example, Nekrasov (20), Milne-Thompson (18) and Bloor (2). We have found convenient a method of this type based on the fact that the surface of a water wave is a vortex sheet.

We work in the coordinate system fixed in the wave, see figure 1. Since the inertia of the air is neglected, we can without loss of generality suppose the velocity of

the air (or upper fluid) is identically zero. Then the surface of the wave is a vortex sheet of strength  $q(s)$ , where  $s$  is arclength along the surface and  $q$  is the tangential velocity of the fluid. The surface has the parametric representation  $Z(s) = X(s) + iY(s)$ . Let  $u - i v$  denote the components of velocity in the fluid. Then from the Biot-Savart law, the velocity at  $z = x + iy$  is given by

$$u - i v = -\frac{i}{2\pi} \int_{-\infty}^{\infty} \frac{q(s_1)}{z - Z(s_1)} ds_1 + \frac{1}{2} c. \quad (1.2.1)$$

The reason for the  $\frac{1}{2}c$  is that the Biot-Savart law gives the velocity only to the extent of an arbitrary constant. The velocity induced by the vortex sheet has equal and opposite limits as  $y \rightarrow \pm\infty$ . Hence, to make the velocity as  $y \rightarrow \infty$  equal to zero and the velocity as  $y \rightarrow -\infty$  equal to  $c$ , the additive constant must be  $\frac{1}{2}c$ .

Plemelj's formula states that

$$\lim_{z \rightarrow Z(s)} \int \frac{f(s_1)}{z - Z(s_1)} ds_1 = P \int \frac{f(s_1)}{Z(s) - Z(s_1)} ds_1 \mp i\pi \frac{f(s)}{Z'(s)} \quad (1.2.2)$$

The minus sign is for  $z$  approaching the surface from above, and the plus sign from below.  $P$  denotes the Cauchy principal value.

From (1.2.1) and (1.2.2), we have

$$u(s) - i v(s) = q(s) e^{-i\theta(s)} = -\frac{i}{2\pi} P \int_{-\infty}^{\infty} \frac{q(s_1)}{Z(s) - Z(s_1)} ds_1 + \frac{q(s)}{2} \frac{1}{\frac{dZ(s)}{ds}} + \frac{c}{2} \quad (1.2.3)$$

where  $\theta(s)$  is the slope of the surface measured from the  $x$  axis. Also

$$\frac{dZ}{ds} = e^{i\theta}, \quad \frac{d\bar{Z}}{ds} = e^{-i\theta}, \quad (1.2.4)$$

where the overbar denotes the complex conjugate. Thus

$$\frac{1}{2} q(s) \frac{d\bar{Z}}{ds} = -\frac{i}{2\pi} P \int_{-\infty}^{\infty} \frac{q(s_1)}{Z(s) - Z(s_1)} ds_1 + \frac{1}{2} c. \quad (1.2.5)$$

Bernoulli's equation (1.1.10) gives

$$q(s) = \left( c^2(1-b) - 2gY(s) + \frac{2T}{R(s)} \right)^{\frac{1}{2}}. \quad (1.2.6)$$

Equation (1.2.5) is then a non-linear, singular, integro-differential equation for  $Z(s)$ . It can be simplified by a change of variable. Introduce  $\phi$  or  $\xi$  as independent variables instead of  $s$ . Then

$$\phi(s) = \int_0^s q(s_1) ds_1, \quad \xi = \frac{2\pi\phi}{cL} \quad (1.2.7)$$

and

$$\frac{1}{2} q^2 \frac{d\bar{Z}}{d\phi} = -\frac{i}{2\pi} P \int_{-\infty}^{\infty} \frac{d\phi_1}{Z(\phi) - Z(\phi_1)} + \frac{1}{2} c; \quad (1.2.8)$$

or since the problem is periodic of period  $L$  for  $Z$  and  $cL$  for  $\phi$ , using that

$$P \int_{-\infty}^{\infty} \frac{d\phi_1}{Z(\phi) - Z(\phi_1)} = \sum_{n=-\infty}^{\infty} P \int_0^{cL} \frac{d\phi_1}{Z(\phi) - Z(\phi_1) - nL} = \frac{\pi}{L} P \int_0^{cL} \cot \left[ \frac{\pi}{L} (Z(\phi) - Z(\phi_1)) \right] d\phi_1, \quad (1.2.9)$$

and writing

$$Z = \frac{L}{2\pi} \zeta, \quad (1.2.10)$$

we have

$$\left(1 - b - \frac{gL}{\pi c^2} \operatorname{Im} \zeta + \frac{2T}{c^2 R}\right) \frac{d\bar{\zeta}}{d\xi} - 1 + \frac{i}{2\pi} P \int_0^{2\pi} \cot \left[ \frac{\zeta(\xi) - \zeta(\xi_1)}{2} \right] d\xi_1 = 0, \quad (1.2.11)$$

where

$$\frac{1}{R} = \frac{2\pi}{L} \operatorname{Im} \left( \frac{d^2 \zeta}{d\xi^2} \frac{d\bar{\zeta}}{d\xi} / \left| \frac{d\zeta}{d\xi} \right|^3 \right). \quad (1.2.12)$$

To equation (1.2.11) must be added some condition that specifies the magnitude of the wave. The simplest procedure conceptually is to specify

$$h = \max(Y) - \min(Y). \quad (1.2.13)$$

Equation (1.2.11) then has solutions of period  $2\pi$  in  $\xi$ ,

$$\frac{L}{2\pi} \zeta = z = x + iy, \quad x = \tilde{x}(\xi; h/L), \quad y = \tilde{y}(\xi; h/L), \quad c = \tilde{c}(h/L), \quad b = \tilde{b}(h/L), \quad (1.2.14)$$

provided  $h/L$  is sufficiently small. These solutions are, however, not isolated for

$$x = \tilde{x}(\xi + \alpha; h/L) + x_0, \quad y = \tilde{y}(\xi + \alpha; h/L) + y_0, \quad c = \pm \tilde{c}(h/L),$$

$$b = \tilde{b}(h/L) - gL y_0 / \pi c^2, \quad (1.2.15)$$

is obviously also a solution of (1.2.11) and (1.2.13) for arbitrary values of  $\alpha$ ,  $x_0$  and  $y_0$ . Equation (1.2.15) describes the same wave displaced horizontally and vertically, moving in the same or opposite direction, with the origin of arclength displaced along the surface. We can remove the degeneracy by putting the origin of coordinates and arclength at a crest or trough, i.e. we can require

$$x(0) = 0, \quad y(0) = 0, \quad \frac{\partial y}{\partial \xi}(0) = 0. \quad (1.2.16)$$

The three equations (1.2.16) then suffice in principle to determine the three arbitrary constants in the general solution (1.2.15). Implementation of (1.2.16) can be made automatic when the solution is assumed to be symmetric. However, for  $T=0$  we also prepared a numerical method which does not assume that the wave is necessarily symmetric. The purpose was twofold; first to provide a check on calculations assuming symmetry, and second to try and find nonsymmetrical solutions. Implementation of (1.2.16) then proved difficult until overcome by a trick; see equation (3.2.13) of chapter 3.

Equations (1.2.11) and (1.2.16) together with (1.2.13) or an equivalent measure of wave magnitude, provide us in principle with a complete set of equations to determine water waves of finite amplitude. This approach is very useful in calculating high amplitude gravity waves.

### 1.3 Some integral properties.

Integral properties of interest are the kinetic and potential energies per unit length. The kinetic energy  $K$  is measured in a frame fixed relative to the fluid. Defining  $W = \Phi + i\Psi = w - cz$ , we have

$$K = \frac{1}{2L} \int_{-\infty}^Y \int_0^L \left| \frac{dW}{dz} \right|^2 dx dy = \frac{1}{2L} \iint d\Phi d\Psi = \frac{1}{2L} \oint \Psi d\Phi . \quad (1.3.1)$$

The physical and potential planes are sketched in figure 1. The last equality of (1.3.1) is Stokes' theorem. The integration along the boundary is in the clockwise direction. Using the periodicity of the solution, and that the fluid is at rest at  $y = -\infty$ , the only contribution to the line integral is from the boundary OAB where

$$\Psi = -cY, \quad \Phi = \phi - cX .$$

It follows that

$$K = -\frac{c}{2L} \left\{ \int Y d\phi - c \int Y dx \right\} = -\frac{c^2}{2} \left\{ \frac{1}{2\pi} \int_0^{2\pi} Y d\xi - \bar{Y} \right\} . \quad (1.3.2)$$

Here  $\bar{Y}$  is the mean height defined as

$$\bar{Y} = \frac{1}{L} \int_0^L Y dx = \frac{1}{L} \int_0^{2\pi} Y \frac{dx}{d\xi} d\xi . \quad (1.3.3)$$

Substituting (1.1.13) and (1.1.14) into (1.3.3) and integrating we have

$$\bar{Y} = \frac{L}{4\pi} \left( \sum_1^{\infty} \frac{A_n^2}{n} - 2 \sum_1^{\infty} \frac{A_n}{n} \right) . \quad (1.3.4)$$

Now, using (1.1.14) and (1.3.4), the kinetic energy is

$$K = \frac{c^2 L}{8\pi} \sum_1^{\infty} \frac{A_n^2}{n} . \quad (1.3.5)$$

The potential energy has two contributions,  $V_g$  due to gravity and  $V_\tau$  due to surface tension. The gravitational potential energy is measured relative to the mean height  $\bar{Y}$ ,

$$V_g = \frac{1}{L} \int_0^L \int_{\bar{Y}}^Y g y dy dx = \frac{g}{2L} \int_0^{2\pi} (Y^2 - \bar{Y}^2) \frac{dX}{d\xi} d\xi, \quad (1.3.6)$$

and upon substitution of the parametric equations for X and Y,

$$V_g = \frac{gL^2}{16\pi^2} \left[ \sum_1^{\infty} \frac{A_n^2}{n^2} + \frac{1}{\pi} \int_0^{2\pi} \left( \sum_1^{\infty} \frac{A_n}{n} \cos n\xi \right) \left( \sum_1^{\infty} A_n \cos n\xi \right) d\xi - \frac{1}{2} \left( \sum_1^{\infty} \frac{A_n^2}{n} \right)^2 \right], \quad (1.3.7)$$

or calculating the integral,

$$V_g = \frac{gL^2}{16\pi^2} \left[ \sum_1^{\infty} \frac{A_n^2}{n^2} + \frac{1}{2} \sum_1^{\infty} \frac{A_n^2}{n^2} A_{2n} + \sum_{m>n}^{\infty} \sum_{n=1}^{\infty} \frac{A_n}{n} \frac{A_m}{m} (A_{n+m} + A_{m-n}) \right]. \quad (1.3.8)$$

The surface tension contribution is

$$V_T = \frac{\Gamma}{L} \int_0^L (ds - dx) = \frac{\Gamma}{L} \int_0^{2\pi} \left\{ \left[ \left( \frac{dX}{d\xi} \right)^2 + \left( \frac{dY}{d\xi} \right)^2 \right]^{\frac{1}{2}} - \frac{dX}{d\xi} \right\} d\xi, \quad (1.3.9)$$

or using (1.1.13) and (1.1.14)

$$V_T = \frac{\Gamma}{2\pi} \int_0^{2\pi} \left\{ \left[ \left( 1 + \sum_1^{\infty} A_n \cos n\xi \right)^2 + \left( \sum_1^{\infty} A_n \sin n\xi \right)^2 \right]^{\frac{1}{2}} - 1 \right\} d\xi. \quad (1.3.10)$$

Other important physical quantities are the momentum per unit length

$$I = \frac{1}{L} \int_0^L \int_{-\infty}^Y \Phi_x dy dx, \quad (1.3.11)$$

the excess flux of momentum due to the wave

$$S = \lim_{D \rightarrow \infty} \left\{ \frac{1}{L} \int_0^L \int_{-D}^Y (p + \Phi_x^2) dy dx - \int_{-D}^{\bar{Y}} p_0 dy \right\}, \quad (1.3.12)$$

where  $p_0 = -g(y - \bar{Y})$  is the hydrostatic pressure in the absence of waves, and the energy flux per unit length F

defined by

$$F = \frac{1}{L} \int_0^L \int_{-\infty}^Y \left[ \rho + \frac{1}{2} \left| \frac{dW}{dz} \right|^2 + g(y - \bar{Y}) \right] \Phi_x dy dx . \quad (1.3.13)$$

Levi-Civita (11), Starr (25), Starr and Platzman (26) and Longuet-Higgins (13) established the following relations

$$I = -\frac{2K}{c} \quad (1.3.14)$$

$$S = 4K - 3V_g \quad (1.3.15)$$

$$F = (3T - 2V_g)c . \quad (1.3.16)$$

Of these three relations, only the first one is valid for  $T \neq 0$ .

Provided  $g \neq 0$ , the following relation gives a useful check on the accuracy of the calculations

$$2g\bar{Y} = -bc^2 . \quad (1.3.17)$$

We will prove it following Lamb (10, p. 420) and Starr (25) in appendix A.

If the amplitude is allowed to vary, the following differential relation governs the rates of change of  $K$ ,  $V_g$  and  $c$

$$\frac{\partial}{\partial b} (K + V_g) = -c \frac{\partial I}{\partial b} . \quad (1.3.18)$$

(1.3.18) is valid only for gravity waves. It is also a useful check on the numerical results. The proof of (1.3.18)

follows Longuet-Higgins (13) and is given in appendix B.

#### 1.4 Simple Bifurcation.

We can write (1.1.16) or (1.2.11) and (1.2.16), together with some amplitude equation such as (1.1.17) or (1.2.13), abstractly as

$$G(u; \epsilon, \tau) = 0, \quad (1.4.1)$$

where the element  $u$  is the solution (the Fourier coefficients  $A_n, n=1,2,\dots$ , or the wave profile for  $0 \leq \xi \leq 2\pi$ , the wavespeed  $c$  and the parameter  $b$ ),  $\epsilon$  is the parameter which determines the magnitude of the wave and  $\tau$  is the surface tension. Since we are only going to consider branches of solutions of (1.4.1) that have one of the two parameters  $\epsilon$  or  $\tau$  constant, the notation can be simplified by writing (1.4.1) as

$$G(u; p) = 0, \quad (1.4.2)$$

where  $p$  now represents the parameter that is allowed to vary.

In practice,  $G$  and  $u$  will be finite dimensional vectors arising from the discretization of the governing equations. To follow solution branches of (1.4.2), determine the existence of limit or bifurcation points, and switch

branches at the latter, we follow Keller (8) and introduce the arclength  $s$  in  $(u, p)$  space. Instead of finding solutions of (1.4.2) in the form  $u = u(p)$  with the parameter  $p$  given, we calculate  $u = u(s)$ ,  $p = p(s)$ . An additional equation of the form

$$N(u, p; s) \equiv \frac{1}{2} \left\| \frac{du}{ds} \right\|^2 + \frac{1}{2} \left( \frac{dp}{ds} \right)^2 - 1 = 0 \quad (1.4.3)$$

is needed to determine  $p$  as a function of  $s$ . A point  $(u(s_0), p(s_0))$  on the branch is a regular point if the Fréchet derivative  $G_u(u(s_0), p(s_0))$  is non-singular. Otherwise we have a critical point. In general, a critical point is either a limit or a bifurcation point, but it can be both. At a limit point, the value of  $p$  has a maximum or a minimum and  $u$  is not a single valued function of  $p$  in the vicinity of the point. Since the arclength  $s$  is always monotonic on a branch, limit points disappear when  $s$  is the parameter. At a bifurcation point two or more solution branches intersect.

The following relations hold if  $s = s_0$  is a simple bifurcation point where two smooth solutions intersect non-tangentially:

$$\left. \begin{aligned} \dim N(G_u^0) = \text{codim } R(G_u^0) = 1 \\ G_p^0 \in R(G_u^0) \end{aligned} \right\} \quad (1.4.4)$$

where  $G_u^0 \equiv G_u(u(s_0), p(s_0))$ ,  $G_p^0 \equiv G_p(u(s_0), p(s_0))$ , and  $N$  denotes the null space and  $R$  the range. Denote by  $\phi_i$  and  $\psi_i^*$  the

unit norm elements which span  $\mathcal{N}(G_u^\circ)$  and the adjoint space  $\mathcal{N}(G_u^{\circ*})$  respectively. (1.4.4) implies the existence of a unique element  $\phi_0$  such that

$$G_u^\circ \phi_0 = -G_p^\circ, \quad \Psi_1^* \phi_0 = 0. \quad (1.4.5)$$

It follows from the definition of  $\Psi_1^*$  and (1.4.5) that

$$\Psi_1^* G_p^\circ = 0; \quad (1.4.6)$$

this equation provides a way to check for bifurcation and distinguish it from limit point behavior.

To find the branches at a simple bifurcation point we first differentiate (1.4.2) twice with respect to  $s$ , evaluate at  $s_0$ , and multiply the second derivative on the left by  $\Psi_1^*$ , giving for each branch ( $u_s^\circ \equiv u_s(s_0)$ ,  $p_s^\circ \equiv p_s(s_0)$ ):

$$G_u^\circ u_s^\circ + G_p^\circ p_s^\circ = 0 \quad (1.4.7)$$

$$\begin{aligned} \Psi_1^* \{ & G_{uu}^\circ (u_s^\circ)^2 + 2 G_{up}^\circ u_s^\circ p_s^\circ + G_{pp}^\circ (p_s^\circ)^2 \} \\ & = -\Psi_1^* \{ G_u^\circ u_{ss}^\circ + G_p^\circ p_{ss}^\circ \} \end{aligned} \quad (1.4.8)$$

The right hand side of (1.4.8) is zero because  $G_p^\circ$  is in the range of  $G_u^\circ$  and  $\Psi_1^*$  is orthogonal to the range of  $G_u^\circ$ . Since the null space of  $G_u^\circ$  is one dimensional, we have from (1.4.7)

$$u_s^\circ = \alpha_0 \phi_0 + \alpha_1 \phi_1, \quad (1.4.9)$$

with

$$\alpha_0 = p_s^0, \quad \alpha_1 = \psi_1^* u_s^0. \quad (1.4.10)$$

Substituting (1.4.9) into (1.4.8) gives the quadratic equation

$$A\alpha_1^2 + B\alpha_1\alpha_0 + C\alpha_0^2 = 0 \quad (1.4.11)$$

with

$$A \equiv \psi_1^* G_{uu}^0 \phi_1 \phi_1 \quad (1.4.12)$$

$$B \equiv \psi_1^* \{ G_{uu}^0 (\phi_0 \phi_1 + \phi_1 \phi_0) + 2G_{up}^0 \phi_1 \} \quad (1.4.13)$$

$$C \equiv \psi_1^* \{ G_{uu}^0 \phi_0 \phi_0 + 2G_{up}^0 \phi_0 + G_{pp}^0 \} \quad (1.4.14)$$

Solution of the quadratic, the so called algebraic bifurcation equation, gives the branches intersecting at the bifurcation point and makes it possible to switch from one branch to the other. Note that prior knowledge of one branch gives one root of the quadratic. For further details and a general treatment see Keller (8). In chapter 3 we describe the actual procedure by which solution branches were followed and simple bifurcation points found. As we shall see later, it is likely that more complex behavior may be associated with high order bifurcation, but the techniques for analysing such bifurcations have not reached the same level of development as those for simple

bifurcation.

CHAPTER 2

WEAKLY NON-LINEAR WAVES

The object of this chapter is to study the solutions of (1.1.16) and determine the slope of symmetrical waves of permanent form. We shall examine analytically the properties of solutions of small but not infinitesimal magnitude as described by formal perturbation series. In later chapters we obtain approximate solutions for finite amplitude using numerical methods.

2.1 Pure and combination waves.

If we suppose that the magnitude of the wave is small, we may expand equation (1.1.16) in powers of the  $A_n$ . We obtain after some algebra an expression

$$\begin{aligned}
 & \frac{1}{2} \mu b - \sum_1^{\infty} \frac{A_n}{n} + \frac{\mu}{2} \sum_1^{\infty} A_n^2 - \frac{\kappa}{2} \sum_1^{\infty} n A_n^2 + \sum_1^{\infty} \alpha_p A_p \cos p\xi \\
 & + \sum_1^{\infty} \sum_{p \neq q}^{\infty} [\alpha_{p,q} \cos(p-q)\xi + \beta_{p,q} \cos(p+q)\xi] A_p A_q + \sum_1^{\infty} [\alpha_{pp} + \beta_{pp} \cos 2p\xi] A_p^2 \\
 & + \sum_1^{\infty} [\alpha_{ppp} \cos p\xi + \beta_{ppp} \cos 3p\xi] A_p^3 + \sum_1^{\infty} \sum_{q \neq p}^{\infty} [\alpha_{qpp} \cos q\xi + \beta_{qpp} \cos(2p-q)\xi \\
 & + \beta'_{qpp} \cos(2p+q)\xi] A_q A_p^2 + \dots = 0, \tag{2.1.1}
 \end{aligned}$$

where the omitted terms are quartic and higher order, and

$$\left. \begin{aligned}
 \alpha_p &= \frac{1}{p} - \mu + \kappa p, & \alpha_{p,q} &= \frac{1}{2}\mu - \frac{1}{4}\kappa(p+q), \\
 \alpha_{pp} &= \frac{1}{2}\mu - \frac{1}{2}\kappa p, & \beta_{p,q} &= \mu - \frac{3}{4}\kappa(p+q), \\
 \beta_{pp} &= \mu - \frac{3}{2}\kappa p, & \alpha_{ppp} &= -\mu + \frac{9}{8}\kappa p, \\
 \beta_{ppp} &= -\mu + \frac{15}{8}\kappa p, & \alpha_{qpp} &= -2\mu + \frac{3}{4}\kappa(2p+q), \\
 \beta'_{qpp} &= -\mu + \frac{3}{8}\kappa(2p+q), & \beta'_{qpp} &= -3\mu + \frac{15}{8}\kappa(2p+q).
 \end{aligned} \right\} \quad (2.1.2)$$

In these equations the dimensionless parameter

$$\mu = 4\pi^2 T / gL^2 \quad (2.1.3)$$

measures the relative importance of surface tension and gravity, while

$$\mu = 2\pi c^2 / gL \quad (2.1.4)$$

is a dimensionless form of the unknown wavespeed.

We characterize the wave magnitude in terms of an amplitude parameter  $\epsilon$  by taking

$$\sum_1^{\infty} \lambda_n A_n = \epsilon, \quad (2.1.5)$$

where the sequence  $\lambda_1, \lambda_2, \lambda_3, \dots$  is chosen depending on the type of wave we want to study. If we now, following Wilton (31), equate the coefficients of  $\cos n\zeta$  in (2.1.1) to zero for  $n=0, 1, 2, \dots$ , we obtain an infinite number of algebraic equations of infinite degree. The counting seems to be

correct, in the sense that truncation at order  $M$  by setting  $A_n = 0$  for  $n > M$  and ignoring coefficients of  $\cos n\xi$  for  $n > M$  gives, together with (2.1.5),  $M+2$  equations for the  $M+2$  unknowns  $A_1, A_2, \dots, A_M, \mu, b$ . The problem seems, therefore, to be well posed, although convergence proofs are lacking.

Let us suppose now that all the  $\lambda_n$  are zero except  $\lambda_N$ , say. Then  $A_N = \xi$ , and if  $|\xi| \ll 1$ , we can expect a solution to exist in which the  $A_n$  are powers of  $\xi$ . In particular, the solution will have  $A_n = 0$  unless  $n$  is a multiple of  $N$ , and further

$$A_n = \theta(\xi^{n/N}), \quad (2.1.6)$$

when  $N$  divides  $n$ . We shall call a solution of this kind a pure wave of degree  $N$  and magnitude  $\xi$ . Pure waves of degree 1 were calculated by Wilton up to order  $\xi^5$ , using the ansatz expressed by (2.1.6). A pure wave of degree  $N$ , amplitude  $\xi$  and  $\kappa = \kappa'$ , say, consists, of course, of pure waves of degree 1, wavelength  $\lambda/N$ , and the same magnitude with  $\kappa = N^2 \kappa'$ . It might therefore be thought that there would be no loss of generality in following Wilton and restricting attention to pure waves of degree 1, but this actually turns out not to be the case.

Since  $A_N$  is the dominant coefficient in a pure wave of degree  $N$ , we expect that the coefficient of  $A_N$  in (2.1.1) must be small and hence

$$\frac{1}{N} - \mu + \kappa N \doteq 0, \text{ i.e. } \mu \doteq \mu_N \equiv \frac{1}{N} + \kappa N. \quad (2.1.7)$$

Only the harmonics of  $\cos N\xi$  are generated and their coefficients are uniquely determined by the equations derivable from (2.1.1), provided the coefficients

$$\alpha_p(N) \equiv \frac{1}{p} - \mu_N + \kappa p \neq 0 \quad (2.1.8)$$

for  $p$  a multiple of  $N$ . Elementary algebra shows that (2.1.8) is violated for  $p = rN$  (i.e.  $\alpha_p(N) = 0$ ) if  $\kappa = \frac{1}{rN^2}$ . When (2.1.8) fails, it is found that the ansatz (2.1.6) is inconsistent and the expansion fails.

Wilton examined in detail the case  $N=1$ ,  $r=2$ ,  $\kappa = \frac{1}{2}$ . He showed that in this case the ansatz (2.1.6) should be replaced by the assumption that both  $A_1$  and  $A_2$  are of order  $\xi$ . It is then found that in the infinitesimal limit

$$A_2 = \pm A_1, \quad (2.1.9)$$

so that the wave of given magnitude (however this is defined) is not unique, but the higher order coefficients are determined uniquely once the sign in (2.1.9) is specified. The two waves with the same  $A_1$  are quite distinct, and cannot be made to coincide by a change of phase. These waves are called Wilton's ripples. The lack of uniqueness or ambiguity can be explained physically by a resonance mechanism due to the fact that infinitesimal waves of

wavelength  $L$  and  $\frac{1}{2}L$  have the same phase speed when  $\kappa = \frac{1}{2}$ .

Wilton noted that the ansatz might also fail when  $\kappa = \frac{1}{r}$ , but stated that only for  $r=2$  was there any ambiguity in the value of  $A_r$  for  $\kappa = \frac{1}{r}$ . This statement is literally correct for  $r > 3$ , but as we shall see in the course of this work there can be ambiguity for  $\kappa$  slightly greater than  $\frac{1}{r}$ . It is false for  $r=3$ . A difference between  $r=2$  and the other cases is that only in the former case is the important interaction quadratic. For  $r \geq 3$ , the interaction is cubic.

We can generalize Wilton's approach by examining the possibility that, with  $\kappa$  given,  $\alpha_p$  vanishes for two or more values of  $p$ . From the definition of  $\alpha_p$ , it is easily seen that a necessary and sufficient condition is

$$\kappa = \frac{1}{MN}, \quad T = \frac{gL^2}{4\pi^2 MN}. \quad (2.1.10)$$

In this case,  $\alpha_N = \alpha_M = 0$ , if

$$\mu_N = \mu_M = \frac{1}{M} + \frac{1}{N}. \quad (2.1.11)$$

Even though  $\frac{1}{\kappa}$  may be an integer with many decompositions into a pair of factors, for only one decomposition at a time can  $\alpha_N$  and  $\alpha_M$  vanish. These considerations suggest the existence of combination waves, in which for an arbitrary pair of integers  $N$  and  $M$ , the coefficients  $A_N$  and  $A_M$  are of comparable order  $\epsilon$  and all the other  $A_n$  are of higher order in  $\epsilon$ . The consistency of the perturbation

expansion should fix the ratio of  $A_N$  to  $A_M$ , as for the Wilton ripple which is the particular case  $N=1$ ,  $M=2$ . We shall see below that combination waves exist for all sets of positive integers  $M$  and  $N$  for appropriate value of  $\kappa$ . The Wilton ripples are the simplest but not particularly typical example.

Clearly without loss of generality, we can now suppose that  $M$  and  $N$  are coprime, and we take for definiteness  $1 \leq N < M$ . We will call such a wave a combination  $(N,M)$  wave. Multiplication of  $N$  and  $M$  by an integer corresponds to dividing  $\kappa$  by the square of the same integer.

The concept of pure and combination waves can be extended to finite amplitude although not without some ambiguity. The wave will be said to be pure if the coefficient of the lowest order harmonic clearly determines the wave in a unique manner. Thus, Crapper's exact capillary waves, for which in our notation

$$A_n = 4n(A_1/4)^n, \quad n=2,3,4,\dots, \quad (2.1.12)$$

are pure waves of degree 1. Similarly, Stokes gravity waves of permanent form found by expansion in  $A_1$ , where  $A_2 = A_1^2 + O(A_1^4)$  etc, are pure waves. If, on the other hand, the lowest order harmonic is relatively insignificant or does not specify the wave uniquely in a clear way, we shall speak of a combination wave. A precise classification for finite amplitude waves does not seem possible, because

as we shall see a combination wave for some value of  $\kappa$  may be the analytic continuation of a pure wave for a different  $\kappa$ .

The existence of combination waves of small magnitude will now be considered. First we deal with the case  $M=2N$ .

## 2.2 Wilton ripples.

Combination waves with  $N=1$ ,  $M=2$  are typical of the case  $M=2N$ . We suppose that  $A_1$  and  $A_2$  are both  $\mathcal{O}(\epsilon)$  and that the remaining  $A_n$  are of smaller order. The consistency of the ordering is easily checked a posteriori. Then the coefficients of  $\cos \xi$  and  $\cos 2\xi$  in (2.1.1) give the equations

$$(1-\mu+\kappa)A_1 + (\mu - \frac{3}{2}\kappa)A_1A_2 = \mathcal{O}(\epsilon^3), \quad (2.2.1)$$

$$(\frac{1}{2} - \mu + 2\kappa)A_2 + (\mu - \frac{3}{2}\kappa)A_1^2 = \mathcal{O}(\epsilon^3). \quad (2.2.2)$$

These equations, together with a form of the amplitude equation (2.1.5)

$$A_1 + A_2 = 2\epsilon, \quad (2.2.3)$$

constitute three equations for the three unknowns  $A_1$ ,  $A_2$ ,  $\mu$  in terms of the given parameters  $\kappa$  and  $\epsilon$ .

We note first that for all values of  $\kappa$  there is a

solution with

$$A_1 = 0, \quad A_2 = 2\varepsilon, \quad \mu = \frac{1}{2} + 2\kappa + O(\varepsilon^2). \quad (2.2.4)$$

In this wave,  $A_{2n+1} = 0$ ,  $A_{2n} = O(\varepsilon^n)$ , and it is a pure wave of degree 2. There is nothing special about  $\kappa = \frac{1}{2}$  for this wave. (There may of course be ambiguity around  $\kappa = 1/(2p)$ ,  $p > 1$ .)

We wish to consider now the solutions for which  $A_1 \neq 0$ . For  $\kappa$  not close to  $\frac{1}{2}$ , there is a solution with

$$A_1 = 2\varepsilon + O(\varepsilon^2), \quad \mu = 1 + \kappa + O(\varepsilon^2), \quad A_2 = \frac{8-4\kappa}{1-2\kappa} \varepsilon^2 + O(\varepsilon^3), \quad (2.2.5)$$

which is recognisable as a pure wave of degree 1. (The difficulties that might arise when  $\kappa \approx 1/n$ ,  $n > 2$ , are the subjects of the following sections.) But this solution is not uniformly valid as  $\kappa$  approaches  $\frac{1}{2}$ . To obtain a uniformly valid solution, we solve (2.2.1) for  $\mu$  and substitute into (2.2.2), neglecting the  $O(\varepsilon^3)$  terms on the right hand sides. This gives

$$\mu = \frac{1 + \kappa - \frac{3}{2} \kappa A_2}{1 - A_2}, \quad (2.2.6)$$

$$A_1^2 = \frac{(1-2\kappa)A_2 + (1+\kappa)A_2^2}{2-\kappa}. \quad (2.2.7)$$

The dependence on  $\varepsilon$  can be found by substituting into (2.2.3), but it is better to work with (2.2.7) which contains the whole phenomenon of Wilton's ripples in a simple way.

First we note that if  $\kappa$  is not close to  $\frac{1}{2}$ , we recover the pure wave (2.2.5). If  $\kappa = \frac{1}{2}$ , we obtain Wilton's formula (2.1.9). Equation (2.2.7) in fact contains the uniformly valid relation between  $A_1$  and  $A_2$ . Once the relation between  $A_1$  and  $A_2$  is established to lowest order, the equations derivable from (1.1.16) or (2.1.1) allow in principle the unique calculation of the remaining  $A_n$  to arbitrary order.

There are now two alternative methods of procedure. The first is to interpret (2.2.7) as a quadratic giving  $A_2$  in terms of  $A_1$ . Thus

$$A_2 = \frac{-1+2\kappa \pm \sqrt{\{(1-2\kappa)^2 + 4(2-\kappa)(1+\kappa)A_1^2\}}}{2(1+\kappa)}. \quad (2.2.8)$$

This is the approach of Pierson and Fife (21), who studied the nature of Wilton ripples for  $\kappa$  close to  $\frac{1}{2}$  by a somewhat different method than that used here. It appears that one should take the positive square root for  $\kappa < \frac{1}{2}$  and the negative square root for  $\kappa > \frac{1}{2}$ , in order to join smoothly with the pure wave (2.2.5) for  $\kappa$  not close to  $\frac{1}{2}$ . However, this leaves uncertain the status of the other root.

The second and more informative approach is to interpret (2.2.7) as specifying  $A_1$  given  $A_2$ . Then we see that solutions exist only if  $A_2$  is such that the right hand side is positive. In figure 2.1, we have plotted the accessible regions of the  $A_2, \tilde{\kappa}$  plane as given by (2.2.7).

It is convenient to use  $\tilde{\kappa} = \kappa/(1+\kappa)$  in order to include the capillary waves in the figure. Notice that  $A_1$  vanishes when  $A_2 = 0$  and  $A_2 = 3\tilde{\kappa} - 1$ . Accessible regions are hatched. The analysis is for weakly non-linear waves, so we cannot say which regions are accessible when  $A_2$  is  $O(1)$ . From Crapper's calculations, we know that  $A_2 < 1.654$  for pure capillary waves of degree 1. (it is equal to 1.819 for the pure capillary wave of degree 2.) For the pure gravity wave of degree 1, Schwartz's (23) results suggest an upper limit of about 0.18 for  $A_2$  (or 0.29 for the limiting pure wave of degree 2). Note that these results also suggest that the highest wave does not have the greatest value of  $A_2$ , so that the  $A_2, \tilde{\kappa}$  plane will be covered more than once near the limiting wave.

The boundary of the region is unknown at present and needs numerical work for its determination. The results of such study will be reported in chapter 4. There is, of course, no reason to believe that the accessible region is singly covered, so the topology of the covering may be fairly complicated. The point  $\tilde{\kappa} = 2/3$ ,  $\kappa = 2$ , has the property that  $A_2$  vanishes at this value for the weakly non-linear pure wave of degree 1. It is an apparent singularity caused by the choice of plot and does not have a physical significance.

The point  $\kappa = \frac{1}{2}$ ,  $\tilde{\kappa} = \frac{1}{3}$  is a fundamental singularity. If  $A_2 \rightarrow 0$  in the vicinity of  $\kappa = \frac{1}{2}$ , it implies that

$A_1 \rightarrow 0$  and the wave disappears. Thus we conclude from this figure that an analytic transformation is not possible from gravity waves of finite amplitude to capillary waves of finite amplitude as the surface tension increases continuously with the wave always having a non-zero magnitude. The significance of the Wilton ripples is now clear. In the vicinity of  $\kappa = \frac{1}{2}$ , there are two weakly nonlinear solutions, one for a gravity-side wave ( $A_2 > 0$ ) and the other for the capillary-side wave ( $A_2 < 0$ ). It can be shown that the wave with  $A_2 < 0$  can be continued analytically to a capillary wave of degree 1. The gravity-side waves can apparently not be continued analytically to gravity waves (at least with small amplitude) for reasons to be given later (section 2.7). Note that although according to (2.2.7) there are two combination waves for each  $A_2$ , depending on the sign of  $A_1$ , these waves are not in fact distinct, since a change of sign of  $A_1$ , leaving  $A_2$  constant, corresponds simply to a phase shift of  $\pi$  or moving the origin horizontally by  $L/2$ . The meaning of the two signs in (2.2.8) is also now apparent. The positive sign gives gravity-side waves, the negative sign gives capillary-side waves. The paradox, that  $A_2$  tends to a finite limit independent of  $A_1$  as  $\kappa - \frac{1}{2}$  increases when the positive sign is taken, is to be interpreted as saying that  $A_1 \rightarrow 3\tilde{\kappa} - 1$  and  $A_1 \rightarrow 0$ ; similarly as  $\kappa - \frac{1}{2}$  decreases when the negative sign is used. The Wilton ripples are the

particular solutions on the line  $\tilde{\kappa} = \frac{1}{3}$  ,  $\kappa = \frac{1}{2}$  , but there are clearly neighboring solutions for  $\kappa$  not exactly equal to  $\frac{1}{2}$ .

There is an interesting difference between capillary-side and gravity-side waves. For  $A_2 < 0$  , the crests of the combination waves are of equal height and unequal spacing, whereas the troughs are of unequal depth but uniform separation  $L/2$  . The waves are symmetrical about troughs but not about crests. The converse is true for the gravity-side waves. Thus the analytic continuation of a pure capillary wave of degree 1 into a Wilton ripple is associated with the creation of another trough, or going in the reverse direction with the disappearance of a trough. Conversely the appearance or disappearance of the gravity-side Wilton ripple as  $\kappa - \frac{1}{2}$  becomes small or large is associated with the creation or disappearance of a crest. Sample profiles showing these changes are shown in figure 2.2.

We now discuss an interpretation of Wilton's ripples as a bifurcation phenomenon in which the wavelength of a pure wave can suddenly double when it attains a certain amplitude.

2.3 Wilton ripples as a 2→1 bifurcation.

The regions marked 'no solution' in figure 2.1 show where no combination (1,2) wave exists. However, pure waves of degree 2 exist in these regions (provided the magnitude is less than some as yet unknown value). Thus if we describe waves by the relation between  $A_1$  and  $A_2$ , we see that there are solutions with  $A_1 = 0$  for arbitrary  $A_2$  (within the limits of existence of pure waves), and there are also solutions with non-zero  $A_1$  provided, according to (2.2.7),

$$A_2 > \frac{2\kappa-1}{1+\kappa} > 0 \quad \text{or} \quad A_2 < \frac{2\kappa-1}{1+\kappa} < 0, \quad (2.3.1)$$

for  $\kappa < 2$ . The result (2.3.1) is of course limited to  $|A_2| \ll 1$ , and is therefore valid only for  $\kappa$  close to  $\frac{1}{2}$ .

These results are shown graphically in figure 2.3, where we sketch  $A_1$  vs  $A_2$  for  $\kappa < \frac{1}{2}$  and  $\kappa > \frac{1}{2}$ , with  $|\kappa - \frac{1}{2}| \ll 1$ , as given by equation (2.2.7). For a given value of  $\kappa > \frac{1}{2}$ , there always exists a pure wave of degree 2, marked by the  $A_2$  axis. For  $A_2 < 0$ , there is also a combination wave which is a capillary-side wave. Thus  $A_2 = 0$  is a bifurcation point, but this is the trivial bifurcation of a flat surface into infinitesimal waves of arbitrary wavelength. For  $A_2 > 0$ , only the pure wave is possible until  $A_2$  reaches the critical value  $(2\kappa-1)/(1+\kappa)$ , at which value the pure wave of degree 2 can bifurcate into a

combination wave of twice the wavelength. The bifurcation wave has the shape shown in figure 2.2, the middle crest being slightly decreased ( $A_1 > 0$ ) or increased ( $A_1 < 0$ ), and is a gravity-side wave. Similarly for  $\kappa < \frac{1}{2}$ , there is a trivial bifurcation at  $A_2 = 0$  into a combination gravity-side wave, and a non-trivial bifurcation at  $A_2 = (2\kappa - 1)/(1 + \kappa)$  of the pure wave of degree 2 into a combination wave. For  $\kappa = \frac{1}{2}$ , the figure would reduce to the two straight lines  $A_1 = \pm A_2$ .

It is to be noted that although the solutions  $A_1$  and  $-A_1$  are mathematically distinct in the formulation, they are physically the same wave displaced a distance  $L/2$ . The difference between the pure wave of degree 2 with  $A_2$  and  $-A_2$  is a similar transformation. The reason why bifurcation occurs for  $A_1 > 0$  when  $\kappa > \frac{1}{2}$ , say, and not also for  $A_1 < 0$ , lies in the constraint that the wave is symmetrical about the origin. When  $A_2 > 0$ , the origin is a crest and the bifurcated waves for  $\kappa > \frac{1}{2}$  are symmetrical about crests. They are not symmetrical about troughs and therefore bifurcation with  $A_1 < 0$ , when the origin is a trough, is excluded for  $\kappa > \frac{1}{2}$ .

It is to be expected that the bifurcation phenomenon will be associated with a change in stability of the pure wave to small disturbances, the combination wave being perhaps stable while the pure wave loses its stability. The stability of the waves is an interesting question, but

although calculations of stability are straightforward they seem to be rather tedious and we shall defer the question for later study. The present work is restricted to an investigation of possible forms of steady waves.

Suppose now that we have a weakly non-linear pure wave of height  $h$  (vertical distance between crest and trough) and wavelength  $\lambda$ . This wave can be described as a pure wave of degree 2, with

$$L = 2\lambda, \quad A_2 = \pi h/\lambda, \quad \kappa = \pi^2 T/g\lambda^2. \quad (2.3.2)$$

Then if the amplitude of the wave is such that

$$h > \frac{4\lambda}{3\pi} \left| \frac{\pi^2 T}{g\lambda^2} - \frac{1}{2} \right|, \quad (2.3.3)$$

the wave can bifurcate into a combination wave of wavelength  $2\lambda$ . In other words, waves such that  $\pi^2 T/g\lambda^2$  is close to  $\frac{1}{2}$  could spontaneously double their wavelength when the amplitude exceeds the critical value given by (2.3.3).

The locus of bifurcation points given by (2.3.3) is only valid for small amplitude. The shape of the curve for finite amplitude can be investigated by numerical means, to be described in chapter 4. We now continue the analysis by studying  $(N, M)$  combination waves.

#### 2.4 Combination (N, M) waves.

The coefficients  $A_n$  of a permanent wave can be derived in principle from the equations obtained by setting the coefficients of  $\cos n\zeta$  to zero in the master equation (2.1.1). As mentioned earlier, pure waves of degree 1 can be constructed by solving recursively, and the series presumably converges if  $A_1$  is sufficiently small, provided  $\kappa \neq \frac{1}{M}$ . If  $\kappa = \frac{1}{M}$ ,  $\alpha_M \neq 0$  and the first approximation to  $A_M$  gives  $A_M \neq \infty$ . The previous sections studied this problem for the case  $M=2$ , and it was seen that the way to avoid the difficulty and obtain a uniformly valid solution was to suppose that  $A_1$  and  $A_2$  are both of order  $\epsilon$ .

We now study the existence of a combination (N, M) wave, with  $2N \neq M$ , for which

$$A_N = O(\epsilon), \quad A_M = O(\epsilon), \quad \kappa - \frac{1}{MN} = O(\epsilon^s) \quad (2.4.1)$$

and the other coefficients of higher order. The value of  $s$  is to be determined, and will be seen below that  $s=2$ . Without loss of generality, we suppose that  $N$  and  $M$  are coprime and  $1 \leq N < M$ . The case  $N=1, M=3$  has special features and is deferred to a later section.

With the assumption (2.4.1) and supposing that  $N < M$ ,  $N \neq \frac{1}{2}M$ ,  $N \neq \frac{1}{3}M$ , it follows from (2.1.1) that

$$A_{2N} = O(\epsilon^2), \quad A_{2M} = O(\epsilon^2), \quad A_{N+M} = O(\epsilon^2), \quad A_{M+N} = O(\epsilon^2), \quad (2.4.2)$$

and all remaining coefficients are of higher order. Equating in (2.1.1) the coefficients of  $\cos N\xi$ ,  $\cos M\xi$ ,  $\cos 2N\xi$ ,  $\cos 2M\xi$ ,  $\cos(N+M)\xi$  and  $\cos(M-N)\xi$  to zero, and neglecting terms smaller than  $O(\varepsilon^3)$ , we obtain

$$\alpha_N A_N + \alpha_{NNN} A_N^3 + 2\alpha_{N,2N} A_N A_{2N} + 2\alpha_{M,M-N} A_M A_{M-N} + 2\alpha_{M,M+N} A_M A_{M+N} + \alpha_{NMM} A_N A_M^2 = 0, \quad (2.4.3)$$

$$\alpha_M A_M + \alpha_{MMM} A_M^3 + 2\alpha_{M,2M} A_M A_{2M} + 2\alpha_{N,M+N} A_N A_{M+N} + 2\beta_{N,M-N} A_N A_{M-N} + \alpha_{MNN} A_M A_N^2 = 0, \quad (2.4.4)$$

$$\alpha_{2N} A_{2N} + \beta_{N,N} A_N^2 = 0, \quad (2.4.5)$$

$$\alpha_{2M} A_{2M} + \beta_{M,M} A_M^2 = 0, \quad (2.4.6)$$

$$\alpha_{M+N} A_{M+N} + 2\beta_{M,N} A_M A_N = 0, \quad (2.4.7)$$

$$\alpha_{M-N} A_{M-N} + 2\alpha_{M,N} A_M A_N = 0. \quad (2.4.8)$$

The  $\alpha$  and  $\beta$  coefficients are given by (2.1.2). However, we can simplify the expressions by substituting the leading order values  $\kappa = 1/MN$ ,  $\mu = 1/M + 1/N$ , except in  $\alpha_N$  and  $\alpha_M$ . Thus,

$$\alpha_{2N} = \frac{1}{M} - \frac{1}{2N}, \quad \alpha_{2M} = \frac{1}{N} - \frac{1}{2M}, \quad \alpha_{M+N} = \frac{1}{M+N}, \quad \alpha_{M-N} = \frac{2N-M}{M(M-N)};$$

$$\alpha_{M,N} = \frac{1}{4M} + \frac{1}{4N}, \quad \alpha_{N,2N} = \frac{1}{2N} - \frac{1}{4M}, \quad \alpha_{M,2M} = \frac{1}{2M} - \frac{1}{2N},$$

$$\alpha_{M,M-N} = \frac{3}{4M}, \quad \alpha_{M,M+N} = \frac{1}{4M}, \quad \alpha_{N,M+N} = \frac{1}{4N};$$

$$\beta_{N,M-N} = \frac{1}{M} + \frac{1}{4N}, \quad \beta_{N,N} = \frac{1}{N} - \frac{1}{2M}, \quad \beta_{M,M} = \frac{1}{M} - \frac{1}{2N},$$

$$\beta_{M,N} = \frac{1}{4M} + \frac{1}{4N};$$

$$\alpha_{NNN} = \frac{1}{8M} - \frac{1}{N}, \quad \alpha_{MMM} = \frac{1}{8N} - \frac{1}{M}, \quad \alpha_{NMM} = -\frac{5}{4M} - \frac{1}{2N},$$

$$\alpha_{MNN} = -\frac{5}{4N} - \frac{1}{2M};$$

$$\alpha_N = N(k - \frac{1}{MN}) - (\mu - \frac{1}{M} - \frac{1}{N}), \quad \alpha_M = M(k - \frac{1}{MN}) - (\mu - \frac{1}{M} - \frac{1}{N}).$$

It is clear from these equations that consistency requires

$$k - \frac{1}{MN} = O(\epsilon^2), \quad \mu - \frac{1}{M} - \frac{1}{N} = O(\epsilon^2). \quad (2.4.9)$$

The procedure now is to substitute from (2.4.5), (2.4.6), (2.4.7), (2.4.8) into (2.4.3) and (2.4.4), and then eliminate  $\mu$  to obtain a relation between  $A_M$  and  $A_N$  of the form

$$\gamma_N A_N^2 - \gamma_M A_M^2 = (\kappa - \frac{1}{MN})(M-N) \quad (2.4.10)$$

where

$$\gamma_N = \frac{(N+10M)}{8MN} , \quad (2.4.11)$$

$$\gamma_M = \frac{2M^4 - 7M^3N + 48M^2N^2 - 28MN^3 - 4N^4}{8M^2N(2M-N)(2N-M)} . \quad (2.4.12)$$

It is evident from these expressions that  $\gamma_N > 0$  for all appropriate pairs  $N, M$ , while  $\gamma_M > 0$  for  $N > \frac{1}{2}M$  and  $\gamma_M < 0$  for  $N < \frac{1}{2}M$ . Then provided  $A_N$  and  $A_M$  satisfy the relation (2.4.10), where  $2N \neq M$ ,  $3N \neq M$ , a combination wave exists. This wave exists in addition to pure waves of degree  $M$ , for which  $A_N = 0$ . Pure waves of degree  $N$  also exist if  $N > 1$ , and have  $A_M = 0$ . If  $N = 1$ , the pure wave has a more complicated structure and will be discussed separately. If  $|\kappa - \frac{1}{MN}| \gg \epsilon^2$ , the combination waves are not infinitesimal and must be studied numerically.

Convergence of the expansions has not been proved, but there is no reason to doubt existence if the amplitudes are sufficiently small and  $\kappa$  is sufficiently close to  $\frac{1}{MN}$ . The pure and combination waves all move with approximately the same speed

$$\mu \doteq \frac{1}{M} + \frac{1}{N} , \quad c^2 \doteq \frac{gL}{2\pi} \left( \frac{1}{M} + \frac{1}{N} \right) . \quad (2.4.13)$$

2.5 The  $M \rightarrow N$  and  $N \rightarrow M$  bifurcations,  $N > \frac{1}{2}M$  .

We consider first the case that  $N > \frac{1}{2}M$  and examine the implications in terms of bifurcation phenomena. Equation (2.4.10) is now a hyperbola in a plot of  $A_N$  vs  $A_M$  as shown in figure 2.4. There are two cases according as  $\kappa > 1/MN$  or  $\kappa < 1/MN$  .

The figure can be interpreted as follows. For arbitrary values of  $\kappa - 1/MN$  of  $O(\epsilon^2)$  , there exist pure waves of degree  $N$  and  $M$  of  $O(\epsilon)$  amplitude. However, the pure waves of degree  $M$  can bifurcate when

$$A_M = \pm \left[ \left( \frac{1}{MN} - \kappa \right) \frac{M-N}{\gamma_M} \right]^{\frac{1}{2}}, \quad \text{for } \kappa < \frac{1}{MN}, \quad (2.5.1)$$

into a combination  $(N,M)$  wave. Similarly, the pure wave of degree  $N$  can bifurcate into a combination  $(N,M)$  wave when

$$A_N = \pm \left[ \left( \kappa - \frac{1}{MN} \right) \frac{M-N}{\gamma_N} \right]^{\frac{1}{2}}, \quad \text{for } \kappa > \frac{1}{MN}. \quad (2.5.2)$$

If  $\kappa = 1/MN$  , the hyperbolae degenerate into two pairs of straight lines

$$\gamma_N^{\frac{1}{2}} A_N = \pm \gamma_M^{\frac{1}{2}} A_M. \quad (2.5.3)$$

There are four types of combination waves depending on the signs of  $A_N$  and  $A_M$  . These waves appear to be different, they cannot be brought into coincidence by a change of phase. These combination waves cannot exist for

arbitrary (small) amplitude. The accessible region is shown in figure 2.5.

Suppose now that we have a weakly non-linear pure wave of height  $h$  and wavelength  $\lambda$ . This wave can be described as a pure wave of degree  $M$ , with

$$L = M\lambda, \quad A_M = \pm \frac{\pi h}{\lambda}, \quad \kappa = \frac{4\pi^2 T}{9M^3 \lambda^2}. \quad (2.5.4)$$

Only the Fourier components which are integer multiples of  $M$  are non-zero. Now according to (2.5.1), this wave can bifurcate into a combination  $(M,N)$  wave by adding a Fourier component  $A_N$ , and the associated harmonics, if

$$h > \frac{\lambda}{\pi} \left[ \left( \frac{M}{N} - \frac{4\pi^2 T}{9\lambda^2} \right) \left( 1 - \frac{N}{M} \right) \frac{1}{M\gamma_M} \right]^{\frac{1}{2}}. \quad (2.5.5)$$

We call this an  $M \rightarrow N$  bifurcation. The properties of combination waves of finite amplitude remain to be elucidated by numerical methods, but it can be expected that as the wave grows, the  $A_N$  component will grow so that the wavelength (interpreted as an average distance between crests or troughs) will change from  $\lambda$  to  $M\lambda/N$ . Thus there is the possibility of an increase of wavelength of capillary-gravity waves as their amplitude increases.

Similarly, we can have a  $N \rightarrow M$  bifurcation if

$$h > \frac{\lambda}{\pi} \left[ \left( \frac{4\pi^2 T}{9\lambda^2} - \frac{N}{M} \right) \left( 1 - \frac{N}{M} \right) \frac{1}{N\gamma_N} \right]^{\frac{1}{2}}. \quad (2.5.6)$$

However, this bifurcation adds a higher harmonic and so could not be expected to reduce the wavelength.

In figure 2.6, we show an example of waves produced by the  $5 \rightarrow 4$  and  $4 \rightarrow 5$  bifurcation.

### 2.6 The case $1 < N < \frac{1}{2}M$ .

When  $\gamma_M < 0$ , as occurs when  $N < \frac{1}{2}M$ , equation (2.4.10) is that of an ellipse and has solutions only for  $\kappa > \frac{1}{MN}$ .  
Provided

$$A_N^2 < \left(\kappa - \frac{1}{MN}\right) \frac{M-N}{\gamma_N} \quad \text{or} \quad A_M^2 < \left(\kappa - \frac{1}{MN}\right) \frac{M-N}{-\gamma_M}, \quad (2.6.1)$$

a pure wave of degree  $N$  (for which  $A_M = 0$ ) or a pure wave of degree  $M$  (for which  $A_N = 0$ ) can bifurcate respectively into a combination  $(M,N)$  wave. In this discussion,  $N > 1$ ; otherwise  $A_M \neq 0$  for the pure wave of degree  $N$ . (Remember that  $N$  and  $M$  are coprime.) In terms of a wave magnitude, defined like equation (2.1.5), we see that  $\epsilon$  must be confined to the region such that the line  $A_N + A_M = \epsilon$  intersects the ellipse (2.4.10), i.e.

$$\epsilon^2 < \left(\kappa - \frac{1}{MN}\right)(M-N) \frac{(\gamma_N - \gamma_M)}{-\gamma_N \gamma_M}. \quad (2.6.2)$$

Thus in the  $\kappa, \epsilon$  plane, the accessible region for the existence of the  $(M,N)$  combination is above the parabola given by (2.6.1), see figure 2.5. In this case, the combination wave can exist only for sufficiently small amplitude. The bifurcation of a pure wave takes place as its

amplitude is reduced.

2.7 The case  $N=1$  ,  $M \geq 4$  .

The analysis of the previous section shows that in the vicinity of  $\kappa = 1/M$  , there exists a pure wave of degree  $M$  . There also exists a combination  $(M,1)$  wave, in which  $A_1$  and  $A_M$  are of comparable magnitude where

$$\frac{10M+1}{8M} A_1^2 + \frac{2M^4 - 7M^3 + 48M^2 - 28M - 4}{8M^2(2M-1)(M-2)} A_M^2 = (M-1)(\kappa - \frac{1}{M}) \quad (2.7.1)$$

and  $M > 3$  . These combination waves can exist only if  $\kappa > 1/M$  and their amplitude is not too large.

We now investigate the structure of the pure wave of degree 1 in the vicinity of  $\kappa = 1/M$  . Since  $\alpha_M$  is now small, it is clear that an expansion in which  $A_M = O(\epsilon^M)$  is not possible, where it is supposed that  $A_1 = O(\epsilon)$  . But we can proceed as follows to demonstrate that a consistent expansion exists with  $A_M = O(\epsilon^{M+2})$  . From the coefficients of  $\cos \xi$  and  $\cos 2\xi$  in (2.1.1), we have

$$\alpha_1 A_1 + \alpha_{111} A_1^3 + 2 \alpha_{1,2} A_1 A_2 = O(\epsilon^4), \quad (2.7.2)$$

$$\alpha_2 A_2 + \beta_{1,1} A_1^2 = O(\epsilon^3). \quad (2.7.3)$$

The  $\alpha$  and  $\beta$  coefficients are given as before by (2.1.2), and we can simplify by putting  $\kappa = 1/M$  ,  $\mu = 1 + 1/M$  except

in  $\alpha_1$ , so that the appropriate values are

$$\alpha_{111} = \frac{1}{8M} - 1, \quad \alpha_{1,2} = \frac{1}{2} - \frac{1}{4M}, \quad \alpha_2 = \frac{1}{M} - \frac{1}{2}, \quad \beta_{11} = 1 - \frac{1}{2M}.$$

Thus, it follows that

$$\alpha_1 = \kappa - \frac{1}{M} - (\mu - 1 - \frac{1}{M}) = -\frac{8M^2 + M + 2}{8M(M-2)} A_1^2. \quad (2.7.4)$$

Since

$$\alpha_M = M(\kappa - \frac{1}{M}) - (\mu - 1 - \frac{1}{M}), \quad (2.7.5)$$

it follows from (2.7.4) that  $\alpha_M = O(\epsilon^4)$ . Thus we see that

$$A_M = O(\epsilon^{M-2}) \quad (2.7.6)$$

is a possibility which allows the equation obtained from the  $\cos M\xi$  term in (2.1.1) to be satisfied. To obtain the value of  $A_M$ , we need the equations

$$\begin{aligned} \alpha_M A_M + 2\beta_{1,M-1} A_1 A_{M-1} + 2\alpha_{1,M+1} A_1 A_{M+1} \\ + \alpha_{M11} A_M A_1^2 = O(\epsilon^M), \end{aligned} \quad (2.7.7)$$

$$\alpha_{M+1} A_{M-1} + 2\alpha_{M,1} A_M A_1 = O(\epsilon^{M-1}), \quad (2.7.8)$$

$$\alpha_{M+1} A_{M+1} + 2\beta_{M,1} A_M A_1 = O(\epsilon^{M+1}). \quad (2.7.9)$$

The terms on the right hand sides of (2.7.7) and (2.7.8) of the stated order are sums and products of  $A_p$ ,  $1 \leq p \leq M-2$ . They are uniquely determined to the required

order by  $A_1$ , as is easily verified by inspection. Eliminating  $A_{M-1}$  and  $A_{M+1}$ , and substituting for  $\mu$  from (2.7.4), we obtain

$$A_M \left[ (M-1) \left( \kappa - \frac{1}{M} \right) - \frac{10M+1}{8M} A_1^2 \right] = O(\varepsilon^M) \quad (2.7.10)$$

where the right-hand-side is uniquely determined by  $A_1$  to the stated order. Thus  $A_M$  is uniquely determined if its coefficient in (2.7.10) does not vanish. In particular, the coefficient does not vanish if  $\kappa = 1/M$ , exactly. In this case, the wave is uniquely determined by  $A_1$ , as stated by Wilton.

However, if  $\kappa > 1/M$  and

$$A_1^2 = \frac{8M}{10M+1} (M-1) \left( \kappa - \frac{1}{M} \right), \quad (2.7.11)$$

the coefficient does vanish. Comparison with (2.7.1) shows that this is just the value of  $A_1$  for which  $A_M = 0$  in the combination  $(M,1)$  wave. Thus (2.7.11) gives the values of  $A_1$  for which there is bifurcation between the pure wave of degree 1 and the combination  $(M,1)$  wave in the vicinity of  $\kappa = 1/M$ . But the structure of this bifurcation is that associated with a limit line, with a relationship between  $A_M$  and  $A_1$  or  $\kappa$  as sketched in figure 2.7. This result shows that a pure wave of small amplitude cannot be continued analytically as  $\kappa \rightarrow 0$  into a gravity wave, because at each value of  $\kappa = 1/M$ , for all integer  $M \geq 4$ , there is a limit line behavior and the pure wave becomes a

combination (1,M) wave. The gravity wave ( $\kappa=0$ ) is therefore a singular limit which cannot be reached smoothly by applying the limit  $\kappa \rightarrow 0$  to a gravity-capillary wave. The numerical studies to be reported in chapter 4 indicate that this result remains true for finite amplitude.

The results also show that the effect of small surface tension on a pure gravity wave of degree 1 could produce either a pure capillary-gravity wave of degree 1 or a combination wave in which a higher harmonic, of order  $\approx 1/\kappa$ , would have the same magnitude. In reality, such higher harmonics would be damped out by viscosity, but the study of viscous effects is beyond the scope of the present work.

### 2.8 Bifurcation of (1,3) combination waves.

The remaining case is  $N=1$ ,  $M=3$ , and  $\kappa \doteq 1/3$ . We now show that a consistent expansion can be developed with  $A_1$  and  $A_3$  both of order  $\mathcal{E}$ . In addition, there is of course a pure wave of degree 3. Equating the coefficients of  $\cos \xi$  and  $\cos 3\xi$  in (2.1.1) to zero we obtain

$$\begin{aligned} \alpha_1 A_1 + \alpha_{111} A_1^3 + 2\alpha_{1,2} A_1 A_2 + \alpha_{1,33} A_1 A_3^2 + 2\alpha_{3,4} A_3 A_4 + 2\alpha_{3,2} A_3 A_2 + \\ + \beta_{311} A_1^2 A_3 = O(\mathcal{E}^4), \end{aligned} \quad (2.8.1)$$

$$\alpha_3 A_3 + \alpha_{333} A_3^2 + 2\alpha_{1,4} A_4 A_1 + 2\beta_{1,2} A_1 A_2 + 2\alpha_{3,6} A_3 A_6 + \beta_{111} A_1^3 + \alpha_{311} A_1^2 A_3 = O(\epsilon^4). \quad (2.8.2)$$

From the coefficients of  $\cos 2\xi$ ,  $\cos 4\xi$ ,  $\cos 6\xi$ , we obtain

$$\alpha_2 A_2 + \beta_{11} A_1^2 + 2\alpha_{1,3} A_1 A_3 = O(\epsilon^3), \quad (2.8.3)$$

$$\alpha_4 A_4 + 2\beta_{1,3} A_1 A_3 = O(\epsilon^3), \quad (2.8.4)$$

$$\alpha_6 A_6 + \beta_{33} A_3^2 = O(\epsilon^3). \quad (2.8.5)$$

All coefficients are given by (2.1.2) with  $\mu = 4/3$ ,  $\kappa = 1/3$ , except for  $\alpha_1$  and  $\alpha_3$  which must be given exact values

$$\alpha_1 = (\kappa - \frac{1}{3}) - (\mu - \frac{4}{3}), \quad \alpha_3 = 3(\kappa - \frac{1}{3}) - (\mu - \frac{4}{3}). \quad (2.8.6)$$

Eliminating  $A_2$ ,  $A_4$ ,  $A_6$ , and excluding the pure wave of degree 3 by supposing that  $A_1 \neq 0$ , we obtain

$$\alpha_1 + \frac{77}{24} A_1^2 + \frac{123}{24} A_1 A_3 - \frac{23}{36} A_3^2 = 0, \quad (2.8.7)$$

$$\alpha_3 + \frac{23}{12} A_1^2 - \frac{29}{120} A_3^2 + \frac{123}{24} \frac{A_1^3}{A_3} = 0. \quad (2.8.8)$$

The consistency relation between  $A_1$  and  $A_3$  is obtained by eliminating  $\mu$ , and gives a cubic for  $A_1/A_3$

$$123 \left( \frac{A_1}{A_3} \right)^3 - 31 \left( \frac{A_1}{A_3} \right)^2 - 123 \frac{A_1}{A_3} - \frac{317}{15} = - \frac{48(\kappa - \frac{1}{3})}{A_3^2}. \quad (2.8.9)$$

Note that for  $\kappa = 1/3$ , there are three real roots

$$A_1/A_3 = -0.76, -0.19, 1.20, \quad (2.8.10)$$

and three possible (1,3) combination waves of given (small) magnitude exist. The maximum and minimum of the cubic on the left-hand-side of (2.8.9) are

$$f_+ = 17.24, \quad f_- = -80.47.$$

There are therefore three roots if  $\kappa \neq 1/3$  provided that

$$-f_+ < \frac{48(\kappa - 1/3)}{A_3^2} < -f_- \quad (2.8.11)$$

and only one root otherwise. The situation in the  $\kappa, A_3$  plane is shown in figure 2.5. In figure 2.8, we sketch the locus of  $A_1$  vs  $A_3$  for  $\kappa > 1/3$  and  $\kappa < 1/3$ . The pure wave of degree 3 is represented by the  $A_3$  axis. It is clear from this figure that for sufficiently small amplitude, a unique combination wave exists. This could be thought of as the pure wave of degree 1 since

$$A_3 \sim -\frac{123}{48} \frac{A_1^3}{\kappa - 1/3} \quad A_1 \rightarrow 0 \quad (2.8.12)$$

As the magnitude grows, another solution branch becomes possible when the coefficient of the third harmonic reaches a critical value.

The previous sections have discussed the form of steady progressive capillary-gravity waves of small magnitude. It has been shown that there exist pure waves and combination waves, and that bifurcation loci occur at which solutions can pick up subharmonics or higher

harmonics which are not integer multiples of the fundamental. Limit line behavior has also been found. Two important questions remain. The first is the stability of the waves and the possible change of stability of a solution on crossing a bifurcation line or passing a limit point. This question will not be treated in this thesis. The second is the property of the solutions for finite amplitude. In the next chapter we will develop the numerical procedures necessary to answer the second question.

CHAPTER 3

NUMERICAL PROCEDURES

3.1 The Fourier series method.

Let us consider a pure wave of wavelength  $\lambda$  and height  $h$ . This can be regarded as a pure wave of degree  $M$  and period  $L = M\lambda$ . We expect that bifurcation of type  $M \rightarrow N$  may occur for some value of  $h$ . The bifurcation will occur when

$$A_M = f_n(\kappa, M, N) \quad (3.1.1)$$

where  $f_n$  is some unknown function. Now  $M \rightarrow N$  bifurcation with period  $L$  must be identical with  $pM \rightarrow pN$  bifurcation with period  $pL$ , where  $p$  is an arbitrary integer. Hence, (3.1.1) must take the form

$$A_M = f_n\left(\frac{M}{N}, \kappa M^2\right) \quad (3.1.2)$$

or in dimensional terms

$$\frac{h}{\lambda} = f_n\left(\frac{M}{N}, \frac{T}{g\lambda^2}\right). \quad (3.1.3)$$

We know that as  $h \rightarrow 0$ ,

$$\frac{T}{g\lambda^2} \rightarrow \frac{M}{4\pi^2 N}, \quad (3.1.4)$$

and the limiting forms of the function are given by (2.3.3) for the  $2 \rightarrow 1$  bifurcation and by (2.5.5) and (2.5.6) for the  $M \rightarrow N$  and  $N \rightarrow M$  bifurcation with  $N > \frac{1}{2}M$ . Similar criteria can be found from (2.6.2) and (2.7.11) for the  $M \rightarrow N$  and  $N \rightarrow M$  bifurcations when  $1 < N < \frac{1}{2}M$  and for the  $1 \rightarrow M$  limit points with  $M \geq 4$ .

Another question of interest is the largest value of  $h/\lambda$  for which waves can exist, and how this depends on  $\kappa$  or  $T/g\lambda^2$  and the type of waves.

There are many possible methods for calculating the shape of steady water waves of finite amplitude. One of the simplest is to truncate equation (1.1.16) obtained in chapter 1 for some integer  $J$  and evaluate at  $\xi_j = \frac{j\pi}{J}$ ,  $0 \leq j \leq J$ , to give the  $J+1$  equations

$$\begin{aligned} & \mu - 2 \left[ \sum_1^J \frac{A_n}{n} (1 - \cos n\xi_j) \right] \left[ \left( \sum_1^J A_n \sin n\xi_j \right)^2 + \left( 1 + \sum_1^J A_n \cos n\xi_j \right)^2 \right] \\ & + 2\kappa \left[ \left( \sum_1^J A_n \sin n\xi_j \right) \left( \sum_1^J n A_n \sin n\xi_j \right) + \left( 1 + \sum_1^J A_n \cos n\xi_j \right) \left( \sum_1^J n A_n \cos n\xi_j \right) \right] \times \\ & \times \left[ \left( \sum_1^J A_n \sin n\xi_j \right)^2 + \left( 1 + \sum_1^J A_n \cos n\xi_j \right)^2 \right]^{-\frac{1}{2}} \\ & - \mu(1-b) \left[ \left( \sum_1^J A_n \sin n\xi_j \right)^2 + \left( 1 + \sum_1^J A_n \cos n\xi_j \right)^2 \right] = 0, \quad (3.1.5) \end{aligned}$$

for the  $J+2$  unknowns,  $A_j$  ( $1 \leq j \leq J$ ),  $\mu$  and  $b$ . We found it more convenient to work with the dimensionless quantities

$\mu = 2\pi c^3/gL$  and  $\kappa = 4\pi^2/gL^2$  instead of  $c^2$  and the surface tension  $T$ . The remaining equation is a specification of wave magnitude. We used mainly equation (1.1.17), but sometimes we specified the parameter  $b$ .

Thus, we have a non-linear algebraic system of equations in  $J+2$  unknowns, depending on two parameters, the surface tension quantity  $\kappa$  and the amplitude quantity  $\xi$ . To include the case  $\kappa \rightarrow \infty$  into the general scheme, we divide equation (3.1.5) by  $1+\kappa$  and work with  $\tilde{\kappa} = \kappa/(1+\kappa)$  and  $\tilde{\mu} = \mu/(1+\kappa)$ , instead of  $\kappa$  and  $\mu$ .

This system will be denoted by

$$G(u; p) = 0, \quad (3.1.6)$$

where for simplicity we are using the same notation for the truncated and for the infinite dimensional problems. Here  $u \equiv (A_1, \dots, A_J, \tilde{\mu}; b)$  and  $p$  is the parameter we are allowing to vary, either  $\tilde{\kappa}$  or  $\xi$ . To solve (3.1.6) we use Newton's method:

an initial guess to the solution  $u^{(0)}$  is given. An approximation to the solution is calculated iteratively

$$G_u(u^\nu; p) \delta u^\nu = -G(u^\nu; p), \quad (3.1.7)$$

$$u^{\nu+1} = u^\nu + \delta u^\nu. \quad (3.1.8)$$

We stopped the iteration when the maximum residual was  $\theta(10^{-4})$ . Here  $G_u$  is the Jacobian matrix of the truncated system.

The linear system (3.1.7) in each iteration is solved by a LU decomposition with column pivoting, where  $L$  is lower triangular with 1's in the diagonal and  $U$  is upper triangular. The Jacobian ( $\det G_u$ ) is the product of the diagonal elements of  $U$ , with a possible sign change depending on the pivoting.

The method was checked by comparing with Crapper's results for capillary waves, Schwartz's for gravity waves, and Wilton's for small amplitude capillary-gravity waves. In all cases the agreement was to the order expected.

A useful check on the accuracy of each calculated solution is to verify that the relation

$$2g\bar{\gamma} = -bc^2 \quad (3.1.9)$$

is satisfied. The error obtained was at most  $O(10^{-8})$ .

The mean water level and the kinetic and gravitational potential energies were calculated by truncating (1.3.4), (1.3.5) and (1.3.8) to  $J$  terms. The surface tension contribution was calculated by approximating the integral using the trapezoidal rule, since the problem is periodic. The mean water level and the potential energies were also calculated by using the trapezoidal rule to approximate the integrals in (1.3.3) and (1.3.6) or (1.3.7). The agreement, as expected, was at least  $O(10^{-8})$ .

The arclength procedure used to find branches of solutions, bifurcation and limit points, is described in

section 3.3.

3.2 The vortex sheet method.

We now show how to solve numerically the non-linear, singular integro-differential equation derived in section 1.2,

$$\left(1 - b - \frac{g L}{\pi c^2} \operatorname{Im} \zeta + \frac{2T}{c^2 R} \right) \frac{d\bar{\zeta}}{d\xi} - 1 + \frac{i}{2\pi} P \int_0^{2\pi} \cot \left[ \frac{\zeta(\xi) - \zeta(\xi_1)}{2} \right] d\xi_1 = 0, \quad (3.2.1)$$

where

$$\frac{1}{R} = \frac{2\pi}{L} \operatorname{Im} \left( \frac{d^2 \zeta}{d\xi^2} \frac{d\bar{\zeta}}{d\xi} / \left| \frac{d\zeta}{d\xi} \right|^3 \right) \quad (3.2.2)$$

and

$$\zeta = \frac{2\pi}{L} Z = \frac{2\pi}{L} (x + iy),$$

together with

$$x(0) = 0, \quad y(0) = 0, \quad \frac{\partial y}{\partial \xi}(0) = 0. \quad (3.2.3)$$

It was convenient to specify  $b$  as the amplitude parameter. Given the value of  $b$ , the solution of (3.2.1) and (3.2.3) will still not be unique until we specify the number of waves in the window or equivalently the shortest period  $\lambda$ . (We neglect the trivial degeneracy associated with the direction of the wave and take  $\lambda > 0$ .)

First consider the case of symmetric waves that

satisfy

$$\zeta(-\xi) = -\bar{\zeta}(\xi) \quad , \quad \zeta(\pi + \xi) = -\bar{\zeta}(\pi - \xi). \quad (3.2.4)$$

It is sufficient to work in the interval  $[0, \pi]$  . Introduce a uniform mesh

$$\xi_j = \pi j / N \quad , \quad j = 0, 1, 2, \dots, N, \quad (3.2.5)$$

and the unknown values

$$\zeta_j \equiv \zeta(\xi_j) = \frac{2\pi}{L} (x_j + iy_j), \quad j = 0, 1, 2, \dots, N$$

at the mesh points.

The derivatives in (3.2.1) and (3.2.2) are replaced by a seven point finite difference formula

$$\frac{d\zeta(\xi_j)}{d\xi} = \left[ 540(\zeta_{j+1} - \zeta_{j-1}) - 108(\zeta_{j+2} - \zeta_{j-2}) + 12(\zeta_{j+3} - \zeta_{j-3}) \right] / \Delta\xi \times 6! + O(\Delta\xi^6) \quad (3.2.6)$$

$$\frac{d^2\zeta(\xi_j)}{d\xi^2} = \left[ -980\zeta_j + 540(\zeta_{j+1} + \zeta_{j-1}) - 54(\zeta_{j+2} + \zeta_{j-2}) + 4(\zeta_{j+3} + \zeta_{j-3}) \right] \times \frac{2}{6!} \times (\Delta\xi)^2 + O(\Delta\xi^6), \quad (3.2.7)$$

where  $\Delta\xi = \pi/N$  .

To calculate the integral introduce an integration mesh at  $\tilde{\xi}_j = \pi(j+\frac{1}{2})/N$  , halfway between the mesh  $\xi_j$  to take care of the principal value, express the values of  $\zeta$  on the integration mesh in terms of the  $\zeta_j$  by a sixth order

Lagrange interpolation formula

$$\begin{aligned} \zeta(\tilde{\xi}_j) = & [150(\zeta_j + \zeta_{j+1}) - 25(\zeta_{j-1} + \zeta_{j+2}) \\ & + 3(\zeta_{j-2} + \zeta_{j+3})] / 256 + O(\Delta \xi^6), \end{aligned} \quad (3.2.8)$$

and, since the integrand is periodic, use the trapezoidal rule

$$P \int_0^{2\pi} \cot \left[ \frac{\zeta(\xi_k) - \zeta(\tilde{\xi}_j)}{2} \right] d\tilde{\xi} \approx \Delta \xi \sum_{j=0}^{2N-1} \cot \left[ \frac{\zeta(\xi_k) - \zeta(\tilde{\xi}_j)}{2} \right], \quad \alpha k \leq M \quad (3.2.9)$$

The values of  $\zeta$  outside the range  $[0, \pi]$  are obtained from the symmetry. The real and imaginary parts of this discretized version of (3.1.1) at the  $N+1$  mesh points gives  $2N$  equations, because the imaginary values of (3.2.1) at  $\xi=0$  and  $\xi=\pi$  are identically zero from symmetry. Further we take  $x_0=0$ ,  $y_0=0$ ,  $x_N=\frac{L}{2}$ ; the first two come from (3.2.3) and the last from symmetry. The last equation of (3.2.3) is automatically satisfied from symmetry. Thus, we have  $2N$  non-linear algebraic equations for the  $2N$  unknowns,  $x_1, x_2, \dots, x_{N-1}; y_1, y_2, \dots, y_N$  and  $c^2$ . The parameters  $b$  and  $T$  are given.

Now consider the case of nonsymmetric waves. This is more difficult. We introduce a uniform mesh

$$\xi_j = \frac{2\pi j}{M+1}, \quad j = 0, 1, 2, \dots, M \quad (3.2.10)$$

and the values  $\zeta_j$  at the mesh points. The values outside the range are given by periodicity. Discretizing the

integro-differential equation as for the symmetrical case and taking real and imaginary parts at the  $M+1$  mesh points, we obtain  $2M+2$  equations for the  $2M+3$  unknowns  $x_j, y_j$  and  $c^2$ . Equations (3.2.3), with a seven point finite difference formula for the derivative, provide a further three equations, giving  $2M+5$  equations for  $2M+3$  unknowns. The system is thus apparently overdetermined. The difficulty arises from the fact that the  $2M+2$  equations derived from the integro-differential equation are not independent because of the degeneracy expressed by (1.2.15). The degeneracy arises from the fact that (3.2.1) is invariant under the addition of constants to  $x$  and  $y$ . In principle, (3.2.3) handles the degeneracy, but it is not clear how it is to be incorporated into the numerical scheme other than by throwing away two of the equations which come from (3.2.1). This was tried but did not work. The problem does not arise in the symmetric case because the imposition of symmetry destroys the degeneracy.

The following trick proved satisfactory and was easy to implement.

First note that when  $b$ , rather than  $h$ , is the parameter, the degeneracy with respect to  $y_0$  disappears because the equation is not invariant under  $y$  translation; hence we can take  $y_0=0$  without loss of generality, and this is done henceforth. Now instead of solving (3.2.1) and (3.2.3), we solve a discretized form of the equation

$$\left(1 - b - \frac{gL}{\pi c^2} I_m \xi + \frac{2T}{cR}\right) \frac{d\bar{\xi}}{d\xi} - 1 + \frac{i}{2\pi} P \int_0^{2\pi} \cot \left[ \frac{\xi(\xi) - \xi(\xi_1)}{2} \right] d\xi_1 + k_1(\xi) x(0) + k_2(\xi) \frac{dy}{d\xi}(0) = 0, \quad (3.2.11)$$

where  $k_1$  and  $k_2$  are arbitrary functions of  $\xi$  chosen so that the Fréchet derivative of (3.2.11) is in general non-singular. This can be done because (3.2.11) is not invariant under translation of  $x$  and  $\xi$ . Then the discretized form of equation (3.2.11) gives  $2M+2$  equations for the  $2M+2$  unknowns  $x_0, x_1, \dots, x_M; y_1, y_2, \dots, y_M; c^2$ . This system has solutions with  $x(0)=0, dy(0)/d\xi=0$ , which provide a solution of (3.2.1) and (3.2.3). The reason this works is that by hypothesis the equations (3.2.1) and (3.2.3) have isolated solutions. Since the Fréchet derivative of (3.2.11) is by construction in general non-singular, (3.2.11) also has isolated solutions. A solution of (3.2.1) and (3.2.3) obviously satisfies (3.2.11). Therefore (3.2.11) has isolated solutions which satisfy (3.2.1) and (3.2.3). The system is now  $2M+3$  equations in  $2M+3$  unknowns.

(When using the Fourier series method, if we allow for nonsymmetric solutions, we also obtain an overdetermined system of equations, and the degeneracy can be eliminated using a similar trick.)

The problem is thus reduced to calculating the in general isolated solutions of a system of non-linear algebraic equations. The equations involve two parameters,

$T$  and  $b$ . The unknowns are the coordinates of the wave at mesh points and the wave speed. The system of equations, for the symmetric or nonsymmetric problem, can be written as

$$G(u; p) = 0, \quad (3.2.12)$$

where  $u$  is the vector of unknowns, and  $p$  is the one parameter we are allowing to vary. The system (3.2.12) is solved by Newton's method. The Jacobian matrix is obtained by calculating first the Fréchet derivative of the exact equations (3.2.1) or (3.2.11)

$$G_u(u; p) \delta u = G(u + \delta u; p) - G(u; p), \quad (3.2.13)$$

and then discretizing it in the analogous way. At each Newton iteration we solve the finite dimensional linear problem

$$G_u(u; p) \delta u = -G(u; p) \quad (3.2.14)$$

by LU decomposition.

The method of solution was tested by comparison with Longuet-Higgins' (13) results for gravity waves, with Crapper's capillary waves (taking  $g=0$ ), and with the results obtained with the Fourier series method. The agreement was very good as reported in the next two chapters. Equation (3.1.9) was also used to check the accuracy of the calculated waves. For gravity waves, relation (1.3.18)

was verified to within a relative error of 0.1%. This error is bigger than the errors in the other checks because it was calculated with only six decimal places and round-off is important.

The mean water level, the kinetic and potential energies were calculated using equations (1.3.2), (1.3.3), (1.3.6) and (1.3.9). The derivatives were approximated using a sixth order finite difference formula and the integrals using the trapezoidal rule.

The implementation of the arclength continuation is described in the following section.

### 3.3 Arclength continuation.

To implement the arclength continuation procedure described in section 1.4, instead of using the actual arclength  $S$  defined by

$$\frac{1}{2} \left\| \frac{du}{dS} \right\|^2 + \frac{1}{2} \left( \frac{dp}{dS} \right)^2 = 1, \quad (3.3.1)$$

it was found more convenient to continue in terms of a pseudo arclength, also denoted by  $s$ , introduced by the equation

$$N(u, p; s) = \frac{1}{2} u_s^*(s_1) [u(s) - u(s_1)] + \frac{1}{2} p_s(s_1) [p(s) - p(s_1)] - (s - s_1) = 0. \quad (3.3.2)$$

Here,  $(u(s_i), p(s_i))$  is some known solution, the star denotes the adjoint element and the value of  $s_i$  is updated every time we calculate a new solution;  $p$  represents the parameter that is allowed to vary, either  $K$  or  $\epsilon$  for the Fourier series method, or,  $T$  or  $b$  for the vortex sheet method, and  $u$  is the vector of unknowns. The system of equations is written as

$$G(u, p; s) = 0 \quad (3.3.3)$$

for any of the formulations given before. As was done before, we will keep the notation of chapter 1 for the truncated, finite dimensional problem.

To use (3.3.2), we need to calculate  $(u_s(s_i), p_s(s_i))$ . First solve for  $u_p(s_i)$  from

$$G_u u_p = -G_p. \quad (3.3.4)$$

Since we already have the LU decomposition of  $G_u$  at  $(u(s_i), p(s_i))$ , the solution of (3.3.4) is inexpensive. From the chain rule we have

$$u_s(s_i) = u_p(s_i) p_s(s_i). \quad (3.3.5)$$

Taking the limit  $s \rightarrow s_i$  of (3.3.2), we have

$$p_s^2(s_i) \{ \|u_p(s_i)\| + 1 \} = 2 \quad (3.3.6)$$

and the value of  $p_s(s_i)$ . The choice of sign for the square root is arbitrary: the positive sign means that  $p$

increases as  $s$  increases. At a limit point where  $p_s = 0$ , it is necessary to choose the other sign to follow the new branch.

To calculate a new solution  $(u(s), p(s))$ , we will solve the inflated system consisting of (3.3.3) and (3.3.2). Newton's method is used. To obtain a first guess for the iteration a one step Euler method is applied

$$\left. \begin{aligned} u(s) &\approx u(s_i) + u_s(s_i)(s-s_i), \\ p(s) &\approx p(s_i) + p_s(s_i)(s-s_i) \end{aligned} \right\} \quad (3.3.7)$$

Each step of Newton's method requires the solution of the following system of linear equations

$$\begin{pmatrix} G_u & G_p \\ N_u^* & N_p \end{pmatrix} \begin{pmatrix} \delta u \\ \delta p \end{pmatrix} = - \begin{pmatrix} G \\ N \end{pmatrix}, \quad (3.3.8)$$

where everything is evaluated at the old iterate, and  $\delta u$  and  $\delta p$  are the corrections to the solution.

Keller (8) suggested the following algorithm to solve (3.3.8):

obtain the vectors  $y$  and  $z$  from

$$G_u y = G_p \quad (3.3.9)$$

and

$$G_u z = -G. \quad (3.3.10)$$

Then

$$\delta p = -\frac{(N + N_u^* z)}{(N_p - N_u^* y)}, \quad (3.3.11)$$

$$\delta u = z - \delta p y. \quad (3.3.12)$$

(3.3.9) and (3.3.10) are solved by doing a LU decomposition with partial column pivoting. This is the most expensive part of the calculation. In this way, even if we are solving an inflated system, we need only to do the LU decomposition of  $G_u$  and obtain its Jacobian by multiplying the diagonal elements of  $U$ , with a possible sign change due to the pivoting.

Newton's method is considered to have converged when the residuals are very small (typically  $\mathcal{O}(10^{-12})$  for the Fourier series method and  $\mathcal{O}(10^{-10})$  for the integro-differential equation). Szeto (29) proved that Newton's method using the above algorithm converges quadratically for regular and limit points, and only linearly near simple bifurcation points.

It was sometimes convenient to use  $s = p$  as the arclength parameter, replacing (3.3.2) with

$$N(u, p; s) \equiv p - s = 0. \quad (3.3.13)$$

Solutions for small amplitude are found using the results of chapter 2 as the first guess for the Newton iteration. Solutions for higher amplitude are obtained using the arclength continuation described above.

Simple bifurcation points at  $s = s_0$  are detected by monitoring changes in sign of the Jacobian and pinpointed by bisection. Numerically the Jacobian is never zero, but the last pivot is  $O(10^{-6})$  times smaller than the others. The right and left eigenvectors of  $G_u$ ,  $\phi_i$ , and  $\psi_i^*$ , are approximated by inverse iteration. Again, this is not expensive since we already have the LU decomposition of  $G_u$ . The product  $\psi_i^* \cdot G_p$  is calculated; it should be close to zero for bifurcation.

Once determined that  $s = s_0$  is a simple bifurcation point, in order to switch to the bifurcating branch, we use the fact that the method of calculation gives an approximation  $(\hat{u}_s(s_0), \hat{p}_s(s_0))$  to the tangent to the original solution branch at the point  $s_0$ . We compute as an approximation to  $\phi_0$  the element

$$\hat{\phi}_0 = \frac{1}{\hat{p}_s(s_0)} \left[ \hat{u}_s(s_0) - \frac{\psi_i^* \hat{u}_s(s_0) \phi_i}{\psi_i^* \phi_i} \right]. \quad (3.3.14)$$

The leading coefficients of the quadratic

$$A\alpha_1^2 + B\alpha_1\alpha_0 + C\alpha_0^2 = 0 \quad (3.3.15)$$

are approximated by

$$A = \frac{\psi_i^*}{\delta} [G_u(u^0 + \delta\phi_i, p^0) - G_u^0] \phi_i \quad (3.3.16)$$

$$B = \frac{2\psi_i^*}{\delta} \left\{ [G_u(u^0 + \delta\phi_i, p^0) - G_u^0] \hat{\phi}_0 + [G_p(u^0 + \delta\phi_i, p^0) - G_p^0] \right\}, \quad (3.3.17)$$

where  $\delta$  is a given small number. This finite difference

approximation is necessary because of the great complexity of the second Fréchet derivatives. Since one root of the quadratic is known (the tangent to the original branch),  $B/A$  suffices to determine the other root:

$$\frac{\bar{\alpha}_1}{\alpha_0} = - \left( \frac{\alpha_1}{\alpha_0} + \frac{B}{A} \right). \quad (3.3.18)$$

Since only the direction of the tangent is important, we can choose it as

$$\bar{u}_s = \frac{\bar{\alpha}_1}{\alpha_0} \phi_1 + \hat{\phi}_0 \quad (3.3.19)$$

and from (3.3.6)

$$\bar{p}_s = \pm \left( \frac{2}{1 + \bar{u}_s^* \cdot \bar{u}_s} \right)^{1/2}. \quad (3.3.20)$$

The sign of the square root depends on the direction in which we want to do the continuation on the bifurcating branch.

In this way, we were able to detect simple bifurcation points and calculate new branches. The method of monitoring the Jacobian will fail, however, if the bifurcation is not simple and the Jacobian has a root of even order. We have not yet been able to check systematically for higher order even bifurcation and the possibility of their existence cannot be excluded and should be kept in mind during the reading of the results.

## CHAPTER 4

### FINITE AMPLITUDE CAPILLARY-GRAVITY WAVES

#### 4.1 Introduction.

The purpose of this chapter is to extend some of the results obtained in chapter 2 for waves of small amplitude to waves of finite amplitude. The structure of capillary-gravity waves appears to be extremely rich, and our contribution is far from being an exhaustive study. We shall concentrate on extending to finite amplitude some of the bifurcation loci examined in chapter 2 and also on investigating limiting waves of greatest height. The equations to be solved and the numerical procedure are described in chapters 1 and 3.

The method of Fourier series truncation (sections 1.1 and 3.1) was completely adequate for the calculation of capillary-gravity waves up to waves of greatest height, but some results were checked using the vortex sheet integro-differential approach (sections 1.2 and 3.2) which is necessary for gravity waves of large amplitude because of the incipient cusp which causes slow decay of the Fourier

coefficients. As will be seen, capillary-gravity waves are limited in height by the surface crossing itself, as for capillary waves with  $g=0$  (Crapper (4)), but the surface remains smooth and the rate of decay of the Fourier coefficients is not significantly affected as the limiting wave is approached.

The coefficients  $A_n$  are dimensionless. Dimensionless groups involving the surface tension which are convenient for the presentation of the results are

$$\kappa = \frac{4\pi^2\tau}{g L^2} \quad \tilde{\kappa} = \frac{\kappa}{1+\kappa} \quad (4.1.1)$$

The latter is useful for the capillary wave limit,  $g \rightarrow 0$ . In the actual calculations, the scales of length and time were fixed by taking  $g=1$ ,  $L=2\pi$ . Continuation along a solution branch was carried out either in an amplitude parameter  $\xi$ , that was either  $b$  or a linear combination of Fourier coefficients, or in the surface tension variable  $\kappa$ . With the integro-differential equation approach, the continuation was either in  $b$  or in the surface tension  $\tau$ . Symmetry of the solutions about  $\xi=0$  and  $\xi=\pi$ , which correspond to a crest or a trough, was supposed.

All numerical calculations were carried out on the CDC STAR 100 computer.

4.2 The finite amplitude 2→1 and 2→3 bifurcations.

In section 2.3, it was shown that a weakly non-linear pure wave of degree 2 bifurcates into a combination (2,1) wave when

$$A_2 \doteq \frac{4}{3} \kappa - \frac{2}{3} \doteq 2(\bar{\kappa} - \frac{1}{3}), \quad |\kappa - \frac{1}{2}| \ll 1. \quad (4.2.1)$$

In physical variables, this condition is equivalent to

$$\frac{h}{\lambda} \doteq \frac{4}{3\pi} \left| \frac{\pi^2 T}{g \lambda^2} - \frac{1}{2} \right| \quad (4.2.2)$$

as the condition for a pure wave of height  $h$  and wavelength  $\lambda$  to bifurcate by the addition of a subharmonic of wavelength  $2\lambda$ .

To extend the bifurcation curve (4.2.1) to waves of finite amplitude, we employed continuation alternatively in  $\varepsilon$  and  $\kappa$ . Starting for  $\kappa > \frac{1}{2}$  with a small amplitude pure wave of degree 2 with  $A_2 > 0$ , we increased the amplitude until a change of sign of the determinant of the Jacobian matrix occurred, indicating that the solution branch went through a critical point. Since it was easily seen that this was not a limit point, as all variables were changing monotonically, a crossing of the bifurcation curve had taken place. A continuation increasing  $\kappa$  was then carried out until the bifurcation curve was crossed again. The process was continued and in this way a rough profile of the bifurcation curve was obtained. The curve

ended at  $\kappa = 1.342$  ,  $A_2 = 0.77$  ,  $h/\lambda = 0.48$  , where the surface crossed itself. The unphysical nature of the solutions for larger amplitudes was not marked by any singularity in the equations for the Fourier coefficients, which could be calculated without difficulty for unphysical solutions.

Note the conclusion that for  $\kappa > 1.342$  the only solutions with  $A_1 = O(\epsilon)$  have  $h = O(\epsilon)$  , while for  $\kappa < 1.342$  there are also solutions with  $A_1 = O(\epsilon)$  ,  $h \gg \epsilon$  .

A similar procedure was carried out for  $\kappa < \frac{1}{2}$  ,  $A_2 < 0$  . In this case, it was found that the bifurcation curve turns around and returns to the small amplitude state with a value of  $\kappa$  lying between 0.170 and 0.160. As will shortly be explained, this result is consistent with the  $2 \rightarrow 3$  bifurcation locus springing from  $\kappa = 1/6$  .

Figures 4.1 and 4.2 show the approximate bifurcation curve, at which a pure wave of degree 2 may bifurcate by the addition of subharmonic and odd superharmonic components, obtained in the way just described. In figure 4.1, the locus is plotted in the  $\kappa, A_2$  plane. Figure 4.2 shows the results in the  $\kappa, h/\lambda$  plane.

It is only for small amplitude waves that it is meaningful to talk of a (M,N) combination wave. When bifurcation occurs at finite amplitude, many Fourier components are introduced. The combination waves which exist only outside the  $A_2 < 0$  bubble in figure 4.1 are analytic continuations of one another as the bifurcation locus is

traversed from  $\kappa = 1/2$  to  $\kappa = 1/6$ . For  $\kappa \doteq 1/2$ ,  $A_3/A_1 \ll 1$ , and for  $\kappa \doteq 1/6$ ,  $A_1/A_3 \ll 1$ . Thus the return of the bifurcation locus to the  $\kappa$ -axis is consistent with the  $2 \rightarrow 3$  bifurcation curve coming from  $\kappa = 1/6$ .

As follows from the results of section 2.5, the bifurcation locus for  $0 < \kappa - 1/6 \ll 1$  is the parabola

$$A_2 = \pm \left\{ \frac{3}{2} \left( \kappa - \frac{1}{6} \right) \right\}^{1/2}, \quad \left( \frac{h}{\lambda} \right)^2 = \frac{3}{2\pi^2} \left( \kappa - \frac{1}{6} \right). \quad (4.2.3)$$

The continuation of the bifurcation locus across  $\varepsilon = 0$  at  $\kappa = 1/6$  initially follows equation (4.2.3), but as  $\varepsilon$  increases the curvature changes and the locus turns down in  $\kappa$ , as seen in figures 4.1 and 4.2. Above  $\kappa = 1/8$  we can speak of this line as being the  $2 \rightarrow 3$  bifurcation line. The reason is that if we continue pure waves of degree 2 from infinitesimal to finite amplitude, keeping  $\kappa$  constant and  $1/8 < \kappa < 1/6$ , we obtain the same solutions as the ones found following the bifurcation locus. These waves have  $A_4 < 0$ . For  $\kappa$  near but less than  $1/8$ , the continuation of an infinitesimal wave of degree 2 to maximum amplitude with  $\kappa$  constant does not have any critical points but has  $A_4 > 0$ . The behavior of pure waves of degree 2 near  $\kappa = 1/8$  is the same as that of pure waves of degree 1 near  $\kappa = 1/2$  (see sections 2.2 and 2.3). Therefore, the finite amplitude bifurcation locus for  $\kappa < 1/8$  describes the subharmonic bifurcation of combination (4,2) waves. In the  $\kappa, A_2$  plane the locus eventually returns to the  $\kappa$ -axis at about

$\kappa=0.062$  , but the wave has nonzero amplitude when this occurs and the crossing is not related to the behavior near singular points described in chapter 2.

The uncertainty in the values of  $\kappa$ ,  $A_2$  and  $h/\lambda$  for the curves shown in figures 4.1 and 4.2 is about 0.01 for  $\kappa$  and about the same for  $A_2$  and  $h/\lambda$  when  $A_2 > 0$  , and about 0.003 for  $A_2$  and  $h/\lambda$  when  $A_2 < 0$  .

The bifurcation point was determined more exactly at a few points on the bifurcation curve and it was verified that the bifurcation conditions were satisfied. Equation (1.4.6) was satisfied to  $O(10^{-8})$ . The bifurcating branches were calculated; the new solutions have wavelength  $L$  and  $A_1 \neq 0$  . To one side of the bifurcation point  $A_1$  is positive and to the other negative, but they represent physically the same solution shifted by  $L/2$  . For  $\kappa=0.3$  , the pure wave of degree 2 bifurcates at  $A_2 = -0.158$  . The combination wave originating at this value was continued in  $A_2$  until it reached its maximum height, with an enclosed bubble, at  $A_2 = -0.48$  ,  $A_1 = 0.34$  ,  $h/\lambda = 0.27$  . Plots of the profiles for this solution branch are shown in figure 4.3. Profiles of combination waves emanating from  $A_2 = \pm 0.032$  , continued in  $\kappa$  were plotted in figure 2.2. These waves start to resemble pure waves of degree 1 as  $\kappa$  moves away from the bifurcation curve.

Most of the calculations were done using 64 Fourier coefficients. The Newton iteration converged quadratically

and three or four iterations were sufficient to reduce the residuals to  $O(10^{-12})$ . Each solution required less than 0.5 sec. on the CDC STAR 100 computer. Some of the higher amplitude waves were recalculated using 128 Fourier coefficients. Then the computing time per solution was about 1.5 sec. In both cases all the last coefficients were  $O(10^{-12})$  and the solutions agreed to at least 8 significant figures.

Bifurcated solutions for  $K=0.48$  and  $K=0.52$  were also calculated using the vortex sheet method with  $N=20$ . Agreement was at least 4 significant figures. Since this method was slower and it was difficult to classify the solutions obtained with it, we used it mainly on gravity waves.

It is noteworthy that Choi (3) observed experimentally a doubling of wavelength like that predicted by our bifurcation analysis for capillary waves produced by wind blowing over water in a wind-water tunnel. A wind of speed 5m/sec initially produced waves of frequency 16Hz which stayed constant, until after a certain fetch where the frequency appeared to drop to about 9Hz. The value of  $K$  corresponding to Choi's experiment is 0.23 (with  $T=72$  dynes/cm). Our results indicate that bifurcation is then possible at  $A_2=-0.14$  or  $h=0.8$  mm. Unfortunately, Choi does not give the waveheight at which the dominant frequency changed from 16 to 9Hz, but we roughly estimated it to be  $h=1.7$  mm. The quantitative agreement is poor but the effects of wind and shear in the water are probably

significant. The observed wave speed is about 6cm/sec. greater than that given by the linear dispersion relation.

#### 4.3 The finite amplitude $M \leftrightarrow N$ bifurcation with $N > \frac{1}{2}$ .

As examples, we followed the  $3 \rightarrow 2$  , the  $5 \rightarrow 4$  and the  $5 \rightarrow 3$  bifurcation lines. These curves were found in the same approximate way as the  $2 \rightarrow 1$  line.

For the  $3 \rightarrow 2$  bifurcation we start with  $\kappa$  just less than  $1/6$  and a pure 3 wave of small amplitude and, by changing the parameters, determine where the determinant of the Jacobian matrix changes sign. This bifurcation line also turns back, at about  $A_3 = 0.14$  ,  $\kappa = 0.11$  , and tends to the  $\kappa$ -axis between 0.075 and 0.087. For small amplitude waves the  $3 \rightarrow 4$  bifurcation starts at  $\kappa = 1/12$  . It therefore appears that the  $3 \rightarrow 2$  and the  $3 \rightarrow 4$  bifurcation lines are different ends of the same line and the (3,2) and the (3,4) combination waves are analytic continuations of one another. The step sizes used in finding the changes of sign of the Jacobian were at most  $|\Delta \kappa| = 0.012$  ,  $|\Delta A_3| = 0.01$  . Figure 4.4 is a sketch of this bifurcation line. It is symmetric with respect to the  $\kappa$ -axis. The maximum error in the curves is of the order indicated.

The  $5 \rightarrow 4$  bifurcation line was followed in the same way, determining the changes of sign of the Jacobian for

a pure wave of degree 5. In the  $\kappa, A_5$  plane, this line turns back and returns to the  $\kappa$ -axis as the  $5 \rightarrow 6$  line, the same behavior occurs for the  $5 \rightarrow 3$  line that joins to the  $5 \rightarrow 7$  line. Both lines are symmetrical about the  $\kappa$ -axis. The step sizes in determining these lines were  $|\Delta\kappa|=0.001$  and  $|\Delta A_5|=0.01$ . Figure 4.5 shows sketches of the curves. The  $(5,4)$  and the  $(5,6)$  combination waves are analytic continuations of each other, as are also the  $(5,3)$  and the  $(5,7)$  waves.

Since all the waves that we calculate are symmetric about  $\xi = \pi$ , each wave displaced horizontally by a distance  $L/2$  is also a solution of the system of equations for the  $A_n$ . Thus if the set  $\{A_n\}$  constitutes a solution, so does the set  $\{(-1)^n A_n\}$ . It follows that the bifurcation loci for pure waves of odd degree  $N$  are symmetrical about the  $\kappa$ -axis in the  $\kappa, A_N$  plane. This is not necessarily true for pure waves of even degree and it was shown in section 4.2 that the  $2 \rightarrow 3$  bifurcation locus is not symmetrical. However, it was found that the  $4 \rightarrow 3$  and  $4 \rightarrow 5$  bifurcation lines join up and are symmetric.

All these calculations employed 128 Fourier coefficients, the computing time for each iteration being about 1.5 seconds on the CDC STAR 100. The number of iterations depended on the initial guess, but convergence was quadratic and typically 3 or 4 iterations were sufficient to reduce the residuals to  $O(10^{-12})$ .

#### 4.4 The $1 \rightarrow M$ limit line.

As shown in chapter 2, the behavior of small pure waves of degree 1 near  $\kappa = 1/M$  is a special kind. For  $M \geq 4$ , a pure 1 wave continued in  $\kappa$  with  $A_1$  kept constant turns as  $\kappa \rightarrow 1/M$  into a combination wave in which  $A_1$  and  $A_M$  are of the same order. If  $\kappa \rightarrow 1/M$  from above, the solution branch has a limit point in  $\kappa$  and turns back, with the magnitude of  $A_M$  increasing. If we start with a pure 1 wave and  $\kappa < 1/M$ , and then increase  $\kappa$ , there is no limit point but  $A_M$  increases rapidly as  $\kappa \rightarrow 1/M$ . This means that pure 1 waves on different sides of  $\kappa = 1/M$  are not analytic continuations of one another.

As an example, an initially pure wave of degree 1 with  $A_1 = 0.05$ , and 128 coefficients retained, was continued down from  $\kappa = 0.22$  to  $\kappa = 0.2011$  where a limit point was encountered, and then on the second branch to  $\kappa = 0.325$ . At this point the surface of the wave crosses itself, with  $A_1 = 0.05$  and  $A_5 = -1.59$ . The solution looks almost like a pure 5 wave, but the crests are of slightly different height and only two troughs enclose a bubble. The calculation was repeated keeping  $A_1 = 0.1$  constant. Now the limit point is at  $\kappa = 0.2038$ , so that the line moves up with increasing  $A_1$ , in agreement with the analysis of section 2.7, according to which the  $1 \rightarrow 5$  limit line is

$$\kappa = \frac{1}{5} + \frac{51}{160} A_1^2 \quad (4.4.1)$$

Also, a pure wave of degree 1 with  $A_1=0.05$  was continued up from  $\kappa=0.171$ . Around  $\kappa=0.200$ ,  $A_5$  starts growing very fast and dominates the behavior. At  $\kappa=0.325$ , the wave, which looks almost like a pure 5 wave with  $A_5=1.56$ , achieves its maximum height by enclosing a bubble. Figure 4.6 is a plot of  $\kappa$  vs  $A_5$  for these solutions with  $A_1=0.05$ . Compare with figure 2.7 (b).

In section 4.5 we give some additional evidence that the  $1 \rightarrow 5$  limit line intersects the highest wave line. This is probably true for all  $1 \rightarrow M$  limit lines, for  $M \geq 4$ .

These results confirm the impossibility of going continuously from a pure capillary-gravity wave to a gravity wave by letting  $\kappa \rightarrow 0$ . We also tested to see if a combination wave could go continuously to a gravity wave. This was done by starting with a (5,4) combination wave at  $\kappa=0.05$ ,  $A_5=0.122$ ,  $A_4=0.179$ , and continuing by decreasing  $\kappa$  with  $A_5$  kept constant. This solution branch has a limit point in  $\kappa$  at  $\kappa=0.0185$ ,  $A_5=0.122$ ,  $A_4=0.072$ , and turns back. The value of  $A_5$  was chosen so that the solutions were outside the  $5 \rightarrow 4$ ,  $5 \rightarrow 6$  bifurcation line. We believe that, in general, it is impossible to continue a combination wave to a gravity wave by letting  $\kappa \rightarrow 0$ .

The (3,1) combination waves are also special. As shown in section 2.8, for  $\kappa$  near  $1/3$  there are three

(1,3) combination waves. One of them has  $A_3 = O(A_1^3)$  as  $A_1 \rightarrow 0$ . The other two exist only for finite amplitude.

We investigated one of the latter solutions for  $k = 0.316$ . The continuation was done in  $A_1$ . There is a limit point at  $A_1 = 0.0818$ ,  $A_3 = -0.2667$ . Continuing the solution to either side a wave of maximum height is obtained. Figure 4.7 is a plot of  $A_1$  and  $A_3$  for this solution. On the top branch the maximum height wave has  $A_1 = 0.453$ ,  $A_3 = -0.558$ . There is also a limit point with respect to  $A_3$  at  $A_1 = 0.103$ ,  $A_3 = -0.202$ . The other branch has a maximum height wave at  $A_1 = 0.151$ ,  $A_3 = -0.409$ . This solution has  $A_2$  negative, and exists inside the  $2 \rightarrow 1$  bifurcation line. There is no inconsistency since the solution is not a combination (2,1) wave.

Figure 4.8 shows plots of the surface profile for different solutions on this branch. The top three plots correspond to the upper branch, the fourth to the limit point in  $A_1$  and the last two to the lower branch.  $A_1$  decreases from the top until the fourth plot and then increases again.

#### 4.5 Waves of maximum height on deep water.

Gravity waves have a maximum height when the surface cusps and includes an internal angle of  $120^\circ$ . This occurs

for the pure wave at  $h/\lambda \doteq 0.1411$  .

Capillary waves, as shown by Crapper (4), have a maximum height of  $h/\lambda=0.730$  , but in this case the wave is limited because it encloses a bubble. For greater heights the surface crosses itself making the solution unphysical, even though there is no mathematical problem in the calculation of the Fourier coefficients or in determining parametric equations for the surface.

In this section we give some answers to the questions of the existence and shape of capillary-gravity waves of maximum height on deep water.

First we reproduced numerically Crapper's results with a pure wave of degree 1 up to the limiting height. We know of no simple analytical criterion to determine from a parametric Fourier representation like (1.1.13) and (1.1.14) if a surface crosses itself. We used some sufficient conditions for the curve to be simple and visual aids to determine when this happened. The method does not give the maximum height to great accuracy, but it turned out to be sufficient for our purposes. For pure capillary waves we found in this way the maximum height to be  $h/\lambda=0.7305$  , which agrees well with Crapper's exact value.

We repeated the calculation using  $\lambda = 1/2$  and  $\lambda = 1/3$  seeking subharmonic bifurcations. None were found. If we apply the intuitive argument that bifurcation occurs when

two different waves move with the same speed we would not expect any bifurcations since the speed decreases monotonically as the height increases. Also the  $2 \rightarrow 1$  bifurcation line does not intersect the line  $\kappa = \infty, \tilde{\kappa} = 1$ .

Waves of greatest height were found in two different ways. The first method was to take Crapper's limiting solution and, by decreasing  $\kappa$  and then changing the amplitude, obtain waves of maximum height for different values of  $\kappa$ . With this method of continuation it was possible to calculate waves with  $\kappa$  down to about 0.04, where the numerical solution started to become inconsistent because the higher coefficients did not remain small. We were working with 128 harmonics. Increasing this number permitted us to go to lower values of  $\kappa$ , but it was found that the higher order coefficients quickly grew more and more important as  $\kappa$  decreased.  $A_2$ , which is positive for capillary waves, changes sign as  $\kappa$  decreases at about  $\kappa = 1.95$  and stays negative afterwards. All the waves of greatest height calculated in this way look similar to each other; they all enclose a single bubble and are all smooth. But as  $\kappa$  decreases the bubble gets smaller and the change of slope faster. Figure 4.9 shows the profiles for these waves for  $\kappa = \infty, 2.333, 0.666, 0.250$  and  $0.042$ .

The second way was to start with pure waves of degree 1 of small amplitude, and increase the waveheight by changing  $A_1$  with  $\kappa$  kept constant. For  $\kappa > \frac{1}{2}$  the waves of

greatest height are the same as those obtained by the first method of continuation. But for  $K < 1/2$ , the highest waves found in this way are multi-bubbled. The number of bubbles depends on the value of  $K$ . For  $\frac{1}{N+1} < K < \frac{1}{N}$ , with  $N \geq 2$  integer, the highest waves have  $N$  crests of different height and enclose  $N$  bubbles, not all completely closed. For example, for  $K=0.493, 0.429$  and  $0.370$ , the highest waves enclose two bubbles; for  $K=0.316$  and  $0.266$ , three bubbles exist, with only the middle one completely closed; for  $K=0.220$ , four bubbles exist, with two closed; for  $K=0.190$ , five bubbles exist, with only the middle one closed; and for  $K=0.163$ , six bubbles exist, with two closed. Figure 4.10 shows the wave profiles of waves of almost maximum height for  $K=0.493, 0.316, 0.220, 0.190$  and  $0.163$ .

Figure 4.11 shows the change of form of a pure wave of degree 1 from infinitesimal to maximum height for  $K=0.190$ .

For small  $K$ , the continuation in  $A_1$  with  $K$  kept constant sometimes hits the  $1 \rightarrow M$  limit lines in the  $K, A_1$  plane. The solution branch with  $K=0.205$  hits the  $1 \rightarrow 5$  limit line at  $A_1=0.1192$  and turns back. After going through this limit point the solution has five crests. For  $K=0.176$  the solution has a limit point at about  $A_1=0.193$  and turns back looking like a modulated 6 wave. For  $K=0.149$  the solutions meet the  $1 \rightarrow 7$  limit line at  $A_1=0.15$ .

For all the smaller  $K$ , for which we used the second

method of continuation, the solutions all have limit points corresponding to  $l \rightarrow M$  limit lines, before getting to the maximum. These solutions were not continued to the highest wave because it would have required more than 128 harmonics to get a consistent solution. Since the  $l \rightarrow M$  limit lines become more concentrated as  $K \rightarrow 0$  and since they are not horizontal in the  $K, A_1$  plane, the continuation of the solutions using  $A_1$  as the parameter will probably always have limit points for very small  $K$ .

Figure 4.12 is a plot of  $\tilde{K}$  vs  $h/\lambda$  for maximum amplitude waves. The continuous line is for single bubbled waves which are the analytic continuation of Crapper's solution. The + signs represent multi-bubbled waves which are the continuation of small amplitude pure waves of degree 1, as described above.

Figure 4.13 is a plot of  $\tilde{K}$  vs  $A_1$ , and of  $\tilde{K}$  vs  $A_2$  for maximum amplitude waves. The continuous lines are for the single bubbled waves which are the analytic continuation of Crapper's waves. The + signs and the x signs represent the values of  $A_1$  and  $A_2$  respectively for the multi-bubbled waves which are the continuation of small amplitude pure waves of degree 1. This figure complements figure 2.1 to show the accessible regions for pure waves of degree 1 in the  $\tilde{K}, A_2$  plane.

In section 2.6, we showed that for  $l < N < \frac{1}{2}M$ , the (M,N) combination wave can exist only for sufficiently

small amplitude. To see if there were other solutions that did not achieve a limiting height in the sense of the surface crossing itself, we continued a (5,4) combination wave on  $\xi = A_5$ , with  $\kappa = 0.05$  kept constant. The solution goes through several limit points in  $A_5$ , but does not attain a maximum height. Figure 4.14 is a plot of  $\tilde{\mu} = \frac{\mu}{1+\kappa}$  vs  $A_5$  for the (5,4) combination wave. The nearly horizontal line represents the pure wave of degree 5 from which the (5,4) combination wave bifurcated. Note that the wave speed is not a monotonic function of  $A_5$  (or of  $h/\lambda$ ).

## CHAPTER 5

### FINITE AMPLITUDE GRAVITY WAVES

#### 5.1 Introduction.

In all numerical studies to date of which we are aware, it appears to have been assumed, either implicitly or explicitly, that steady, one-dimensional gravity waves are unique in the sense that given the height, wavelength and direction only one wave exists. Owing to the time-reversibility of the Euler equations, it follows that the wave must be symmetrical about its crest and trough. There is no doubt that permanent gravity waves of sufficiently small amplitude are unique, but to our knowledge there is no proof of uniqueness or symmetry for waves of all amplitudes up to the maximum. Garabedian (5) proved that the waves are indeed symmetric and unique in the special case that all the crests and troughs are equal.

The object of this chapter is to give evidence that symmetrical gravity waves of large amplitude are not unique. In chapter 4 we found that finite amplitude capillary-gravity waves are not unique for general values of

the surface tension. However, the limit  $T \rightarrow 0$  is highly singular and we have already shown that gravity waves cannot be obtained as the continuous limit of a capillary-gravity wave as  $T \rightarrow 0$ , so the non-uniqueness of capillary-gravity waves does not imply the non-uniqueness of gravity waves. On the other hand, Wilton's ripples can be explained "physically" as fixed points of the non-linear resonance between a wave and its first harmonic which travel at the same speed. Since there exist permanent gravity waves of large but different amplitude that move at the same speed, because the wave speed is not a monotonic function of wave height, analogy suggests as a possibility some combination may exist that is also a gravity wave of permanent form. The argument is weak, but it does suggest that if gravity waves are not unique, it may only be for waves with heights close to the maximum and that the method of study will need to be one that can handle waves of large height.

Our procedure is to study numerically the solutions of the singular integro-differential equation given in section 1.2, with  $T=0$ . This equation has the property that it can be solved accurately for waves close to the limiting  $120^\circ$ -cusped wave, with a reasonable amount of computation, using the methods of sections 3.2 and 3.3 that allow the systematic search for other solutions different from those obtained from the Stokes expansion.

For almost all the computations reported here, it was convenient to use  $b$  as the parameter that determined the wave magnitude. It is clear that  $b \leq 1$  is necessary. Since  $p=0$  at the surface, from Bernoulli's equation (1.1.10) we have that when  $b=1$ , the origin is at the highest crest and is a stagnation point; the wave is then a limiting wave with a  $120^\circ$  cusp. The identity  $2g\bar{Y} = -bc^2$  implies that at  $y=\bar{Y}$ ,  $q^2=c^2$ , and that the speed at the highest crest is less than  $c$ . Therefore, without loss of generality we can take the origin at the highest crest and confine attention to the fixed range  $0 < b < 1$ . The height is then determined as a function of  $b$ . Infinitesimal waves are given by  $b \ll 1$ .

Given the value of  $b$ , the solution of (1.2.11) and (1.2.16) will still not be unique until we specify the number of waves in the window or equivalently the shortest period  $\lambda$ . (We neglect the trivial degeneracy associated with the direction of the wave and take  $c > 0$ .) Then the existence theory of finite amplitude water waves implies that for  $0 < b < b_c$  there is a unique solution of period  $2\pi$ , which is moreover symmetrical about  $\xi=0$  and  $\xi=\pi$ . The assumption that water waves are unique is equivalent to the statement

$$b_c = 1. \quad (5.1.1)$$

We shall present evidence that this statement is incorrect

and that there are values of  $b$  for which more than one wave, with  $\lambda=L$ , exists. Let us introduce the name regular wave for the symmetric water waves that are the continuation to finite amplitude of the weakly non-linear waves calculated by Stokes by expansion in wave amplitude. The regular waves are those calculated by Schwartz (23), Longuet-Higgins (13) and others. The new types of waves, which we may call irregular waves, arise from subharmonic bifurcations of the regular waves. We shall show that regular wave solutions of (1.2.11) and (1.2.16) with more than one wave in the window, i.e. with  $\lambda=L/n$  where  $n>1$  is the number of waves in the window, may bifurcate at critical values of  $b$  into solutions with  $\lambda=L$  which are not regular waves. We shall call  $n$  the class of the regular wave solution. Regular waves of class 1 do not appear to have any critical values of  $b$  and are not connected continuously with the irregular waves. It is perhaps for this reason that their existence has apparently so far been overlooked. Irregular waves have crests of different heights so there is no contradiction with Garabedian (5).

The following equations of section 1.3 provide useful checks on the accuracy of the numerical computations

$$2g\bar{\gamma} = -bc^2 \quad (5.1.2)$$

$$\frac{\partial(K+V_g)}{\partial b} = -c \frac{\partial I}{\partial b} \quad (5.1.3)$$

Equation (5.1.3) relates the properties of waves on a

solution branch.

In all the calculations, the length and time scales are normalized to

$$g=1, L=2\pi. \quad (5.1.4)$$

While the first solutions were being computed, it was noticed that the mesh points tended to concentrate near the troughs where the curvature changes relatively slowly. In order to resolve properly the crests which become sharp when the wave height increases, while keeping the number of mesh points as small as possible, a change of independent variables was introduced. A new independent variable  $\gamma$  is defined by

$$\xi = \gamma - \frac{\alpha}{n} \sin n\gamma, \quad 0 \leq \gamma \leq 2\pi, \quad (5.1.5)$$

where  $n$  is the number of waves in the window and  $0 \leq \alpha < 1$ . This transformation concentrates points at the crests where  $\xi$  is equal to  $\gamma$  and an integer multiple of  $2\pi/n$ . The closer  $\alpha$  is to 1, the greater the concentration. It was found that very steep waves could be resolved satisfactorily with  $\alpha = 0.99$ , which was the usual value taken. The calculations were done for one case with  $\alpha = 0.999$  to verify that the results were independent of  $\alpha$ . The method worked well for regular waves. However, the spacing of the crests on the irregular waves is not necessarily uniform. In this case, (5.1.5) was replaced for calculations along the new branches of irregular waves by



obtained from the estimate. From this new solution a better approximation to the position of the crest is found. Usually only two or three iterations were necessary to calculate  $\xi_c$  to within  $10^{-3}$  of the true value.

### 5.2 Numerical results for regular waves of class 1.

Fortran programs to implement the numerical procedures were run on the CDC STAR 100 at Minneapolis. The symmetric code was first checked by calculating regular waves and comparing with the results given by Longuet-Higgins (13). The wave height was used as the continuation parameter and his table 2, which runs from  $h/\lambda=0.04527$  to  $h/\lambda=0.14053$ , was reproduced. The calculated values of  $c$  agreed to six significant figures and the other parameters, energies and fluid velocity at crest and trough, agreed to the published figures. These calculations were done with  $N=40$ . Each individual wave required about 4 seconds of computing time. The latest published value for the height of the limiting wave of greatest height is (Longuet-Higgins and Fox (15))  $h/\lambda=0.14107$ . The maximum value of  $c$  occurs at  $b=0.9725$ ,  $h/\lambda=0.13873$ . These calculations check not only our program but also the use of Padé approximants to sum high order series, since the latter method is not rigorous and is based on the uncertain (but apparently in

this case valid) assumption that a large but finite number of terms contains the behavior of the solution near singularities.

We then repeated the calculations using  $b$  as a parameter with  $N=80$ . These calculations were also carried out with the non-symmetric code and produced the same results. For the same values of  $b$  or  $h/\lambda$ , agreement to six significant figures was obtained. Equation (5.1.2) was checked, the integral being evaluated by the trapezoidal rule. The error detected in this relation was typically  $O(10^{-8})$ . The relative error in equation (5.1.3) was less than 0.1%. This error is bigger because the calculations to evaluate (5.1.3) were done with only six significant figures. The derivatives were approximated by a fourth order difference formula. We concluded that the code was satisfactory, provided the wave was not too close to the limiting wave of maximum height.

The method worked very well for  $b \leq 0.998$ ,  $h/\lambda \leq 0.14087$ . Newton's method converged quadratically. The iteration was terminated when the residuals were less than  $10^{-10}$ ; this usually took 3 or 4 iterations. For larger values of  $b$ , the method started to fail; convergence became slow and the residuals could not be made to tend to zero. We expect that the failure is associated with the truncation error in resolving the sharp peak.

Table 1 lists some of our calculated values of  $\theta_m$ ,  $c$ ,

$h/L$  ,  $\omega$  ,  $K$  ,  $V_g$  and  $\bar{Y}$  for a range of  $b$  for regular waves of class 1, where  $\theta_m$  is the maximum slope,  $c$  is the wave speed,

$$\omega = 1 - \frac{q_{crest}^2 q_{trough}^2}{c^2} = 1 - c^2(1-b)^2 + 2(1-b)y_{trough} \quad (5.2.1)$$

is Longuet-Higgins' (13) parameter (units have been chosen so that the speed of infinitesimal waves of wavelength  $L$  is unity), and  $K$  and  $V_g$  are the average kinetic and potential energies per unit length.

Longuet-Higgins and Fox (15) predicted that the wave speed and energies would oscillate infinitely often as  $h \rightarrow h_{max}$ . We appear to have been able to pick up the first relative minima of these quantities. The maximum slope is difficult to calculate. We used the slope of the chord between mesh points and their bisections. Values of  $\theta_m > 30^\circ$  were found, as predicted by Longuet-Higgins and Fox; our results for  $b \leq 0.996$  agree well with the extrapolation curve shown in figure 12 of their paper. The disagreement at the top of the table is probably due to inadequate resolution at the peak.

We followed the solution branch for regular waves of class 1 from  $b=0$  to  $b=0.998$ , with both the symmetric and non-symmetric programs. The Jacobian never changed sign and we conclude that there are no simple bifurcation points on this branch. We cannot, however, at present rule out completely the possibility of higher order even

bifurcations, but the indications are that they are absent.

5.3 Bifurcation of regular class 2 waves: a new type of symmetrical solution.

In our studies of capillary-gravity waves (chapter 2), we showed that these waves could undergo subharmonic bifurcation. In the simplest case, associated with Wilton's ripples, a regular wave of wavelength  $\lambda$  could bifurcate continuously into a wave of wavelength  $2\lambda$  when

$$\frac{h}{\lambda} = \frac{4}{3\pi} \left| \frac{\pi^2 \tau}{g \lambda^2} - \frac{1}{2} \right| + O \left( \frac{\pi^2 \tau}{g \lambda^2} - \frac{1}{2} \right)^2. \quad (5.3.1)$$

This behavior was called a  $2 \rightarrow 1$  bifurcation. The numerical results (chapter 4) show that the bifurcation exists for finite amplitude capillary-gravity waves for values of  $\tau$  not close to  $g \lambda^2 / 2\pi$ , but the theoretical and numerical results showed that the bifurcation locus in an  $h, \tau$  plane does not intersect  $\tau=0$ . Nevertheless, the results suggested that a search for  $2 \rightarrow 1$  bifurcation for gravity waves would be of interest and we now describe the results.

We first followed the solution branch for  $0.1 < b < 0.99$  for regular waves of class 2 (with two periodic waves in the window,  $\lambda = L/2$  and  $n=2$ ) using the symmetric code and  $N=40$ . No significant differences were found in the properties of the regular waves of class 2 and those of

class 1 found previously after the appropriate changes of scale were made. The sign of the Jacobian was monitored and it was observed that a critical point exists for  $b=b_c$ , where

$$0.87969 < b_c < 0.87970, \quad h/\lambda = 0.1289. \quad (5.3.2)$$

The criterion (1.4.6) was tested and found to be satisfied with an error  $O(10^{-7})$ , confirming the existence of a simple bifurcation.

The tangent vector to the new branch was computed as described in section 3.3 and the new branch was followed by pseudo arclength continuation. Figure 5.1 shows a plot of  $c$  vs  $b$  for the regular wave of class 2 and the symmetric (by construction) bifurcated solution. The regular wave of wavelength  $L/2$  bifurcates into an irregular wave of wavelength  $L$ . The tangent to the new branch in the

$c, b$  plane is horizontal at the bifurcation point. The crests in the new solutions are of unequal height. From symmetry consideration, the two branches must describe physically identical waves translated relative to one another through  $L/2$  and hence  $(dc/db)_c$  must be zero on the new branch. It is sufficient therefore to present results for  $b > b_c$ . Table 2 contains properties of the new type of solution and in figure 5.2 are presented plots of the wave profile for various values of  $b$  from the bifurcation value to  $b=1$ . Note that as  $b \rightarrow 1$ , the highest crest

tends to the  $120^\circ$  cusp, while the lower crest stays rounded.

To check the accuracy of the scheme, the calculations were repeated with  $N=60$  and  $N=80$ . The discretization error was proportional to  $N^{-6}$  as expected for a sixth order scheme. The accuracy drops for  $b > 0.99$  and no attempt was made to compute the wave of greatest height. The behavior near the sharp crest would, of course, be that described by Longuet-Higgins and Fox (15).

To corroborate further the existence of new solutions, we used the Fourier series method described in sections 1.1 and 3.1, which consists in solving

$$gk \sum_1^{\infty} \frac{A_n}{n} (\cos n\xi - 1) - \pi c^2 \left[ \left( 1 + \sum_1^{\infty} A_n \cos n\xi \right)^2 + \left( \sum_1^{\infty} A_n \sin n\xi \right)^2 \right]^{-1} = 0, \quad (5.3.3)$$

for  $0 \leq \xi \leq \pi$ . This approach assumes symmetrical waves. The numerical method truncates the series to  $J$  terms, satisfies (5.3.3) at  $J+1$  equally spaced points in  $[0, \pi]$ , and solves the resulting  $J+1$  equations in the  $J+1$  unknowns  $A_1, A_2, \dots, A_J, c^2$  by Newton's method. Iteration is stopped when the residuals were  $O(10^{-10})$ . The method of continuation and the determination of bifurcation points and new branches proceeds as described before. We followed the branch of regular solutions of class 2, starting with a wave of small amplitude. Taking  $J=512$ , the bifurcation

was found to occur at  $b_c = 0.8793$  . The higher coefficients were  $O(10^{-9})$  ; the machine round off is  $O(10^{-13})$  . A bifurcated solution was calculated for  $b = 0.8785$ ; its properties checked to five figures with those found by the integro-differential equation method. The Fourier series method is not a good one for steep gravity waves since the sharp crests produce a slow decay of the Fourier coefficients. The amount of computing time to calculate a Fourier series solution with  $J = 512$  was about 80 secs. The integro-differential equation with  $N = 80$  took 15 secs. per solution; with  $N = 40$  only 4 seconds were required.

Note that the value of  $b_c$  and the corresponding  $h/\lambda$  (0.1289) are less than the values at which  $c$  has its maximum ( $b = 0.9725$  ,  $h/\lambda = 0.1387$  ). The bifurcation also occurs for smaller values of  $b$  than those at which  $K$  and  $\sqrt{g}$  have their maxima.

No further symmetrical bifurcations on the new branch were found. Both solution branches were followed with the non-symmetrical program, but no simple bifurcation points were found, other than the symmetrical  $2 \rightarrow 1$  bifurcation at  $b_c$  . We cannot exclude, however, the possibility of bifurcation into non-symmetrical solutions through a high order even bifurcation, but no indications of such behavior were seen.

Equations (5.1.2) and (5.1.3) were checked for the branch of solutions of irregular waves and were satisfied

to the same accuracy as on the original branch.

#### 5.4 Bifurcation of regular class 3 waves.

We now describe the results of calculations following the solution branch for regular waves of class 3 (i.e.

$\lambda = L/3$ ,  $n=3$ ). Using the symmetrical wave formulation, we found a symmetrical bifurcation for

$$0.87901 < b_c < 0.87902, \quad h/\lambda = 0.1288, \quad (5.4.1)$$

calculated the tangent vector to the new branch, and computed the new solutions. The values of  $b$  and  $h/\lambda$  are very close to those for the  $2 \rightarrow 1$  bifurcation. These results were obtained with  $N=60$  and  $N=80$ . About 15 seconds on the CDC STAR 100 were required for each solution. A few solutions were calculated with  $N=120$  to check that the discretization error was  $O(N^{-6})$ .

In this case, the solutions for  $b > b_c$  and  $b < b_c$  are physically distinct. For  $b > b_c$ , the origin is the highest crest. The other two crests inside the window are equal to one another and smaller. The troughs are of the same depth. In the wave, the highest crests are separated by a pair of lower crests. As  $b \rightarrow 1$ , the highest crest tends to a  $120^\circ$  cusp and the others remain rounded. The wave height increases but the wave speed and energies decrease

as  $b$  increases along this branch.

For  $b < b_c$ , the situation is reversed. The origin is not the highest crest. The two crests inside the window are equal and highest. In this wave, a pair of high crests is separated by a single lower one. The troughs are again of equal depth. As  $b$  decreases, the wave height increases until the highest crest is cusped. The wave speed and energies increase at first and then decrease as the limiting wave is approached.

Since the waves for  $b > b_c$  and  $b < b_c$  are physically distinct, there is no reason why  $d\epsilon/db$  should vanish on the new branch at the bifurcation point, and in fact it is non zero.

Figure 5.3 shows a plot of wave speed vs  $b$  for the regular class 3 wave and the bifurcated symmetric solutions. Some properties of the new waves are listed in table 3. Figure 5.4 shows some wave profiles. Since there are two crests of different heights, the value of  $b$  for the wave is not unique and depends on which crest is chosen as origin. If  $\Delta h$  is the height of the other crest above the one at the origin, the value of the parameter,  $b'$  say, obtained taking the other crest as origin is

$$b' = b + 2\Delta h/c^2 \quad (5.4.2)$$

For  $b > b_c$ , we have  $b' < b_c$ , and vice versa. The dashed line in figure 5.3 shows  $\epsilon$  vs  $b'$ .

It was not possible to check these calculations with the Fourier method, as sufficient resolution of a wave with three crests at the steepness where it bifurcates required a value of  $J$  of at least 750, and the program became too expensive to run.

A check was made, however, by repeating the calculations with the non-symmetric program. The symmetric bifurcation of class 3 waves produces waves which are not symmetric about all the crests. Thus, if symmetry is not imposed, the regular wave will bifurcate at  $b = b_c$  into the symmetric waves as calculated and two apparently non-symmetrical waves which are, however the same wave with the origin at the other crests about which the wave is not symmetric. Hence,  $b = b_c$  must be a non-simple bifurcation of the non-symmetric formulation. Four branches of solutions pass through the bifurcation point; a regular wave of class 3, a symmetric irregular wave, and two non-symmetric irregular waves. The irregular waves are physically identical, the difference between them being a horizontal displacement. A non-symmetric wave with value  $b = b_1$ , say, is identical to the symmetric wave with  $b' = b_1$ . The properties of the non-symmetric branches are therefore given by table 3 with  $b'$  instead of  $b$ . Corresponding to the existence of four branches, we expect the Jacobian to have a double zero. (The branches at a  $n$ th order zero of the Jacobian correspond to the roots of  $n$  quadratic

polynomials.)

Following the regular branch with the non-symmetric program, we found no change of sign of the Jacobian between  $b = 0.8$  and  $b = 0.9$ . This confirms that the bifurcation is not simple. Closer examination showed that two diagonal elements of the matrix  $U$  of the LU decomposition were small near  $b = 0.879$ ; their magnitudes were  $10^{-4}$  smaller than the other elements on the diagonal. These two elements changed sign, but not exactly at the same value of  $b$ , the difference being  $O(10^{-4})$ . The calculation was carried out with  $M = 80, 120$  and  $160$ . No discernible changes in the separation as  $M$  changes could be detected. The residuals of the Newton iteration around the bifurcation point were  $O(10^{-7})$ . The difference appears to be within the limits of numerical error and we can conclude that a double zero of the Jacobian does exist as predicted. We also calculated a non-symmetrical branch. The value of  $c$  vs  $b$  is shown on figure 5.3 as a dashed line. Its properties agreed to five significant figures with those of the symmetrical branch on making the identification of  $b$  and  $b'$ .

### 5.5 Discussion.

We have presented numerical evidence that permanent gravity waves of finite amplitude are not unique when their height is sufficiently large. Two new types of wave with wavelength  $L$  have been calculated, coming respectively from the bifurcation of regular wave trains of wavelength  $L/2$  and  $L/3$ . The bifurcation points were calculated by finding the values of a parameter  $b$  in the range  $(0,1)$  at which the Fréchet derivative of the equation defining the system for each value of  $b$  is singular and testing that a bifurcation criterion is satisfied. Branches were followed by Keller's method of pseudo arclength continuation.

The Fréchet derivative is calculated approximately by a discretization or truncation of the exact system. We have not proved convergence. However, the scheme appears to behave satisfactorily as the number of mesh points is changed and there is no reason to doubt that the results are genuine and not an artifact of the numerics. Three methods, of which one was very different from the others, have been employed and give consistent answers.

Important questions which remain unanswered are the existence of bifurcation at small values of  $h/\lambda$  and the possibility of bifurcation into genuinely non-symmetric solutions. Unfortunately, it appears that the latter type

of bifurcation, if it exists, is probably of high order and consequently difficult to detect, at least by the present method. Consider for example a wave of class 4. Suppose an infinitesimal perturbation onto a symmetric bifurcation branch changes the heights of the five crests in the window  $[0, 2\pi]$  by  $(\epsilon, \epsilon, -\epsilon, \epsilon, \epsilon)$ . On the new branch on the other side of the bifurcation point, the change would be  $(-\epsilon, -\epsilon, \epsilon, -\epsilon, -\epsilon)$ . These waves are physically distinct and hence  $dc/db \neq 0$  for this branch; but they are physically the same as  $(-\epsilon, \epsilon, \epsilon, \epsilon, -\epsilon)$  and  $(\epsilon, -\epsilon, -\epsilon, -\epsilon, \epsilon)$  respectively. Hence the bifurcation must be of second order. Similar arguments can be made for bifurcation into non-symmetric waves. Progress in answering the questions may therefore have to wait on the refinement of the techniques for detecting high order bifurcations.

APPENDIX A

Here we are going to prove that for capillary-gravity waves

$$2g\bar{\gamma} = -bc^2. \quad (\text{A.1})$$

The momentum conservation equations (1.1.2) and (1.2.3) can be written

$$u \frac{\partial u}{\partial x} + v \frac{\partial u}{\partial y} = - \frac{\partial(\rho + g\gamma)}{\partial x}; \quad u \frac{\partial v}{\partial x} + v \frac{\partial v}{\partial y} = - \frac{\partial(\rho + g\gamma)}{\partial y}, \quad (\text{A.2})$$

and from the continuity equation (1.1.1)

$$u \frac{\partial v}{\partial x} + v \frac{\partial v}{\partial y} = \frac{\partial}{\partial x}(uv) + \frac{\partial}{\partial y}(v^2). \quad (\text{A.3})$$

Integrating (A.3), and using Stokes' theorem

$$\int_0^1 \int_{-\infty}^{\gamma} \left[ \frac{\partial}{\partial x}(uv) + \frac{\partial}{\partial y}(v^2) \right] dx dy = \oint uv dy - v^2 dx. \quad (\text{A.4})$$

Since the top and bottom of the circuit are streamlines along which  $u dy - v dx$ , no contribution results from the integration along these parts. As  $v$  is periodic, the contribution of the remaining two portions cancel so that the integral is zero.

Hence,

$$0 = \iint \left[ u \frac{\partial v}{\partial x} + v \frac{\partial v}{\partial y} \right] dx dy = - \iint \frac{\partial(\rho + g\gamma)}{\partial y} dx dy = \oint (\rho + g\gamma) ds = 0. \quad (\text{A.5})$$

Since  $\rho + g\gamma$  is periodic, the last equality of (A.5) gives

$$\int_0^L (p + gY) dx = \int_0^L (p_1 - gD) dx. \quad (\text{A.6})$$

Here for simplicity, we are supposing for the moment that the bottom is the horizontal line  $y = -D$ , where the pressure is  $p_1$ . As before the surface is  $y = Y$  and the pressure there is  $p$ .

Therefore

$$\int_0^L (p - p_1) dx = -g \int_0^L (Y + D) dx = -gL(D + \bar{Y}). \quad (\text{A.7})$$

By comparing pressures in the same vertical line

$$\frac{1}{2} q^2 + p + gY = \frac{1}{2} c^2 + p_1 - gD = c^2 \frac{(1-b)}{2} \quad (\text{A.8})$$

or

$$p - p_1 = -g(Y + D) + \frac{1}{2} (c^2 - q^2). \quad (\text{A.9})$$

Integrating from 0 to L we have

$$\int_0^L q^2 dx = c^2 L. \quad (\text{A.10})$$

Thus, from integrating Bernoulli's equation (A.8) along the surface we have

$$2g\bar{Y} = -bc^2 \quad (\text{A.11})$$

since

$$\int_0^L p dx = -T \int_0^L \frac{1}{R} dx = -T \int_0^L \frac{Y_{xx}}{(1+Y_x^2)^{3/2}} dx = 0. \quad (\text{A.12})$$

APPENDIX B

We will now prove the relation

$$\frac{\partial}{\partial b} (K+V_g) = -c \frac{\partial I}{\partial b} . \quad (\text{B.1})$$

Using (1.3.1), (1.3.2) and (1.3.6) we have

$$\begin{aligned} L \frac{\partial}{\partial b} (K+V_g) &= \frac{\partial}{\partial b} \left\{ \int_0^L \int_{-\infty}^Y \frac{1}{2} (\Phi_x^2 + \Phi_y^2) dy dx + \frac{1}{2} g \int_0^L (\Upsilon - \bar{\Upsilon}) dx \right\} = \\ &= \int_0^L \left\{ \int_{-\infty}^Y (\Phi_x \frac{\partial \Phi_x}{\partial b} + \Phi_y \frac{\partial \Phi_y}{\partial b}) dy + \left[ \frac{1}{2} \frac{\partial \Upsilon}{\partial b} (\Phi_x^2 + \Phi_y^2) + g \Upsilon \frac{\partial \Upsilon}{\partial b} \right]_{y=Y} \right. \\ &\quad \left. - g \bar{\Upsilon} \frac{\partial \bar{\Upsilon}}{\partial b} \right\} dx . \end{aligned} \quad (\text{B.2})$$

The kinematic and dynamic boundary conditions (1.1.7) and (1.1.10) can be written as

$$\frac{(\Phi_x + c)^2 + \Phi_y^2}{2} + g \Upsilon = \frac{c^2(1-b)}{2} , \quad (\text{B.3})$$

$$-\Upsilon_x \Phi_x + \Phi_y = c \Upsilon_x . \quad (\text{B.4})$$

For  $\Upsilon=0$  ,  $\Upsilon$  is a well defined function of  $x$  . Therefore

$$\begin{aligned} L \frac{\partial}{\partial b} (K+V_g) &= \int_0^L \left\{ \int_{-\infty}^Y \left[ \frac{\partial}{\partial x} (\Phi_x \Phi_b) + \frac{\partial}{\partial y} (\Phi_y \Phi_b) \right] dy - \frac{\partial \Upsilon}{\partial b} [c \Phi_x + c^2 b]_{y=Y} - g \bar{\Upsilon} \frac{\partial \bar{\Upsilon}}{\partial b} \right\} dx \\ &= \oint (\Phi_y \Phi_b dx - \Phi_x \Phi_b dy) - \int_0^L c \Phi_x \frac{\partial \Upsilon}{\partial b} dx + g \bar{\Upsilon} \frac{\partial}{\partial b} \int_0^L \Upsilon dx - g \bar{\Upsilon} \frac{\partial \bar{\Upsilon}}{\partial b} L . \end{aligned} \quad (\text{B.5})$$

Here we used equation (A.1) and that  $\Phi$  is harmonic. As before, only the integral along the surface is non-zero.

$$\begin{aligned} L \frac{\partial}{\partial b} (K+V_g) &= \int_0^L \Phi_b (\Phi_y - \Phi_x \gamma_x) dx - c \int_0^L \gamma_b \Phi_x dx = \\ &= c \int_0^L [\Phi_b \gamma_x - \gamma_b \Phi_x] dx. \end{aligned} \quad (\text{B.6})$$

In the last equality we used (B.4).

Now

$$\begin{aligned} L \frac{\partial I}{\partial b} &= \frac{\partial}{\partial b} \left\{ \int_0^L \int_{-\infty}^Y \Phi_x dy dx \right\} = \int_0^L \left\{ \int_{-\infty}^Y \Phi_{xb} dy + \left[ \frac{\partial Y}{\partial b} \Phi_x \right]_{y=Y} \right\} dx = \\ &= \int_0^L \left\{ \frac{\partial}{\partial x} \left( \int_{-\infty}^Y \Phi_b dy \right) - [\gamma_x \Phi_b]_{y=Y} + [\gamma_b \Phi_x]_{y=Y} \right\} dx = \\ &= \int_0^L (\gamma_b \Phi_x - \gamma_x \Phi_b)_{y=Y} dx. \end{aligned} \quad (\text{B.7})$$

In obtaining the last equality we used that

$$\int_0^L \frac{\partial}{\partial x} \left( \int_{-\infty}^Y \Phi_b dy \right) dx = \int_{-\infty}^Y \Phi_b dy \Big|_{x=L} - \int_{-\infty}^Y \Phi_b dy \Big|_{x=0} = 0 \quad (\text{B.8})$$

by periodicity.

Comparison of (B.6) and (B.7) gives the desired relation (B.1).

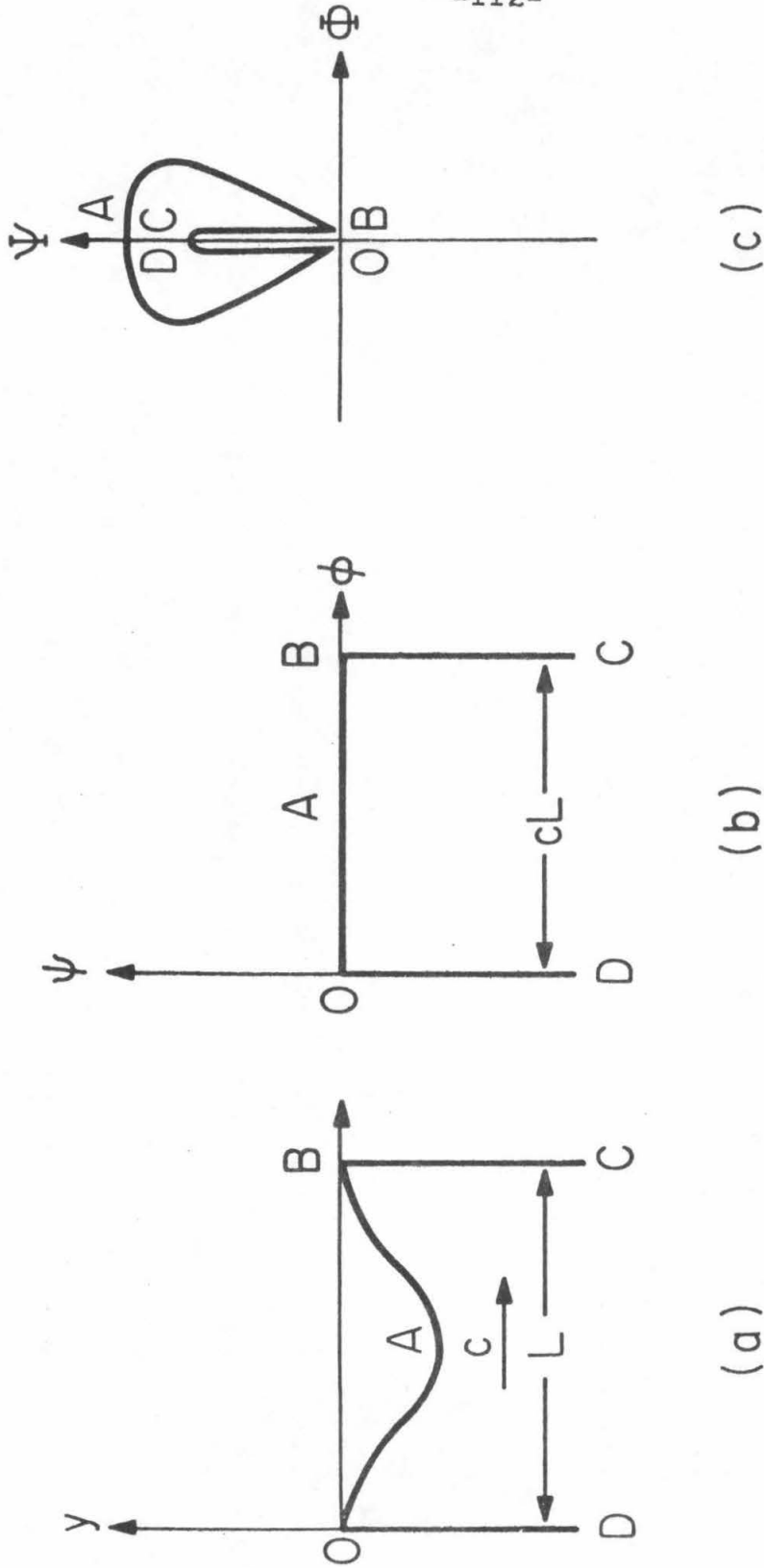


Figure 1. Sketch of the physical and potential planes. (a) Physical plane. (b) Potential plane relative to the wave. (c) Potential plane relative to the fluid.

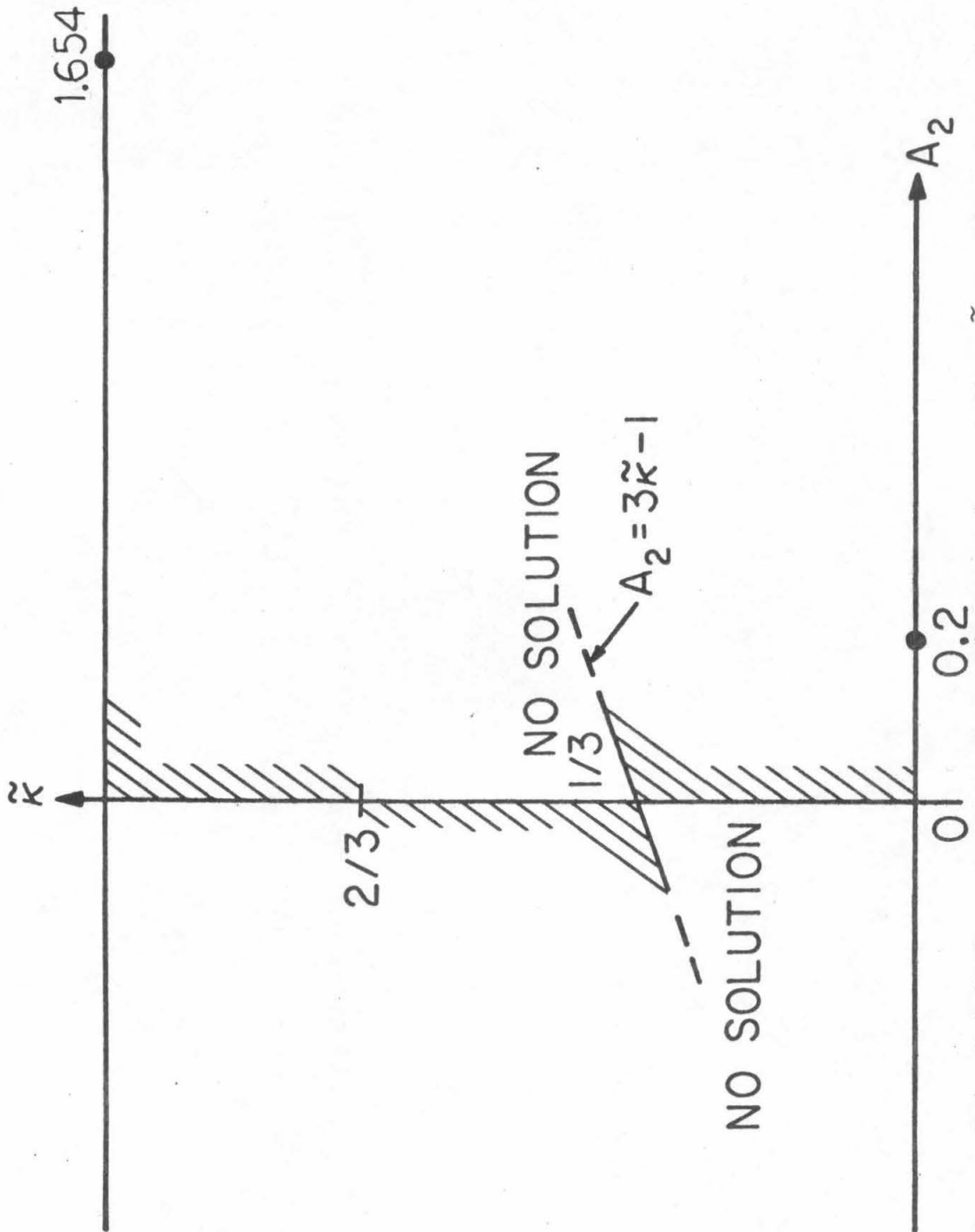
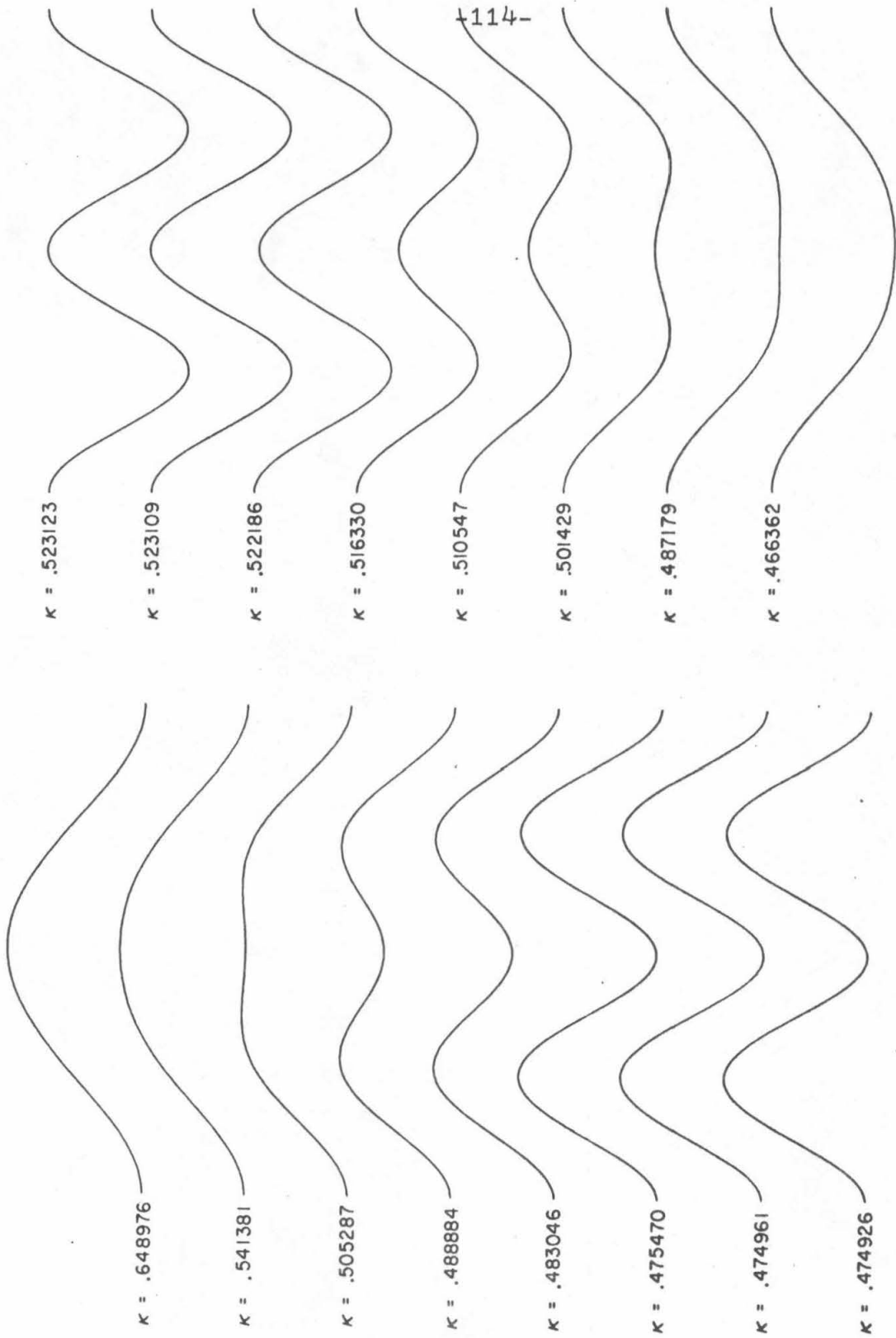


Figure 2.1. Hatched areas show accessible region of the  $\tilde{\kappa}, A_2$  plane for combination (1,2) waves and pure waves of degree 1. The dots on the  $\tilde{\kappa}=0$  and  $\tilde{\kappa}=1$  lines show the values for the limiting gravity and capillary waves of greatest height.



(a)  
 Figure 2.2. Combination (1,2) waves near  $k=1/2$ . (a) Capillary side waves with  $A_1 + \frac{1}{2}A_2 = -0.016$ . (b) Gravity side waves with  $A_1 + \frac{1}{2}A_2 = 0.016$ . Vertical scale is magnified 54 times.

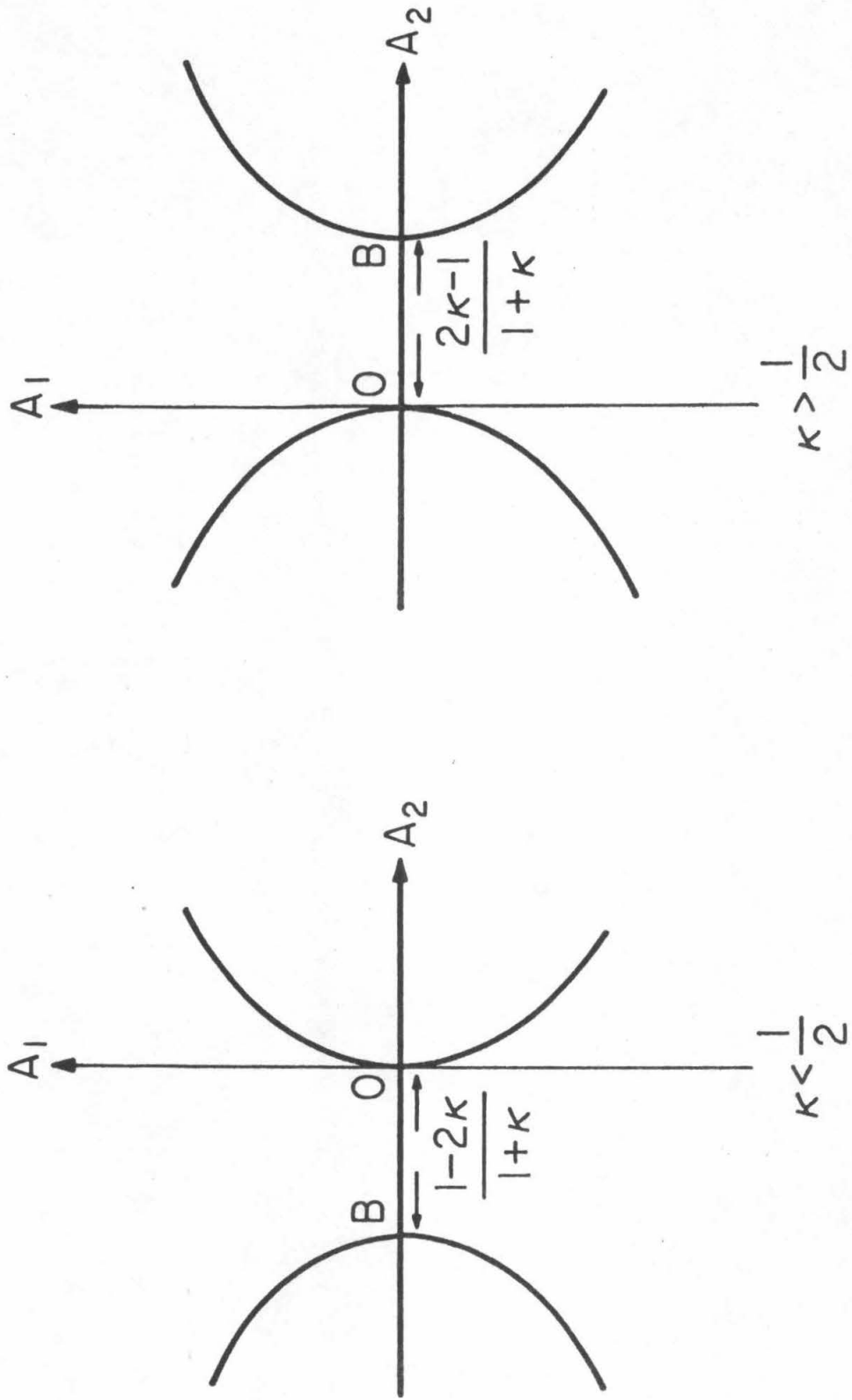


Figure 2.3. Loci of values of  $A_1$  as a function of  $A_2$  as given by equation (2.2.7). Finite amplitude bifurcation points marked by B. The origin is the trivial bifurcation point for infinitesimal waves.

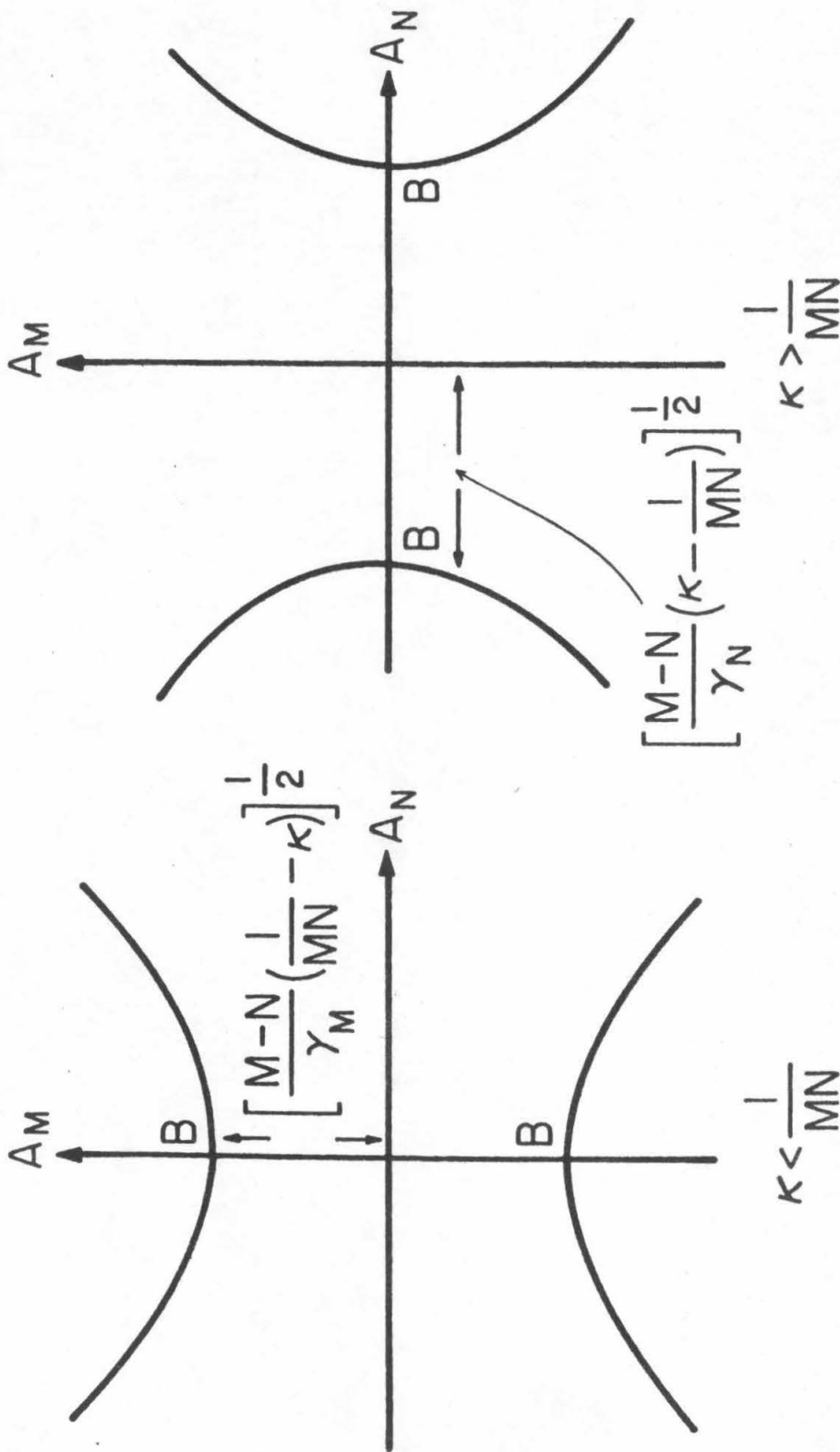


Figure 2.4. Sketch of relation between  $A_M$  and  $A_N$  in vicinity of  $\kappa = 1/MN$  for  $\frac{1}{2}M < N < M$ . The axes are pure waves of degree  $N$  or  $M$ . The hyperbolae (equation (2.4.10)) are combination  $(M,N)$  waves.  $B$  denotes finite amplitude bifurcation points.

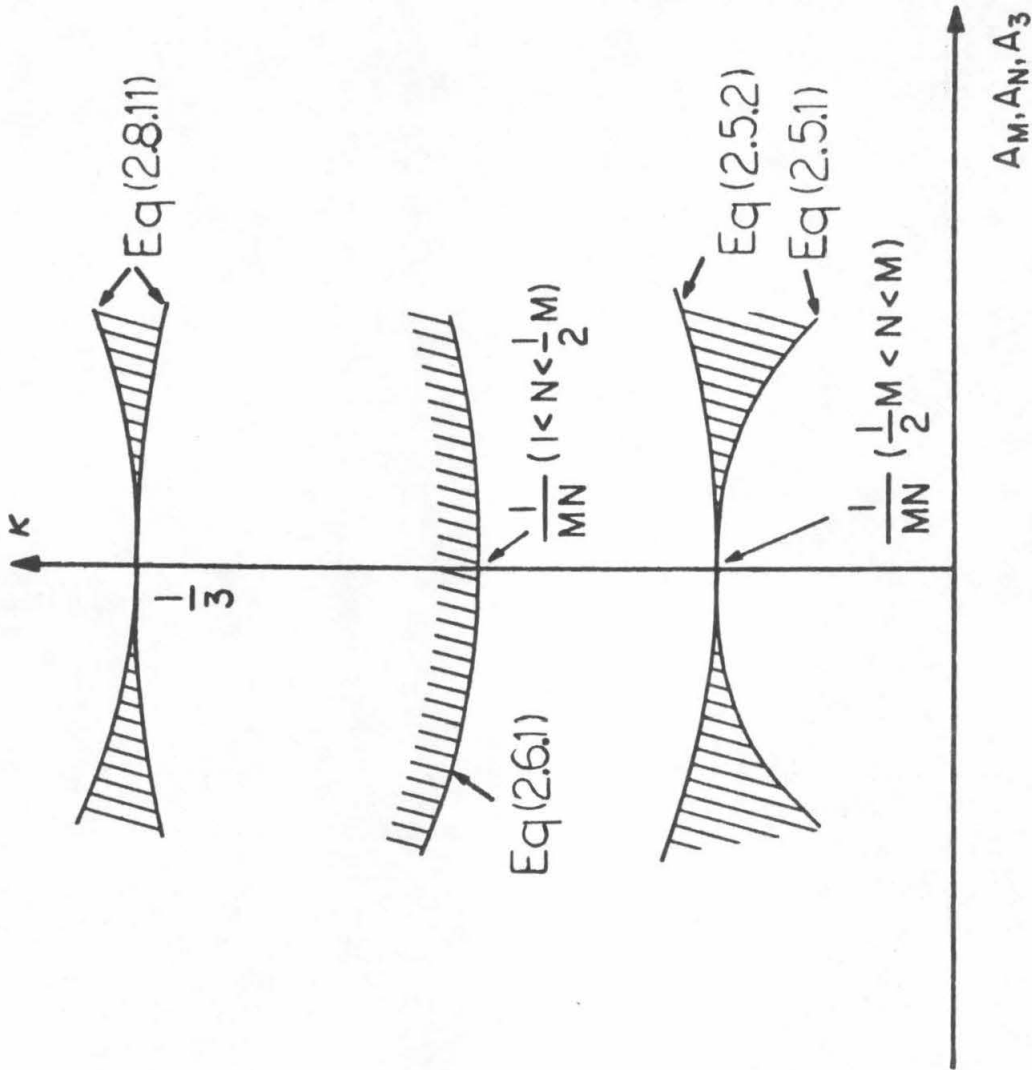


Figure 2.5. Sketch showing accessible regions (hatched) of the  $\kappa, A_M$  or  $A_N$  planes for combination  $(M, N)$  waves and  $\frac{1}{2}M < N < M$  or  $1 < N < \frac{1}{2}M$  ( $M \geq 5$ ) in the vicinity of  $\kappa = 1/3$ . Also shown is the region where three (1,3) waves exist near  $\kappa = 1/3$ .

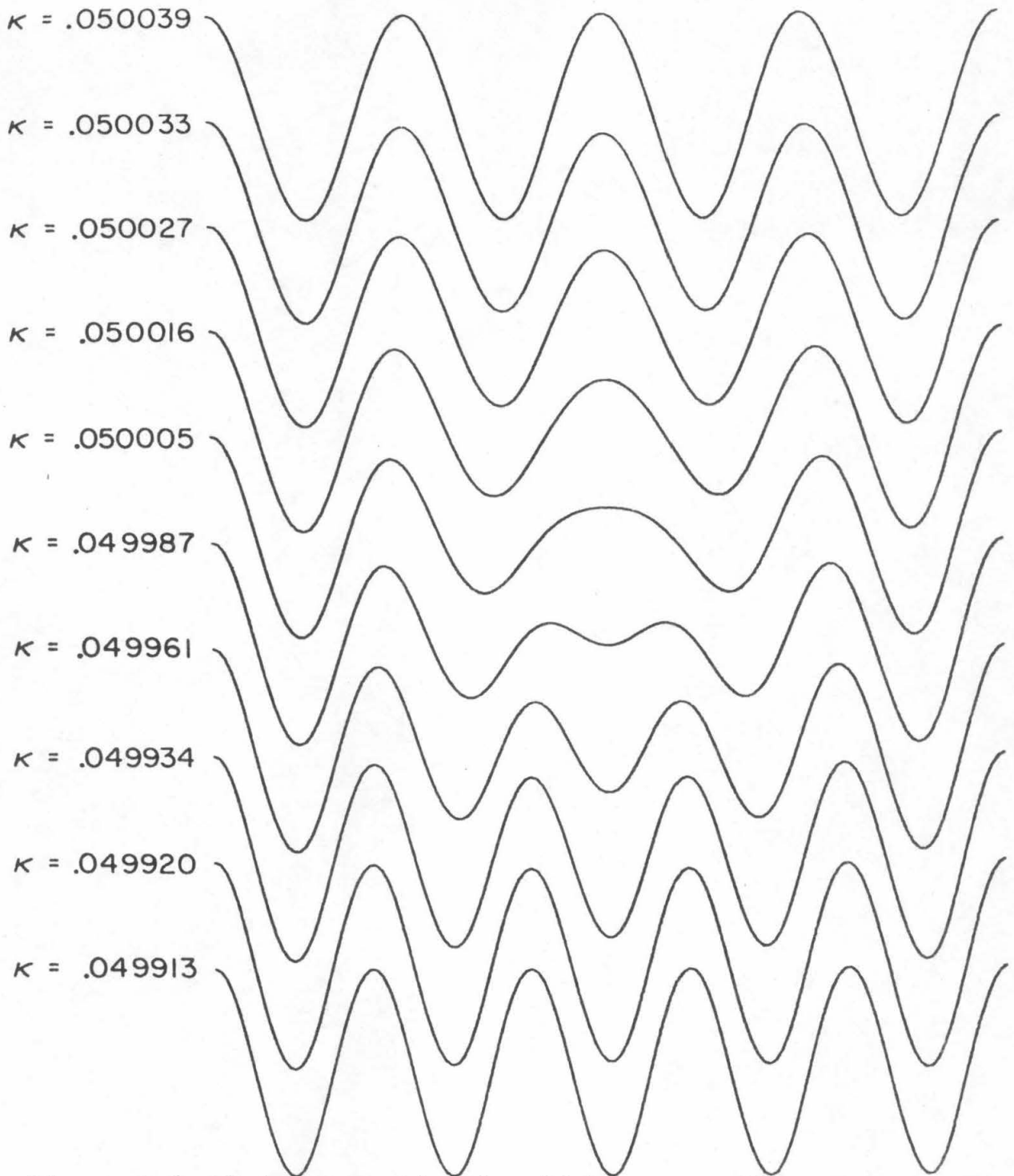
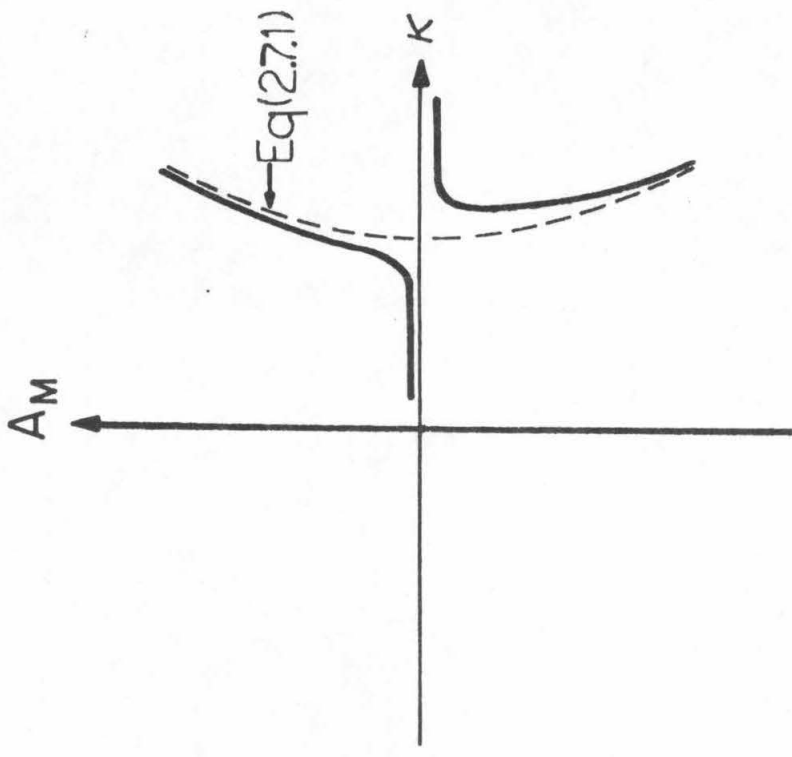
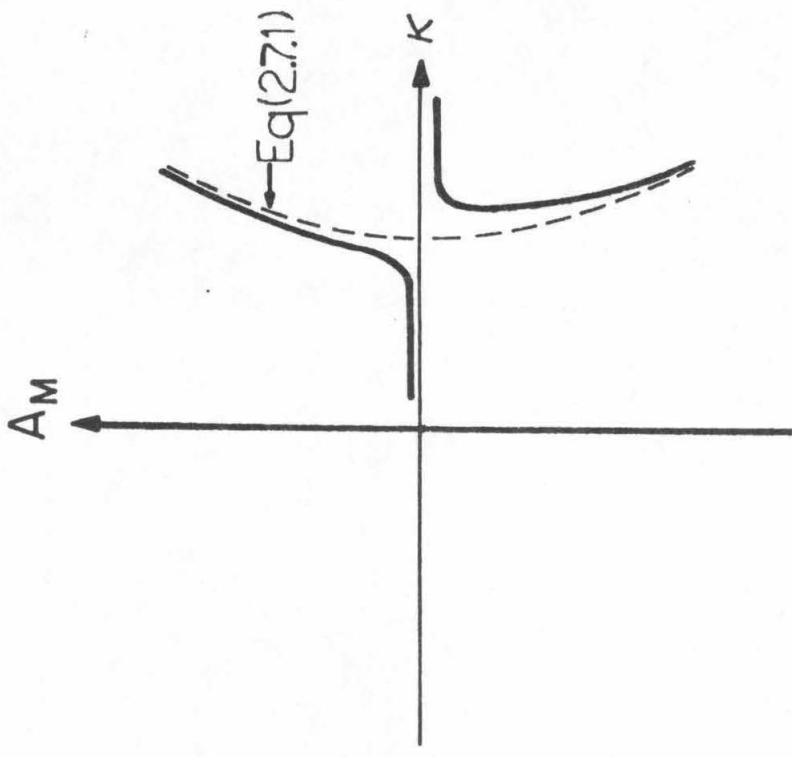


Figure 2.6. Plots of combination (5,4) waves with  $A_4/4 + A_5/5 = 0.00267$  near  $\kappa = 1/20$ , showing smooth transition from a pure wave of degree 5 to one of degree 4 and vice versa. Vertical scale is magnified 333 times.

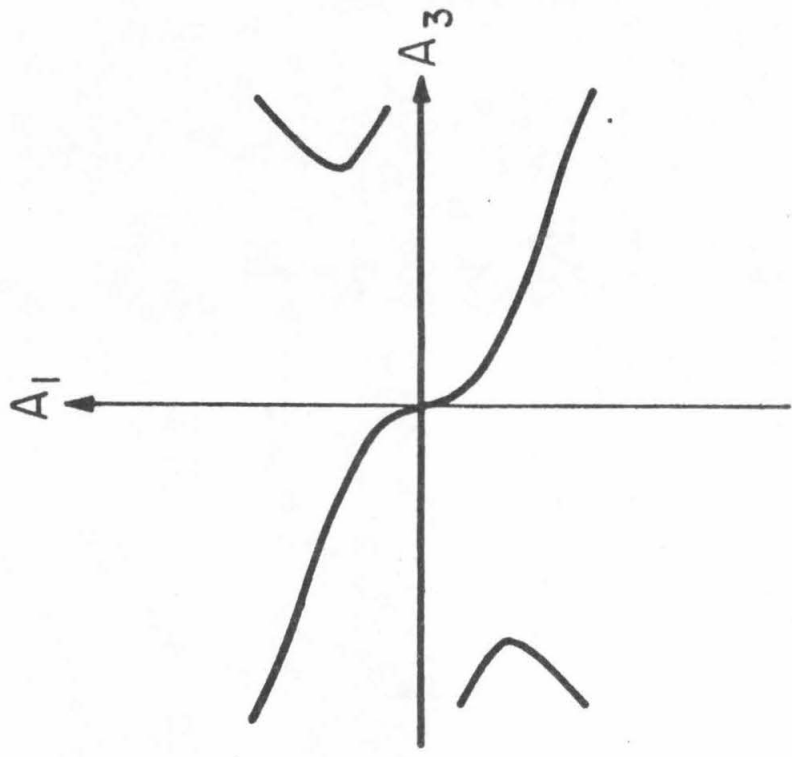


(a)

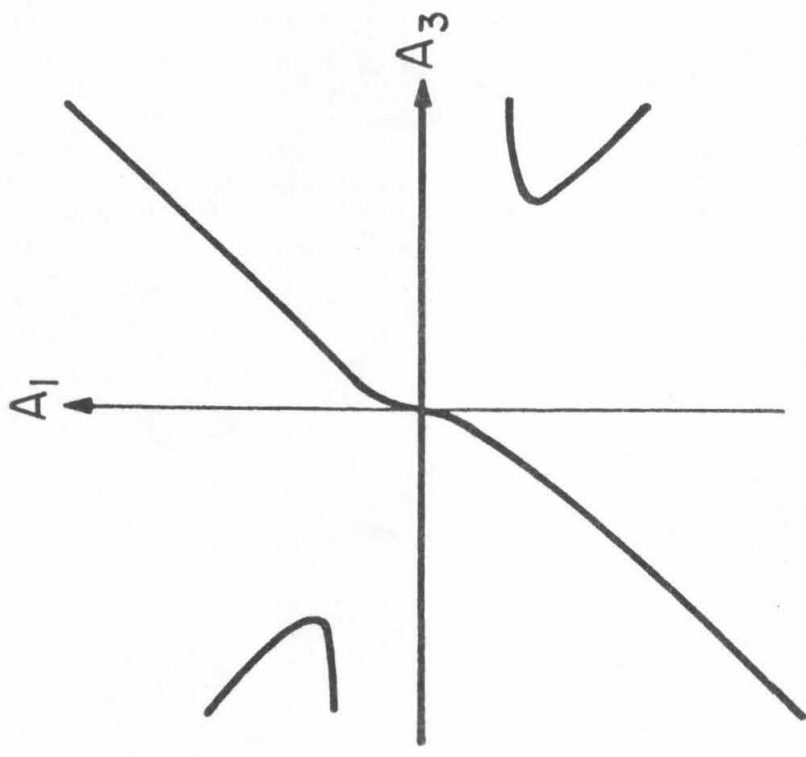


(b)

Figure 2.7. Sketch of the relations between  $A_1$ ,  $A_M$  and  $\kappa$  in the vicinity of  $\kappa = 1/M$ . (a) Relation between  $A_M$  and  $A_1$  for  $\kappa = \text{constant}$ . (b) Relation between  $A_M$  and  $\kappa$  for  $A_1 = \text{constant}$ .



$$\kappa > \frac{1}{3}$$



$$\kappa < \frac{1}{3}$$

Figure 2.8. Relation between  $A_1$  and  $A_3$  for combination (1,3) waves near  $\kappa=1/3$ .

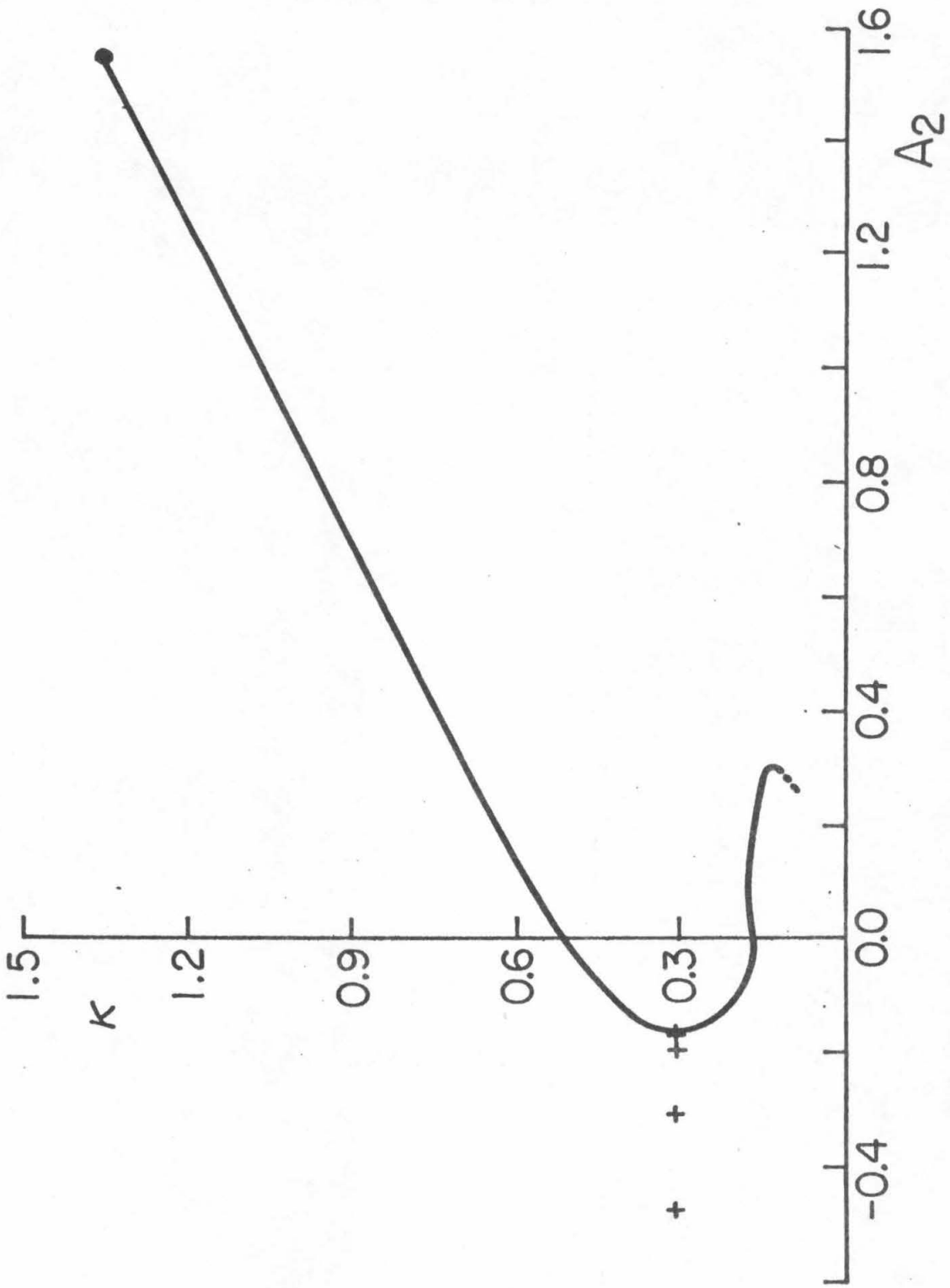


Figure 4.1. Sketch of the  $2 \rightarrow 1$  and  $2 \rightarrow 3$  bifurcation line in the  $\kappa, A_2$  plane. The dot shows the wave of maximum height. The dash line indicates that the line continues. + signs represent the solutions plotted in figure 4.3.

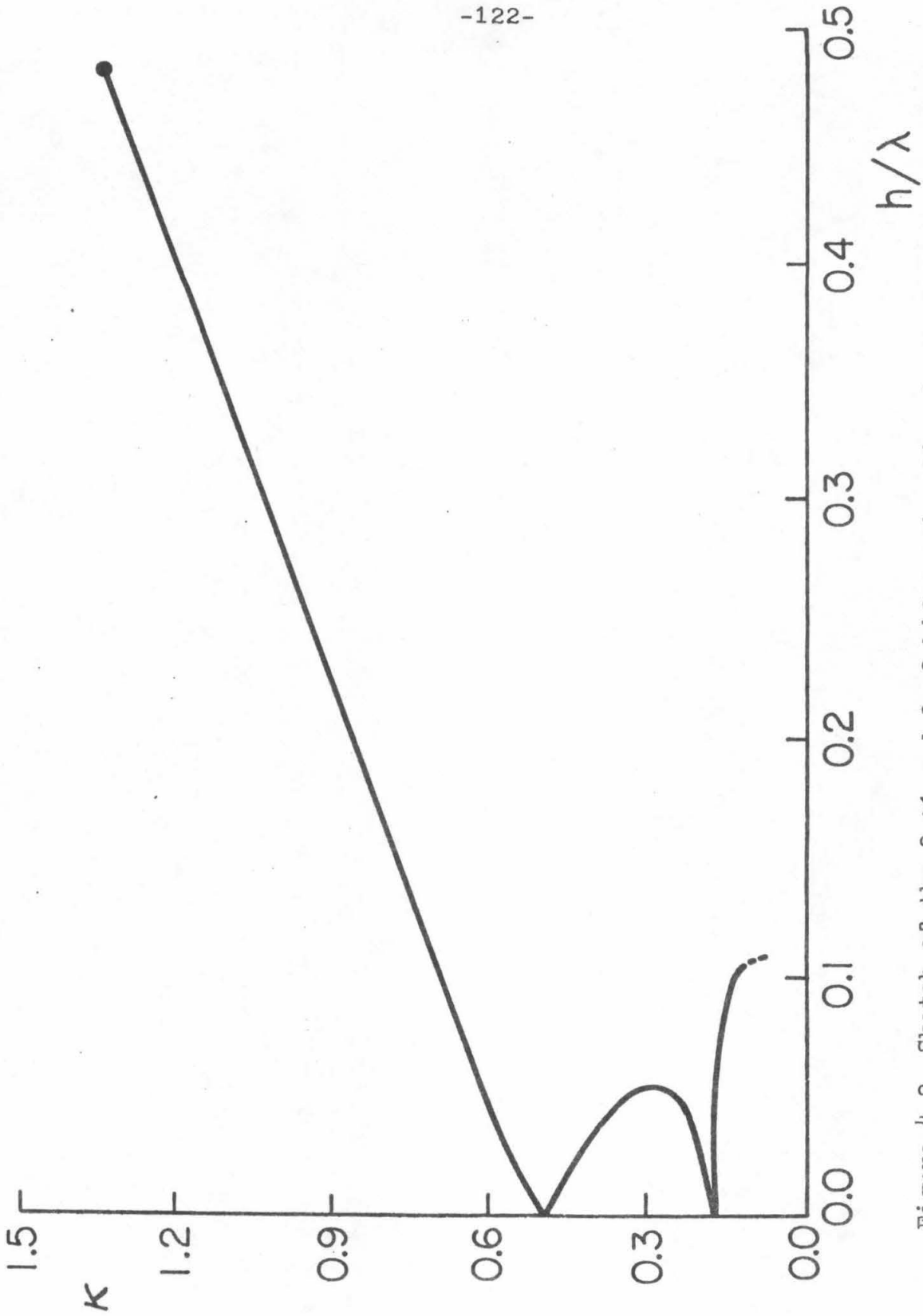


Figure 4.2. Sketch of the  $2 \rightarrow 1$  and  $2 \rightarrow 3$  bifurcation line in the  $\kappa, h/\lambda$  plane. In this case,  $\kappa = \pi^2 T / g \lambda^2$ .

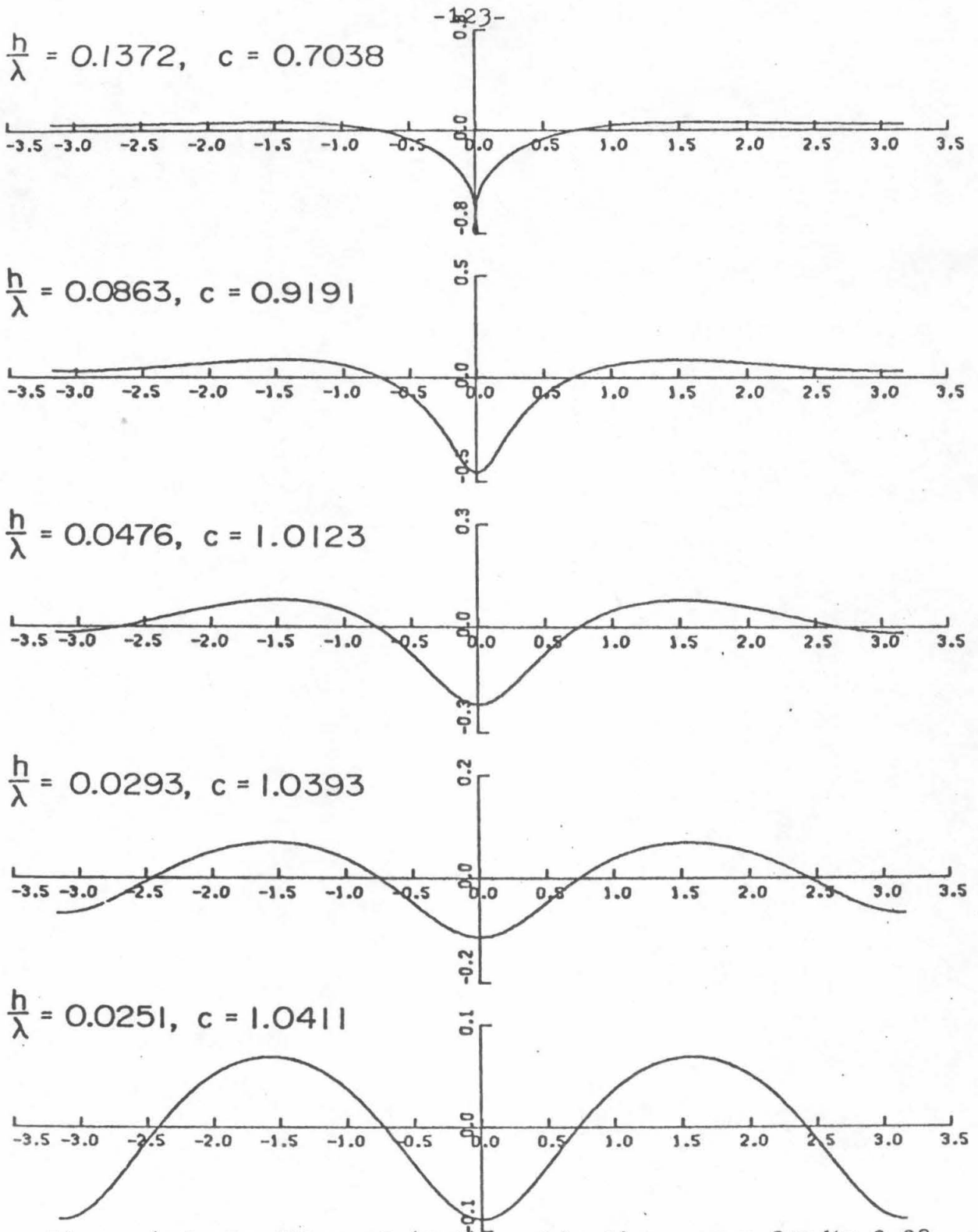


Figure 4.3. Profiles of (2,1) combination waves for  $\kappa = 0.03$ . The lowest profile corresponds to just after the bifurcation point and the top one to the highest wave. The  $\gamma$  origin is at  $\bar{\gamma}$ .

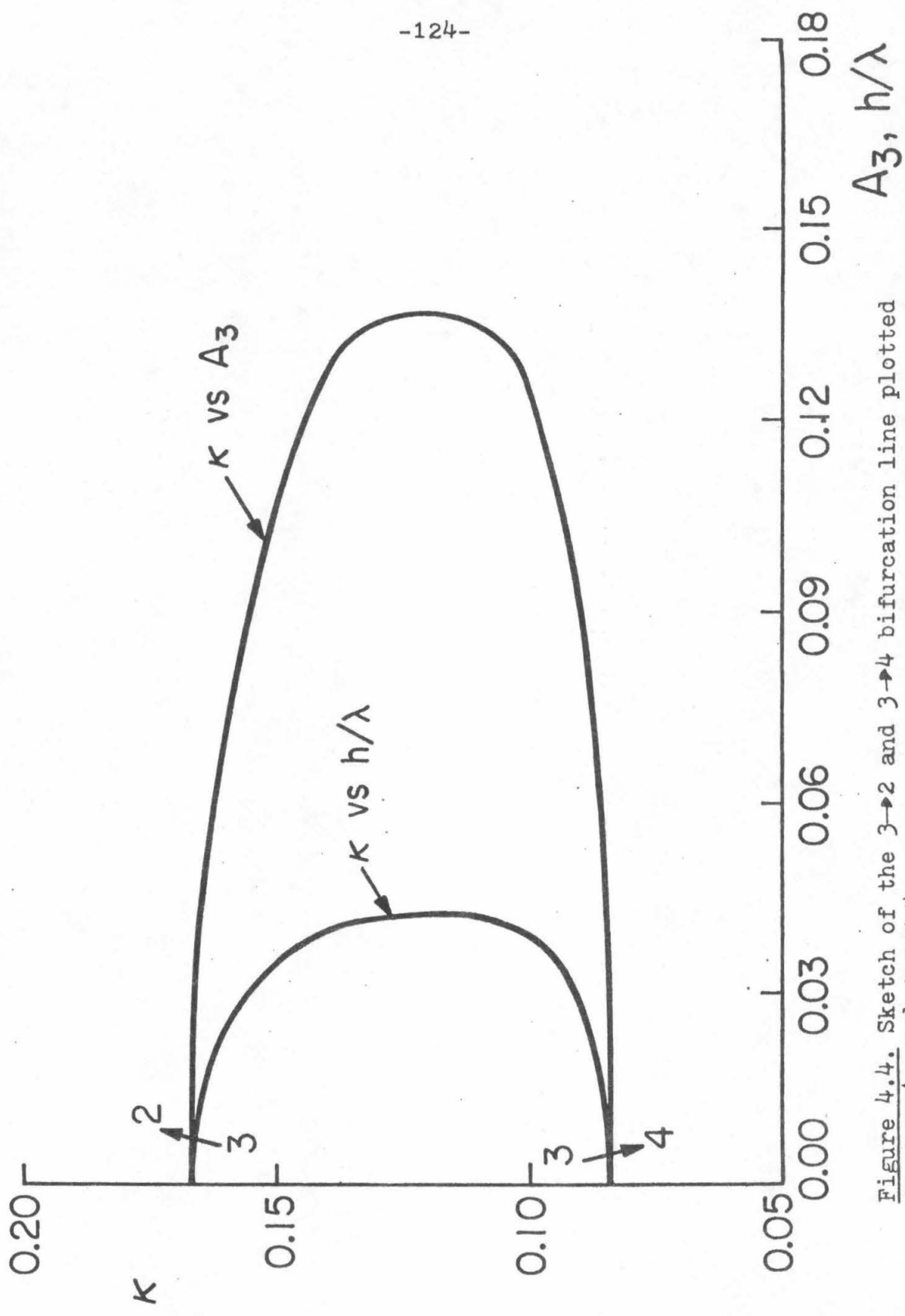
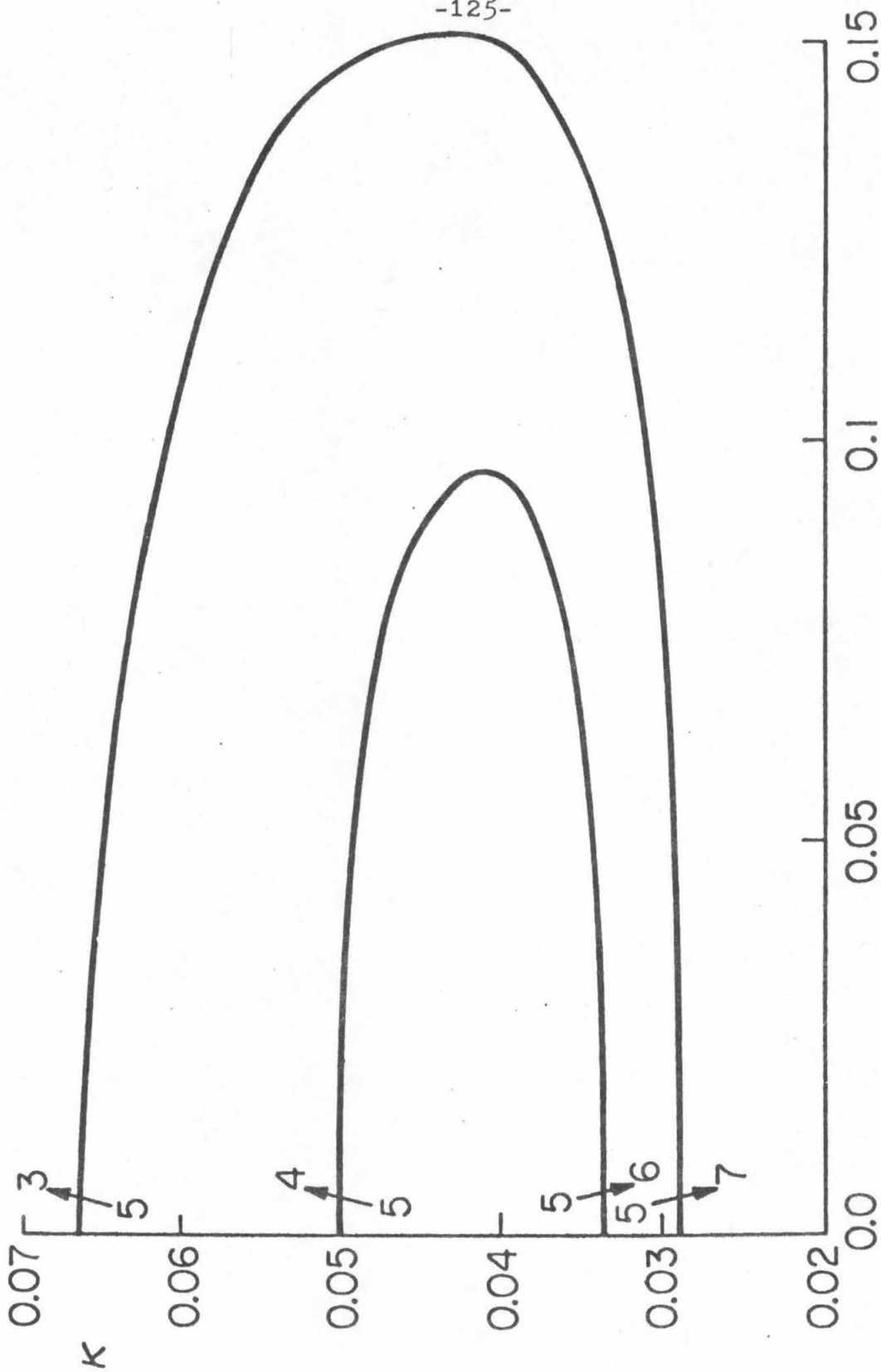


Figure 4.4. Sketch of the  $3 \rightarrow 2$  and  $3 \rightarrow 4$  bifurcation line plotted as  $\kappa$  vs  $A_3$  and  $\kappa$  vs  $h/\lambda$ .



A5

Figure 4.5. Sketch of the  $5 \rightarrow 3$ ,  $5 \rightarrow 4$ ,  $5 \rightarrow 6$  and  $5 \rightarrow 7$  bifurcation lines in the  $\kappa, A_5$  plane.

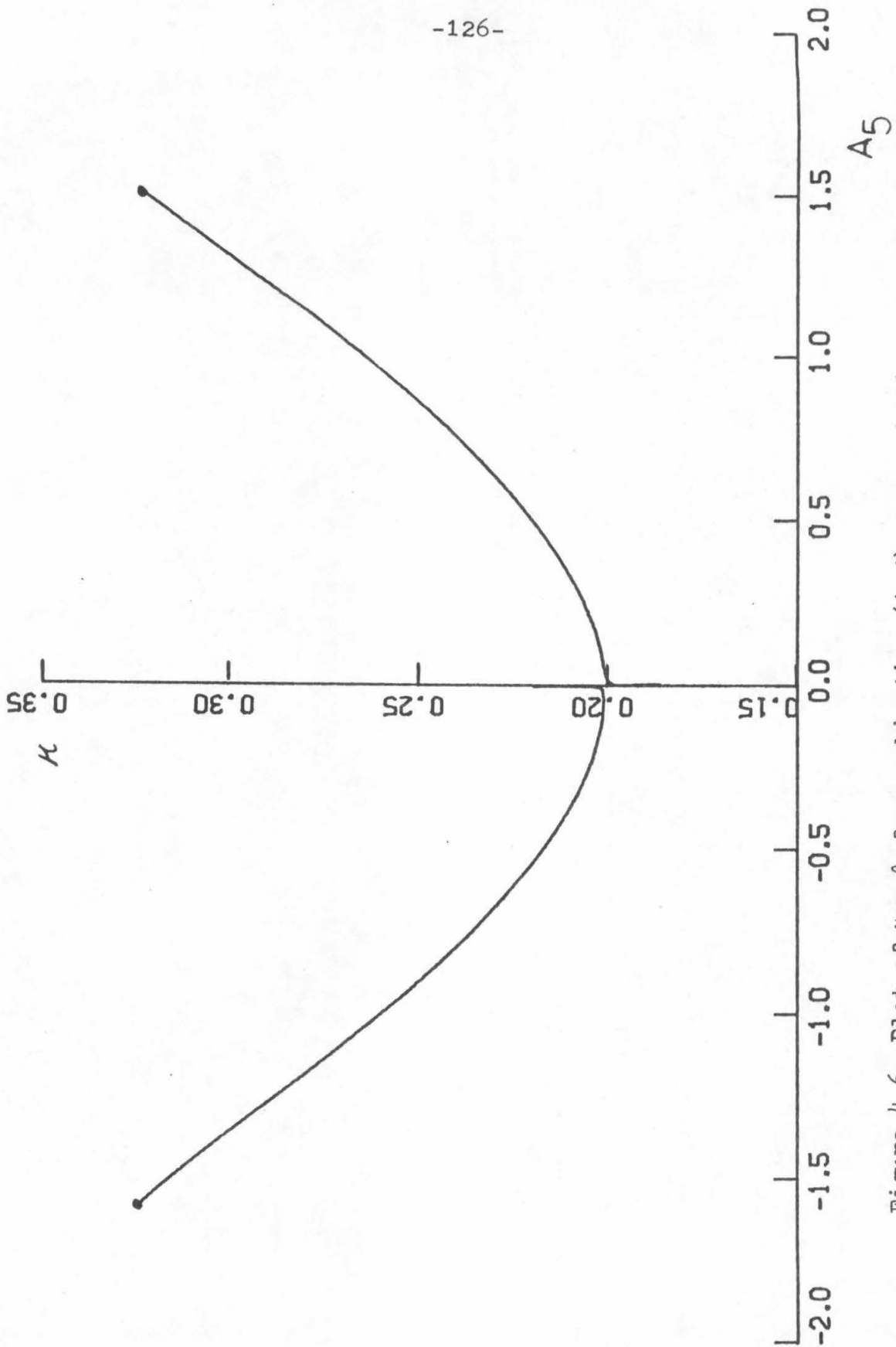
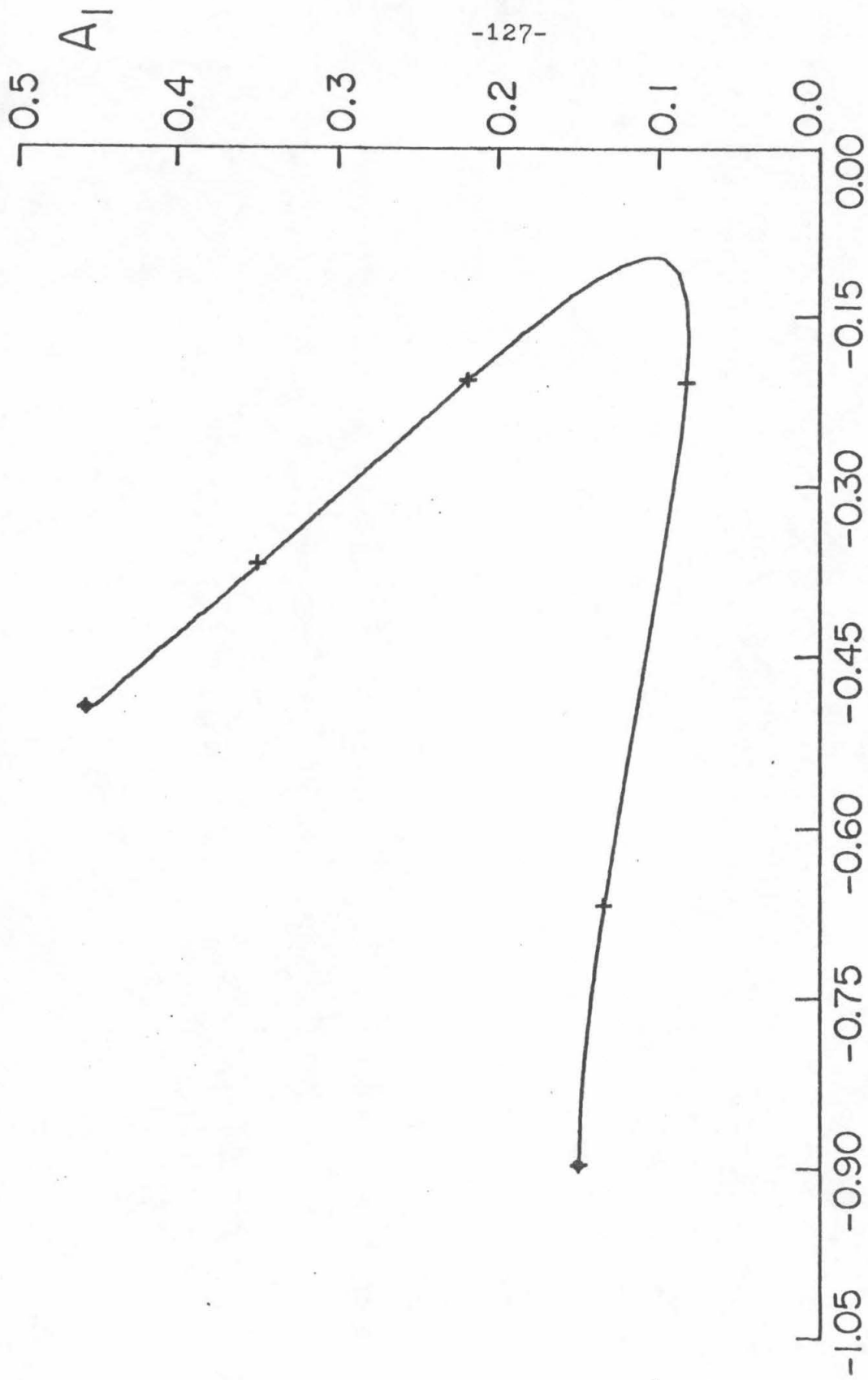


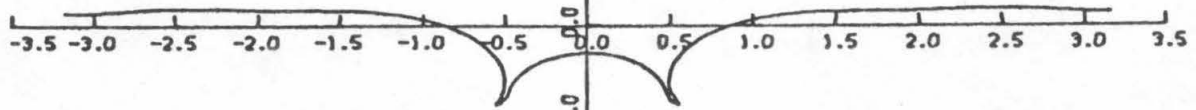
Figure 4.6. Plot of  $\kappa$  vs  $A_5$  for combination (1,5) waves with  $A_1 = 0.05$ . The dots represent waves of maximum height.



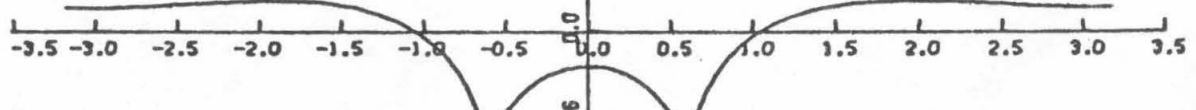
A3

Figure 4.7. Plot of  $A_1$  vs  $A_2$  for a (1,3) combination wave with  $\kappa=0.316$ . The dots represent waves of maximum height. The + signs represent the solutions of figure 4.8.

$\frac{h}{\lambda} = 0.1433, A_1 = 0.1507,$   
 $c = 0.8987$



$\frac{h}{\lambda} = 0.1087, A_1 = 0.1340,$   
 $c = 1.0443$



$\frac{h}{\lambda} = 0.0438, A_1 = 0.0818,$   
 $c = 1.1256$



$\frac{h}{\lambda} = 0.0723, A_1 = 0.2165,$   
 $c = 1.0845$



$\frac{h}{\lambda} = 0.1081, A_1 = 0.3354,$   
 $c = 1.0053$



$\frac{h}{\lambda} = 0.1422, A_1 = 0.4527,$   
 $c = 0.8541$



Figure 4.8. Profiles of (1,3) combination waves with  $\kappa = 0.316$ , for different points on the  $A_1$  vs  $A_3$  diagram of figure 4.7. y origin is at mean water level.

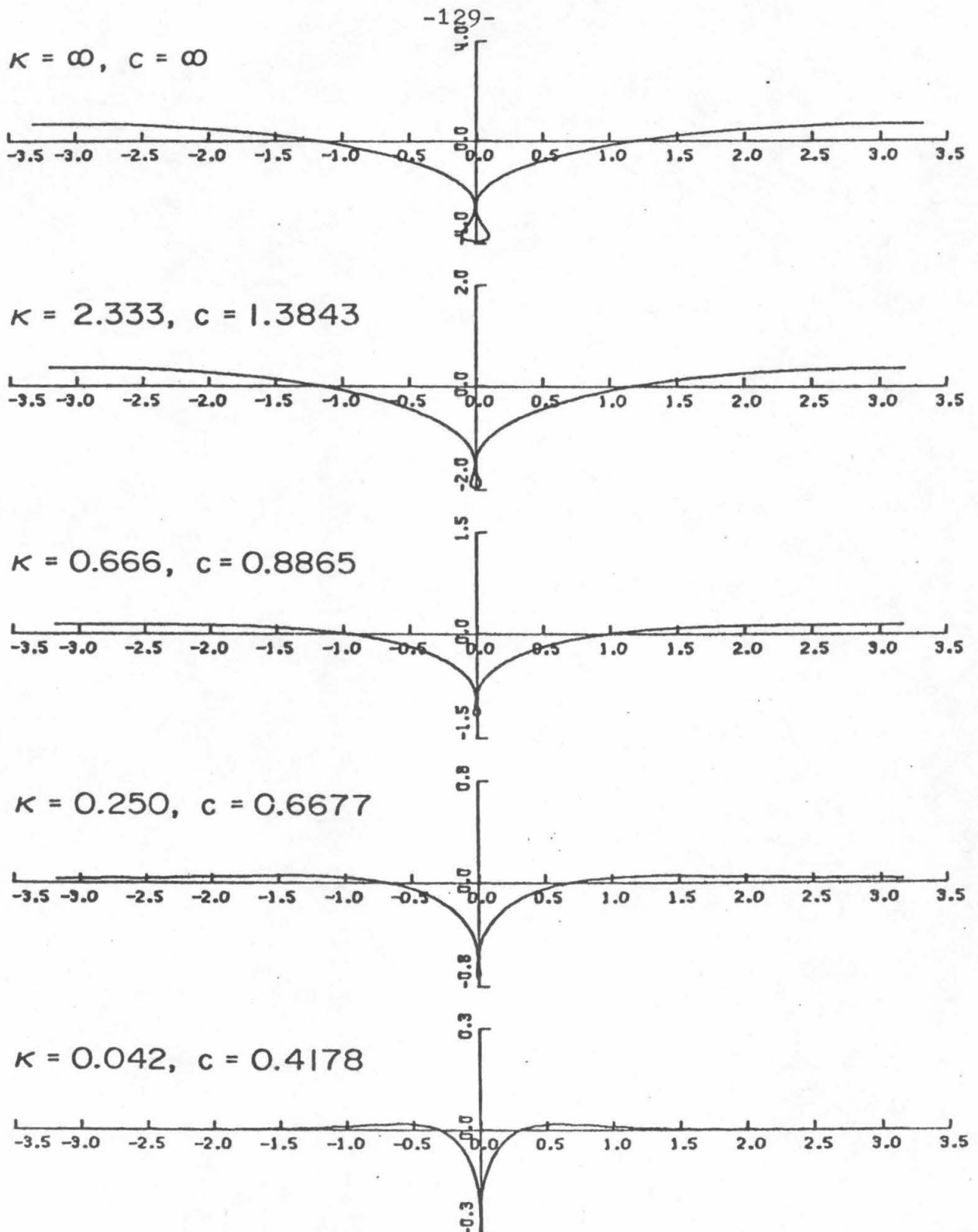


Figure 4.9. Profiles of waves of maximum height for  $\kappa = \infty, 2.333, 0.666, 0.250$  and  $0.042$ . These waves are the analytic continuation of Crapper's limiting solution.  $y$  origin is at  $\bar{Y}$ .

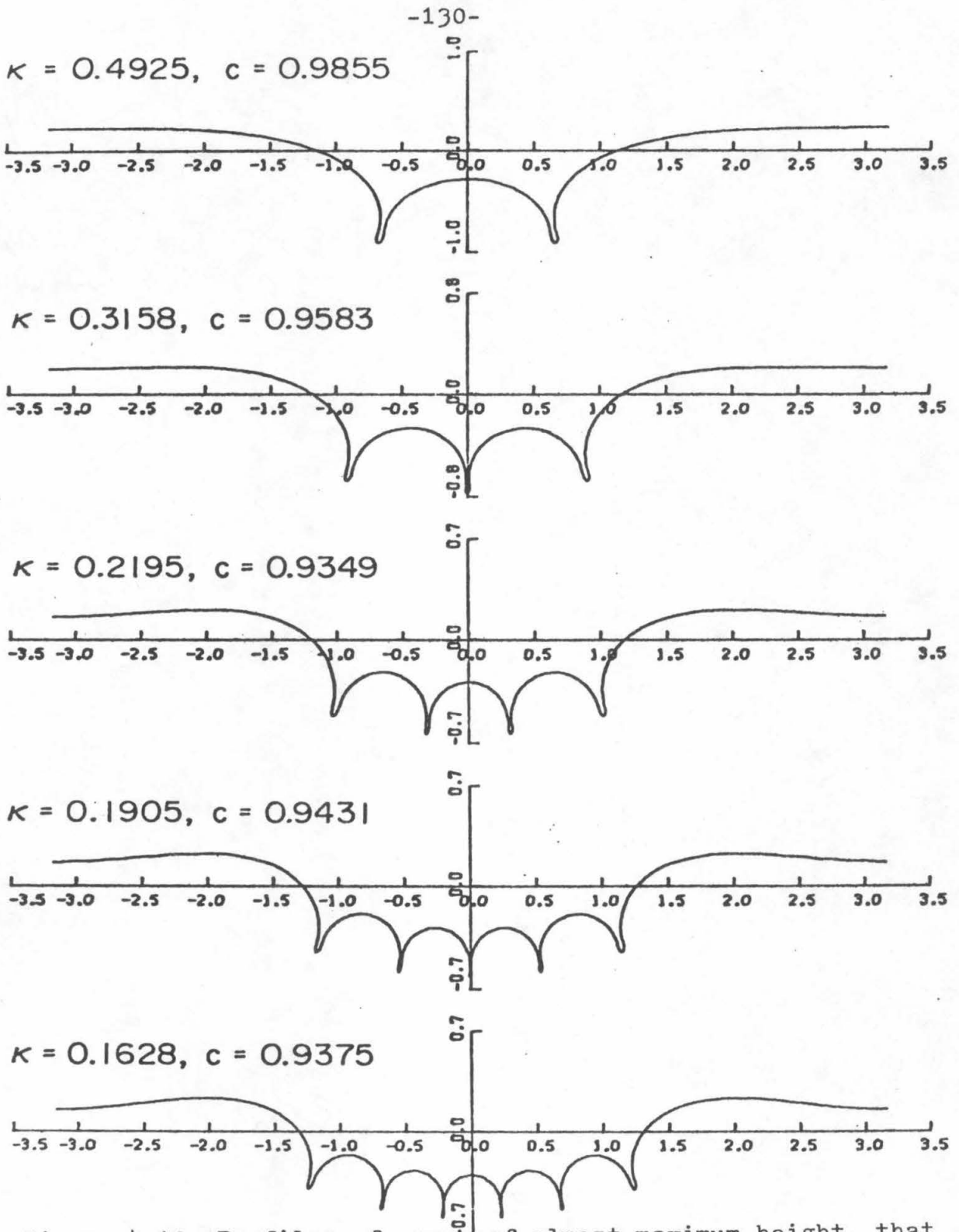


Figure 4.10. Profiles of waves of almost maximum height, that are the analytic continuation of pure waves of degree 1, for several values of  $\kappa$ . Origin is at mean water level.

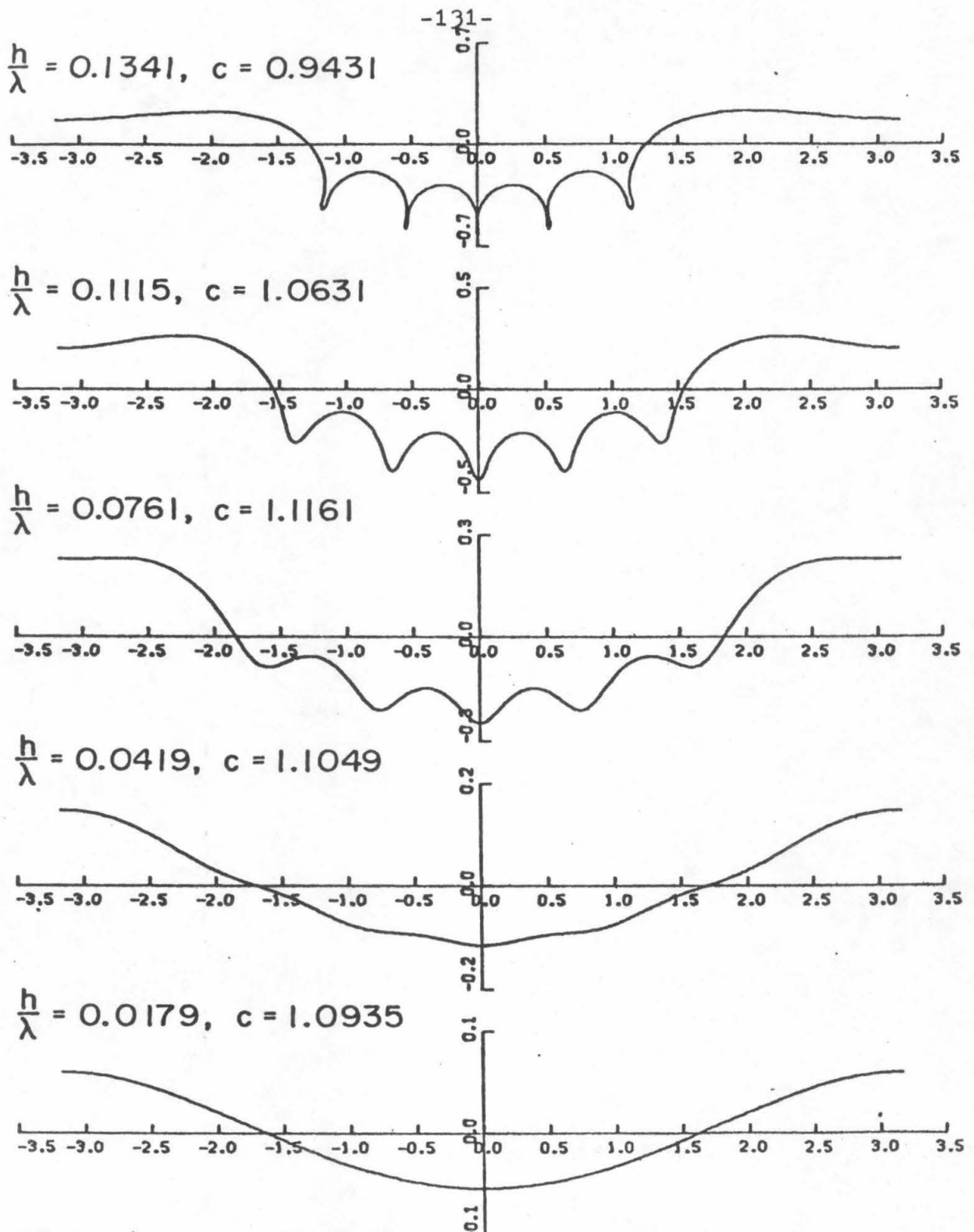


Figure 4.11. Profiles for different heights for a wave with  $\kappa = 0.190$  that started as a pure wave of degree 1 for small amplitude. Origin is at mean water level.

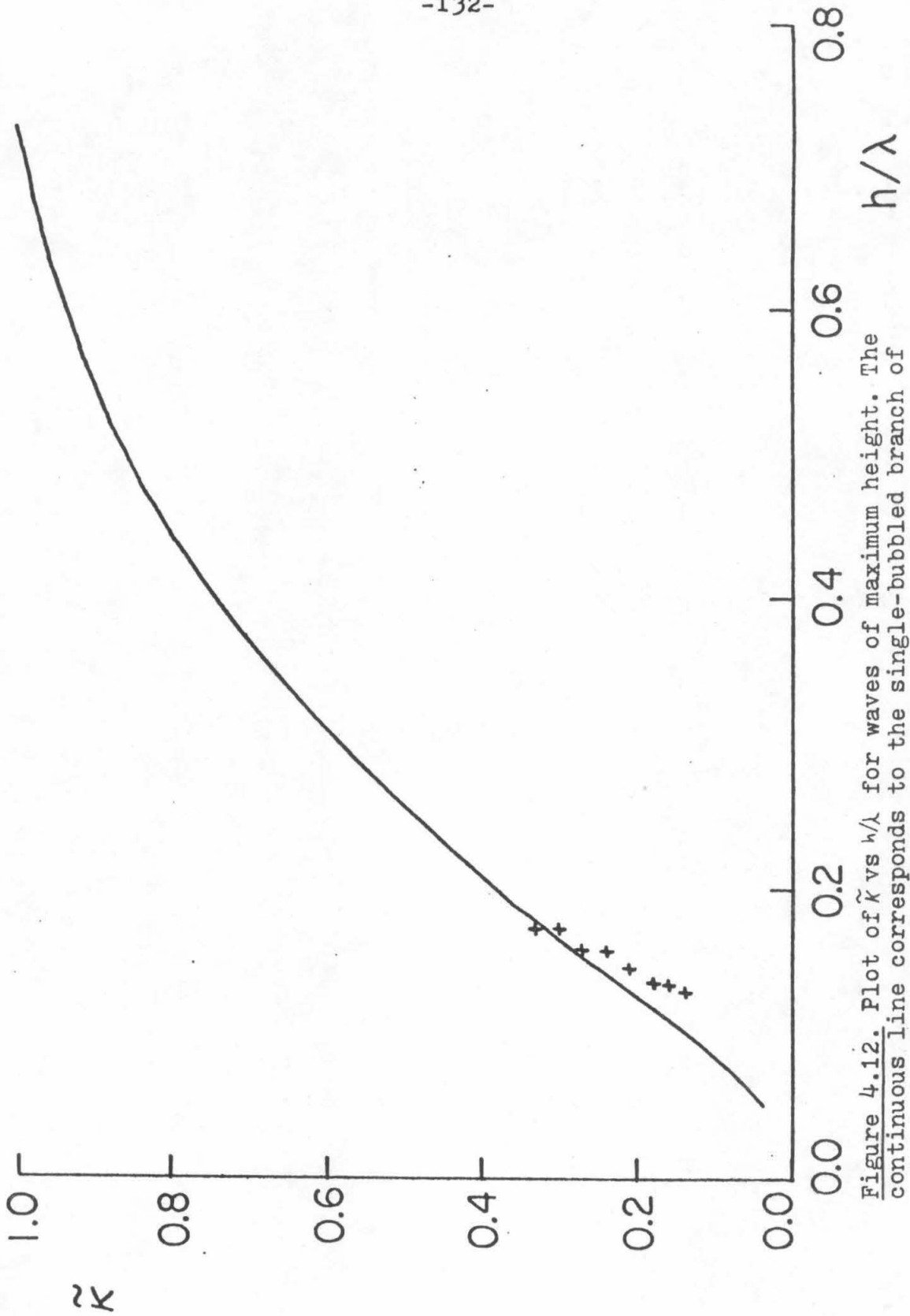


Figure 4.12. Plot of  $\tilde{k}$  vs  $h/\lambda$  for waves of maximum height. The continuous line corresponds to the single-bubbled branch of solutions which includes Crapper's solution. The + signs correspond to multi-bubbled waves that started as pure waves of degree 1 for  $\kappa < \frac{1}{2}$ .

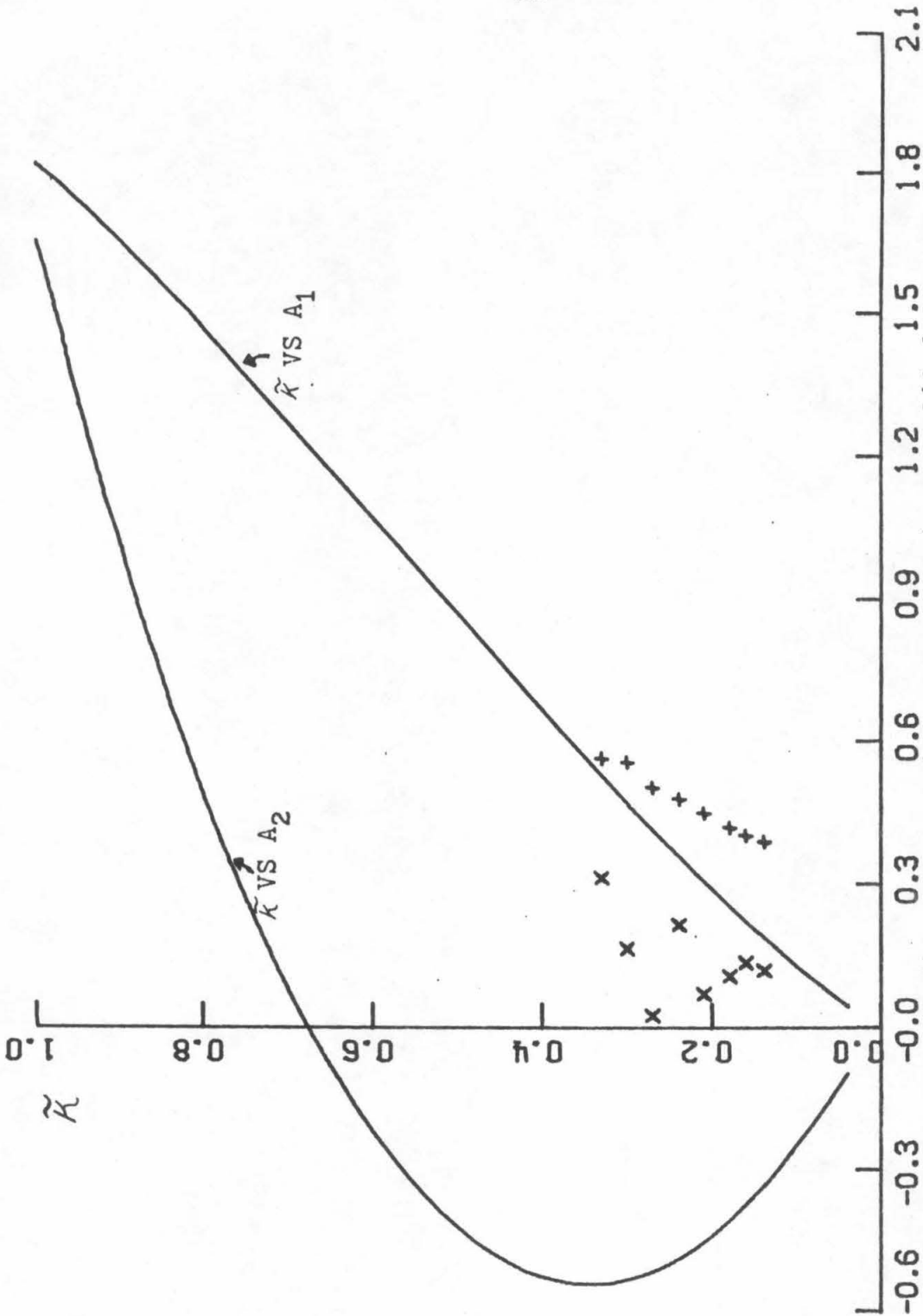
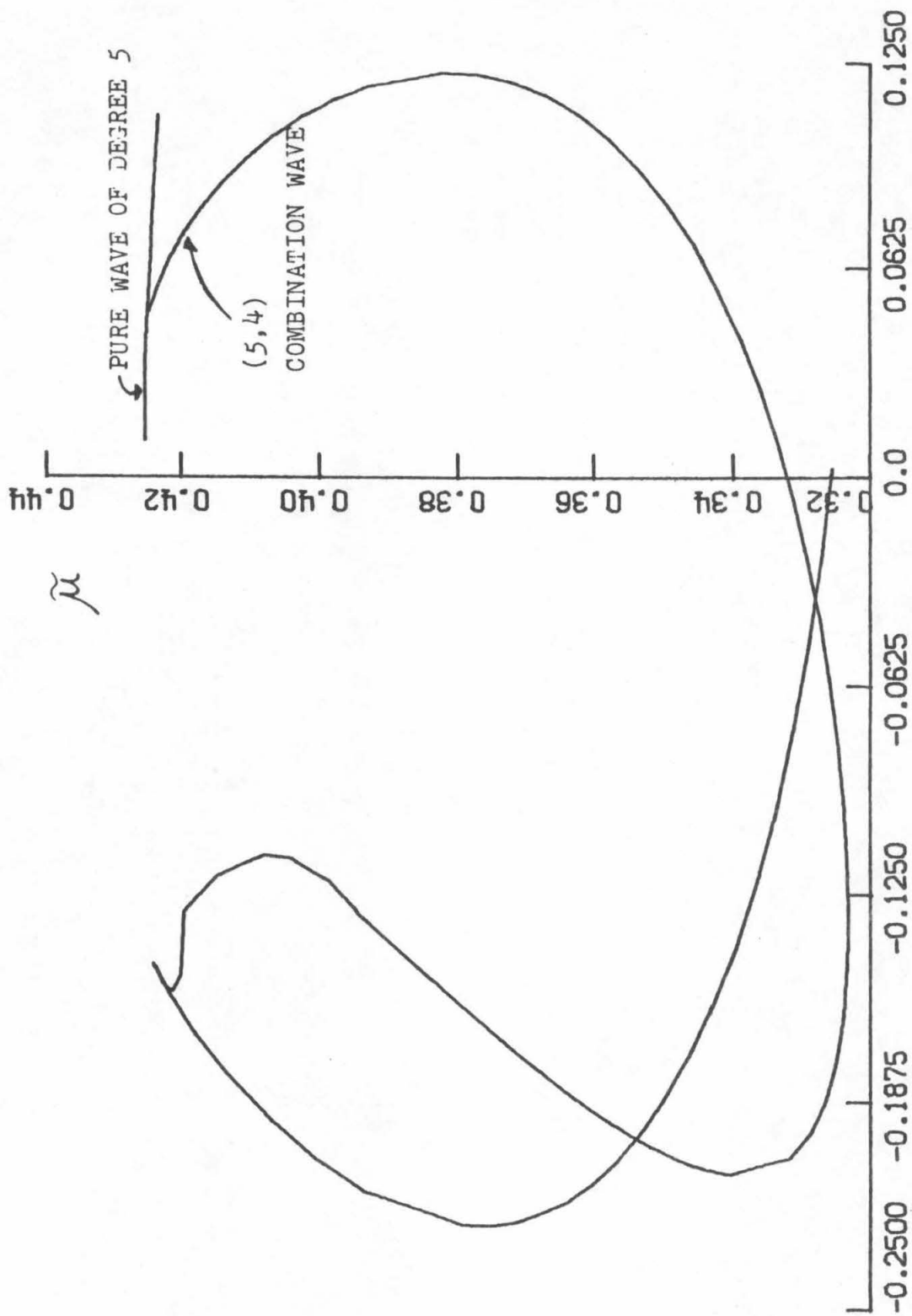


Figure 4.13. Plot of  $\tilde{K}$  vs  $A_1$  and of  $\tilde{K}$  vs  $A_2$  for maximum amplitude waves. The continuous lines are for the single-bubbled waves that are the analytic continuation of Crapper's solution. The + signs and the signs represent the values of  $A_1$  and  $A_2$  respectively for the multi-bubbled waves that are the continuation of small amplitude pure waves of degree 1.



$A_5$

Figure 4.14. Plot of  $\mu$  vs  $A_5$  for a (5,4) combination wave with  $\kappa = 0.05$  kept constant.

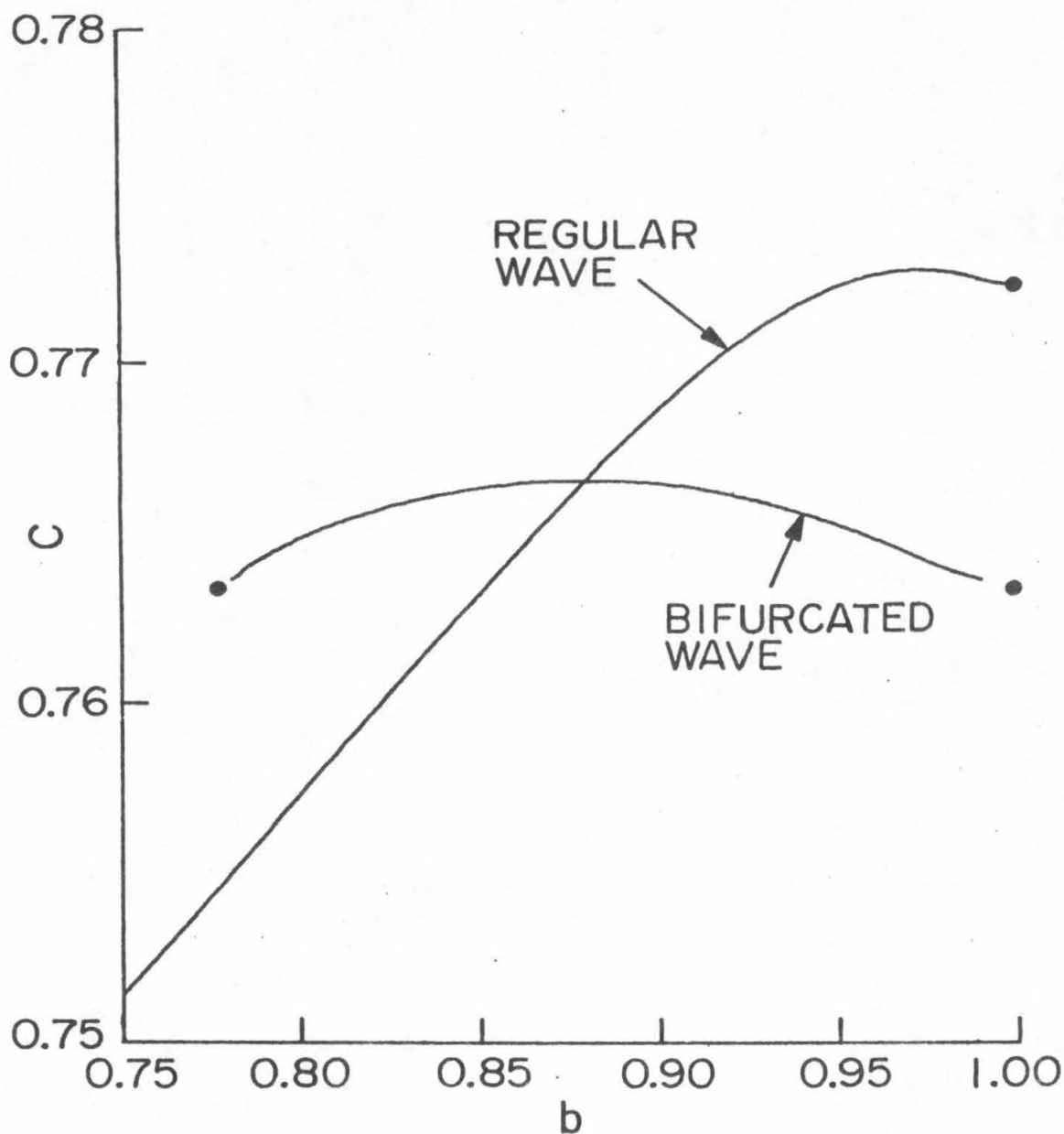


Figure 5.1. Wave speed vs amplitude parameter  $b$  for regular waves of class 2 and the bifurcated solutions. The two parts of the bifurcated solution describe physically identical waves shifted by  $L/2$ . The dots represent schematically the limiting waves.

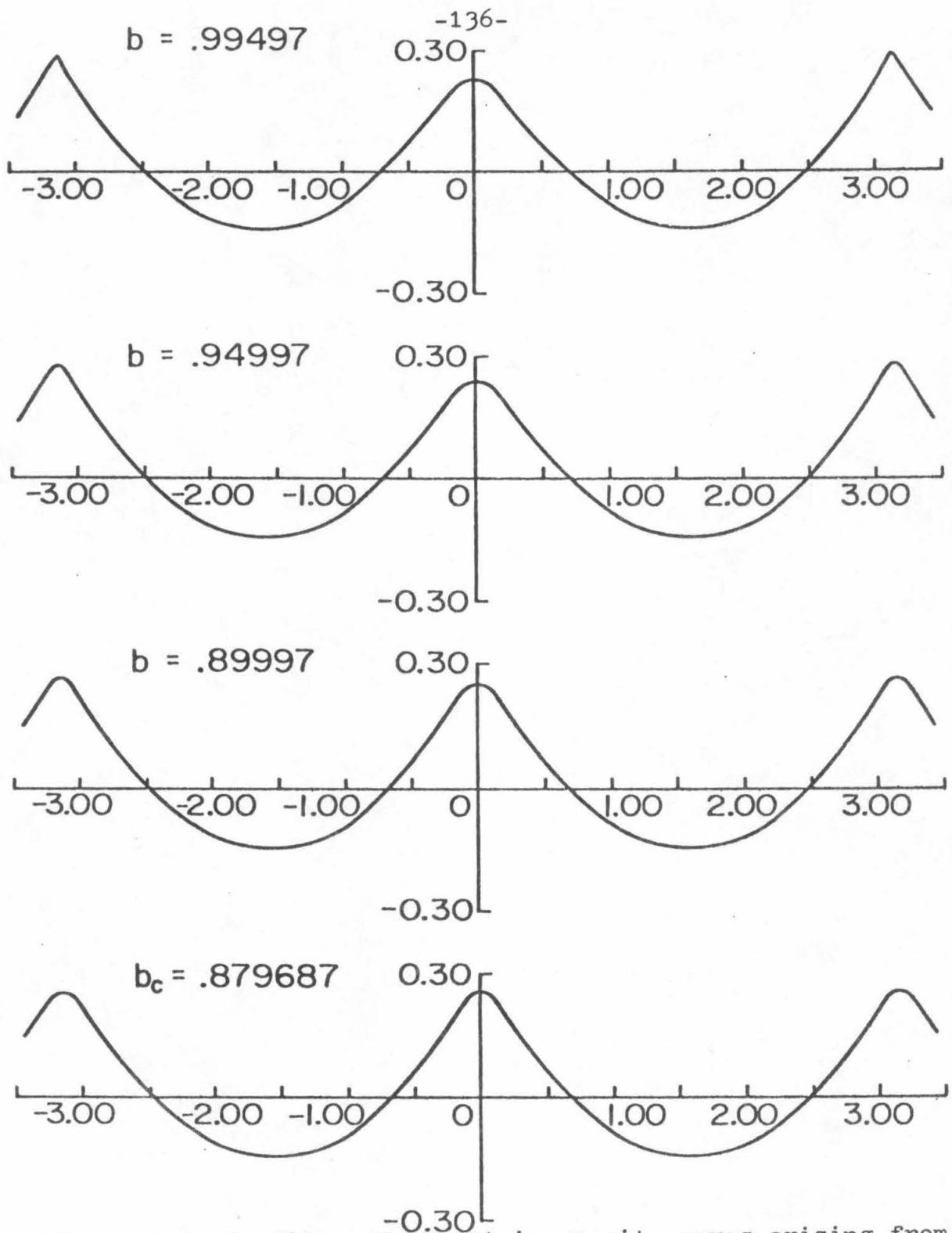


Figure 5.2. Profiles of symmetric gravity waves arising from the  $2 \rightarrow 1$  bifurcation. The horizontal axis is at the mean water level. The lowest wave corresponds to the bifurcation point.

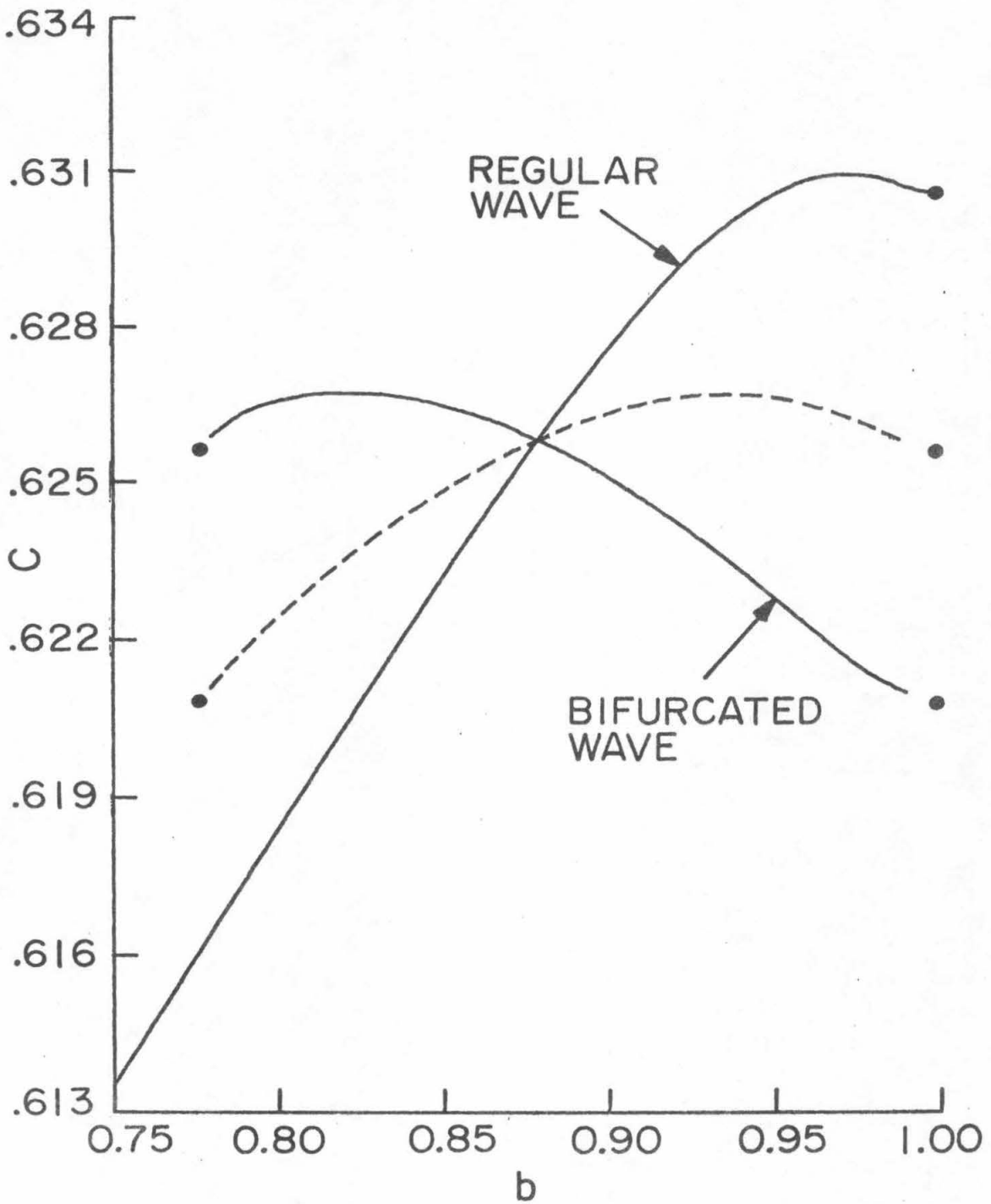


Figure 5.3. Wave speed vs  $b$  for regular waves of class 3 and the bifurcated symmetric irregular waves. The dashed line shows  $c$  vs  $b'$  (eq. (5.4.2)) or  $c$  vs  $b$  for both spurious "non-symmetric" solutions.

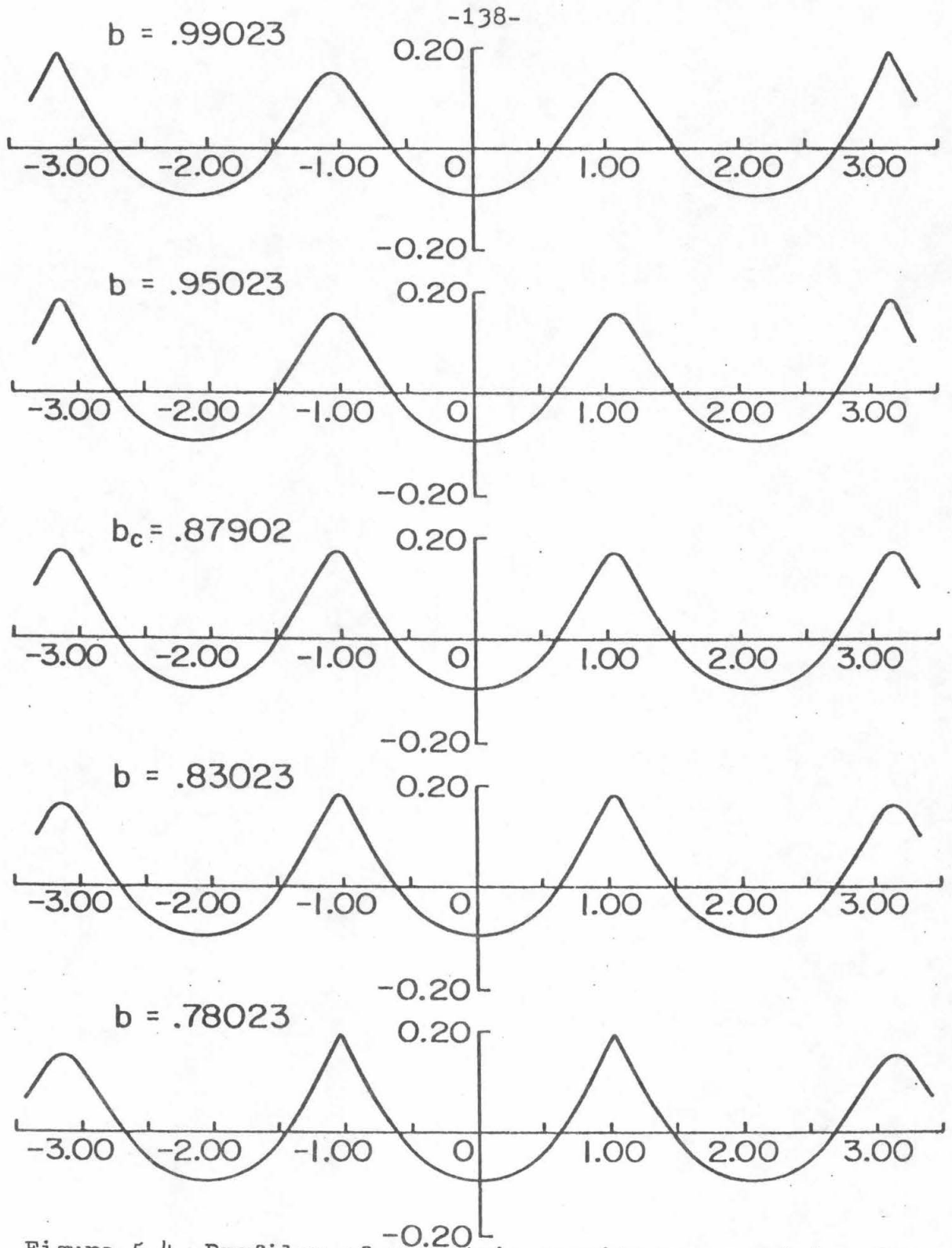


Figure 5.4. Profiles of symmetric gravity waves arising from the bifurcation of regular waves of class 3. The axis is at the mean water level. Middle plot is at the bifurcation point.

Table 1.

b	$\theta_{max}^{\circ}$	c	$\frac{h}{L}$	$\omega$	K	$V_g$	$\bar{y}$
.998	30.07	1.09233	.14087	.9964	.038295	.034567	-.59539
.997	30.13	1.09231	.14077	.9946	.038290	.034564	-.59477
.996	30.16	1.09232	.14068	.9929	.038291	.034564	-.59419
.995	30.15	1.09235	.14059	.9911	.038296	.034568	-.59632
.994	30.01	1.09238	.14050	.9893	.038304	.034574	-.59306
.9925	29.99	1.09243	.14037	.9867	.038323	.034588	-.59223
.9825	29.52	1.09280	.13957	.9689	.038505	.034745	-.58665
.9775	29.28	1.09291	.13917	.9600	.038604	.034835	-.58376
.9725	29.03	1.09295	.13876	.9511	.038693	.034922	-.58085
.9675	28.81	1.09292	.13835	.9422	.038767	.034999	-.57782
.960	28.47	1.09273	.13769	.9288	.038844	.035089	-.57315
.950	28.03	1.09225	.13678	.9110	.038877	.035155	-.56668
.945	27.78	1.09193	.13630	.9022	.038862	.035165	-.56336
.940	27.61	1.09154	.13580	.8933	.038828	.035158	-.55999
.930	27.16	1.09064	.13477	.8756	.038703	.035096	-.55312

Table 1. Properties of steep regular waves of class 1.

Table 2.

b	$\theta_{\max}^{\circ}$	c	$\frac{h}{L}$	K	$V_g$	$\bar{Y}$	$\frac{\Delta h}{L}$
.87969	25.2	.76660	.06445	.009276	.008488	-.2585	0
.87997	25.3	.76660	.06446	.009277	.008489	-.2586	-.00002
.88997	25.6	.76658	.06492	.009270	.008483	-.2615	-.00096
.89997	26.0	.76650	.06536	.009252	.008466	-.2644	-.00190
.90997	26.4	.76637	.06578	.009220	.008438	-.2672	-.00284
.91997	26.8	.76618	.06617	.009177	.008399	-.2700	-.00378
.92997	27.2	.76594	.06655	.009122	.008350	-.2728	-.00472
.93997	27.6	.76564	.06691	.009055	.008290	-.2755	-.00564
.94997	28.0	.76529	.06726	.008979	.008222	-.2782	-.00656
.95997	28.5	.76489	.06759	.008896	.008148	-.2808	-.00744
.96997	28.9	.76445	.06791	.008809	.008072	-.2834	-.00828
.97997	29.4	.76401	.06825	.008729	.008001	-.2860	-.00905
.98997	29.9	.76368	.06862	.008675	.007955	-.2887	-.00968

Table 2. Properties of symmetrical 2→1 bifurcated waves  $\Delta h$  is the height difference of the maxima. Note that K and  $V_g$  decrease monotonically as h increases.

Table 3.

b	$\theta_m$	c	$\frac{h}{L}$	K	$V_g$	$\bar{Y}$	b'
.78023	29.8°	.62589	.04598	.003983	.003633	-.1528	.9881
.79023	29.0°	.62637	.04556	.004035	.003679	-.1550	.9705
.80023	28.4°	.62660	.04527	.004071	.003712	-.1571	.9584
.81023	27.9°	.62673	.04500	.004099	.003738	-.1591	.9475
.82023	27.5°	.62677	.04473	.004120	.003759	-.1611	.9373
.83023	27.1°	.62675	.04446	.004134	.003773	-.1631	.9273
.84023	26.7°	.62667	.04417	.004142	.003782	-.1650	.9175
.85023	26.3°	.62653	.04387	.004145	.003786	-.1669	.9076
.86023	25.9°	.62634	.04356	.004141	.003785	-.1687	.8978
.87023	25.6°	.62611	.04324	.004132	.003779	-.1706	.8879
.87902	25.2°	.62586	.04294	.004119	.003770	-.1721	.8790
.88023	25.2°	.62583	.04297	.004117	.003768	-.1724	.8779
.89023	25.6°	.62552	.04324	.004097	.003753	-.1742	.8678
.90023	26.0°	.62516	.04350	.004072	.003732	-.1759	.8577
.91023	26.4°	.62476	.04374	.004042	.003707	-.1776	.8476
.92023	26.8°	.62434	.04398	.004007	.003678	-.1794	.8374
.93023	27.2°	.62387	.04420	.003968	.003644	-.1810	.8273
.94023	27.6°	.62338	.04441	.003925	.003607	-.1827	.8173
.95023	28.0°	.62287	.04461	.003879	.003568	-.1843	.8077
.96023	28.5°	.62235	.04481	.003832	.003528	-.1860	.7985
.97023	28.9°	.62184	.04501	.003786	.003488	-.1876	.7903
.98023	29.4°	.62138	.04521	.003746	.003453	-.1892	.7836
.99023	29.9°	.62106	.04545	.003719	.003430	-.1910	.7798

Table 3. Properties of waves obtained from bifurcation of regular waves with wavelength  $\frac{1}{3}L$ . The critical wave is  $b = 0.87902$ .

REFERENCES

- (1) T.B. Benjamin and J.E. Feir, The disintegration of wave trains on deep water. Part 1. Theory, J. Fluid Mech. 27, 417-430 (1967).
- (2) M.I.G. Bloor, Large amplitude surface waves, J. Fluid Mech. 84, 167-179 (1978).
- (3) I. Choi, Contributions a l'étude des mecanismes physiques de la generation des ondes de capillarité-gravite a une interface air-eau. Thesis. University d'Aix Marseille (1977).
- (4) G.D. Crapper, An exact solution for progressive capillary waves of arbitrary amplitude, J. Fluid Mech. 2, 532-540 (1957).
- (5) P.R. Garabedian, Surface waves of finite depth, J. Analyse Math. 14, 161-169 (1965).
- (6) W.J. Harrison, The influence of viscosity and capillarity on waves of finite amplitude, Proc. Lond. Math. Soc. 7, 107-121 (1909).
- (7) G. Keady and J. Norbury, On the existence theory for irrotational water waves, Math. Proc. Camb. Phil. Soc. 83, 137-157 (1978).
- (8) H.B. Keller, Numerical solution of bifurcation and nonlinear eigenvalue problems. Applications of Bifurcation Theory, 359-384, Academic Press, 1977.

- (9) Y.P. Krasovskii, The theory of steady-state waves of large amplitude, Dokl. Akad. Nauk SSSR 130, 1237-1240 (1960).
- (10) H. Lamb, Hydrodynamics, Cambridge University Press, 1932.
- (11) T. Levi-Civita, Questioni de meccanica classica e relativista, II, 25-29, Bologna: N. Zanichelli, 1924.
- (12) \_\_\_\_\_, La détermination rigoureuse des ondes permanentes d'ampleur finie, Math. Ann. 93, 264-314 (1925).
- (13) M.S. Longuet-Higgins, Integral properties of periodic gravity waves of finite amplitude, Proc. R. Soc. Lond. A 342, 157-174 (1975).
- (14) \_\_\_\_\_, The instabilities of gravity waves of finite amplitude in deep water, Proc. R. Soc. Lond. A 360, 471-505 (1978).
- (15) M.S. Longuet-Higgins and M.J.H. Fox, Theory of the almost-highest wave. Part 2. Matching and analytic extension, J. Fluid Mech. 85, 769-786 (1978).
- (16) L.F. McGoldrick, An experiment on second-order capillary-gravity resonant wave interactions, J. Fluid Mech. 40, 251-272 (1970).
- (17) J.H. Michell, The highest waves in water, Phil. Mag. 36, 430-437 (1893).

- (18) L.M. Milne-Thompson, Theoretical Hydrodynamics, p. 413, Macmillan, 1968.
- (19) A.H. Nayfeh, Triple and quintuple-dimpled wave profiles in deep water, Phys. of Fluids 13, 545-550 (1970).
- (20) A.I. Nekrasov, On waves of permanent type I., II., Izv. Ivanovo-Voznesensk. Politekhn. Inst. 3, 52-65 (1921).
- (21) W.J. Pierson and P. Fife, Some nonlinear properties of long crested periodic waves with lengths near 2.44 centimeters, J. Geophys. Res. 66, 163-179 (1961).
- (22) A.H. Schooley, Double, triple and higher order dimples in the profiles of wind-generated water waves in the capillary-gravity transition region, J. Geophys. Res. 65, 4075-4079 (1960).
- (23) L.W. Schwartz, Computer extension and analytic continuation of Stokes' expansion for gravity waves, J. Fluid Mech. 62, 553-578 (1974).
- (24) I.I. Sekerzh-Zen'kovich, On the theory of stationary capillary-gravitational waves of finite amplitude, Dokl. Akad. Nauk SSSR 109, 913-915 (1956).
- (25) V.P. Starr, Momentum and energy integrals for gravity waves of finite height, J. Marine Res. 6, 175-193 (1947).

- (26) V.P. Starr and G.W. Platzman , The transmission of energy by gravity waves of finite height, J. Marine Res. 7, 229-238 (1948).
- (27) G.G. Stokes, On the theory of oscillatory waves, Camb. Trans. Phil. Soc. 8, 441-473 (1847).
- (28) \_\_\_\_\_, Mathematical and Physical Papers, Vol. I, 197-229, 314-326, Cambridge 1880.
- (29) R.K.H. Szeto, The flow between rotating coaxial disks, Ph.D. Thesis, Calif. Inst. of Tech., 54-73, 1978.
- (30) J.F. Toland, On the existence of a wave of greatest height and Stokes' conjecture, Proc. R. Soc. A 363, 469-485 (1978).
- (31) J.R. Wilton, On ripples, Phil. Mag. 29, 688-700 (1915).
- (32) H. Yamada, Highest waves of permanent type on the surface of deep water, Rep. Res. Inst. Appl. Mech., Kyushu Univ. 5, 37-52 (1957).
- (33) E. Zeidler, Beiträge zur Theorie und Praxis freier Randwertaufgaben, Akademie-Verlag Berlin, 1971.